Auburn University

EVALUATION OF FATIGUE CRACKING IN I-65 MOBILE DELTA CROSSING BRIDGES

Volume II
Filler Plate Weld Cracks

by

J. Michael Stallings
Thomas E. Cousins
Bradley P. Christopher

sponsored by

The State of Alabama Highway Department
Montgomery, Alabama

Highway Research Center
Harbert Engineering Center
Auburn University, Alabama 36849-5337

September 1993

EVALUATION OF FATIGUE CRACKING IN I-65 MOBILE DELTA CROSSING BRIDGES

Volume II
Filler Plate Weld Cracks

by

J. Michael Stallings
Thomas E. Cousins
Bradley P. Christopher

sponsored by

The State of Alabama Highway Department
Montgomery, Alabama

September 1993

DISCLAIMER

The contents of this report reflect the views of the authors who are responsible for the facts and accuracy of the data presented herein. The contents do not necessarily reflect the official views or policies of the State of Alabama Highway Department or Auburn University. The report does not constitute a standard, specification, or regulation.

ACKNOWLEDGEMENT

The material contained herein was obtained in connection with a research project, "Evaluation of Fatigue Cracking in I-65 Mobile Delta Crossing Bridges" (ST-2019-16), conducted by the Highway Research Center at Auburn University. The research project was sponsored by the State of Alabama Highway Department. The traffic control, test load vehicles, bridge inspection vehicles and operators were provided by the Alabama Highway Department's Ninth Division and Maintenance Bureau. The interest, cooperation, and assistance of many personnel from the Alabama Highway Department is gratefully acknowledged. The assistance of graduate student Scott Rutland during the instrumentation, field testing, and data reduction portions of this project is also gratefully acknowledged.

TABLE OF CONTENTS

LIST OF TABLES

LIST OF FIGURES

SUMMARY

The I-65 Mobile Delta Crossing Bridges, located approximately 20 miles north of Mobile, Alabama, constitute a six mile section of interstate highway over the Mobile River delta plains. The tied arch span portion of the bridges extends 800 feet across the Mobile River. In late 1990, Alabama Highway Department bridge inspectors discovered filler plate weld cracks in numerous double angle members of the floortrusses at the tied arch span (northbound and southbound).

The objective of the project reported here was to use field testing to evaluate the stress conditions at the arch span in order to make an accurate prediction about the severity of existing filler plate weld cracks and the potential of future fatigue cracking in the double angles. The weld cracks were caused by pressures generated by confined rust between the filler plates and double angle legs of the floortruss members.

Field measurements were made at quarter-span and mid-span locations along the southbound arch span. The test data indicated that the four outer diagonals at each test location were the most critical members. The highest stress range found at the extreme fiber of any of the critical members was 4.4 ksi. This value is less than half the design AASHTO fatigue limit of 10 ksi for the filler plate weld details. The fatigue strength of the cracked weld details were judged not to be significantly less than the as designed (uncracked) details.

Further conclusions were drawn concerning the double angle tension members based on fracture mechanics principles. Fatigue-crack-initiation threshold estimates

indicate that fatigue cracking will not occur. Fatigue life calculations show that if fatigue cracks initiate, they will grow at a sufficiently slow rate to be found in the normal two year bridge inspections.

Based on the findings of the project, fatigue cracking at the filler plate welds of the double angles in the arch span floortrusses is not expected and does not pose a future problem. Repairs at the filler plates in the double angle tension members with cracked welds is not warranted.

CHAPTER ONE

INTRODUCTION

BACKGROUND

The I-65 Delta Crossing Bridges, located approximately 20 miles north of Mobile, Alabama, constitute a six mile section (northbound and southbound) of interstate highway over the Mobile River delta plains. The bridges consist of three basic types of spans: precast concrete spans, steel plate girder spans, and a steel tied arch span. The bridges were constructed in the late 1970's and early 1980's and opened to traffic in October, 1981.

In late 1990, Alabama Highway Department (AHD) bridge inspectors discovered filler plate weld cracks in numerous tension and compression double angle members of the floortrusses at the tied arch portion of the bridge (northbound and southbound). A typical double angle with filler plates is shown in Figure 1. Photos of typical filler plate weld cracks are illustrated in Figures 2 and 3. Note that the small rectangular object on top of the filler plate in Figure 3 is a block of rust that had collected on top of the filler plate and solidified.

The ends of the filler plates were attached to the back to back legs of the double angles with groove welds. The welds were approximately two inches long and were ground flush with the ends of the filler plates. The double angles and filler plates were made of unpainted A588 weathering steel and were susceptible to corrosion.

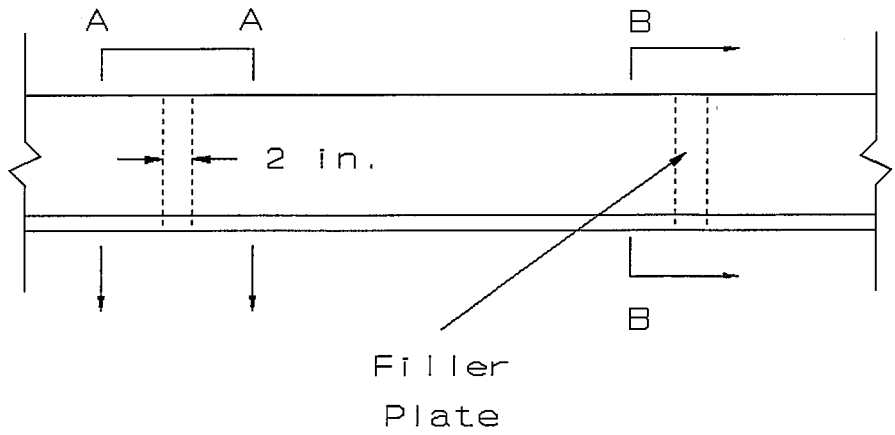

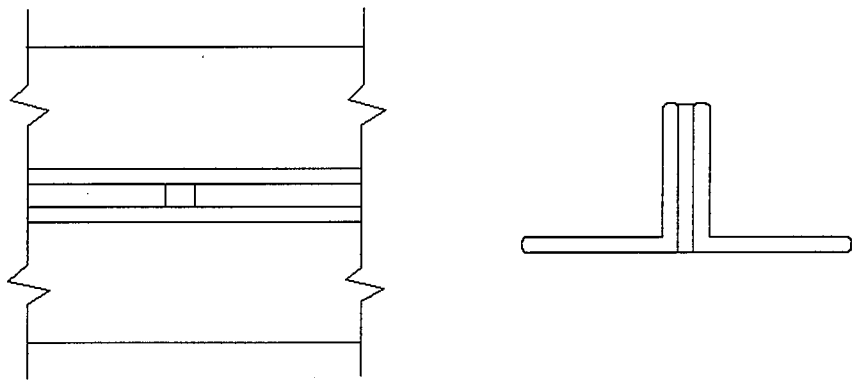

Figure 1. Typical Double Angle with Filler Plates

Figure 2. Filler Plate Weld Crack

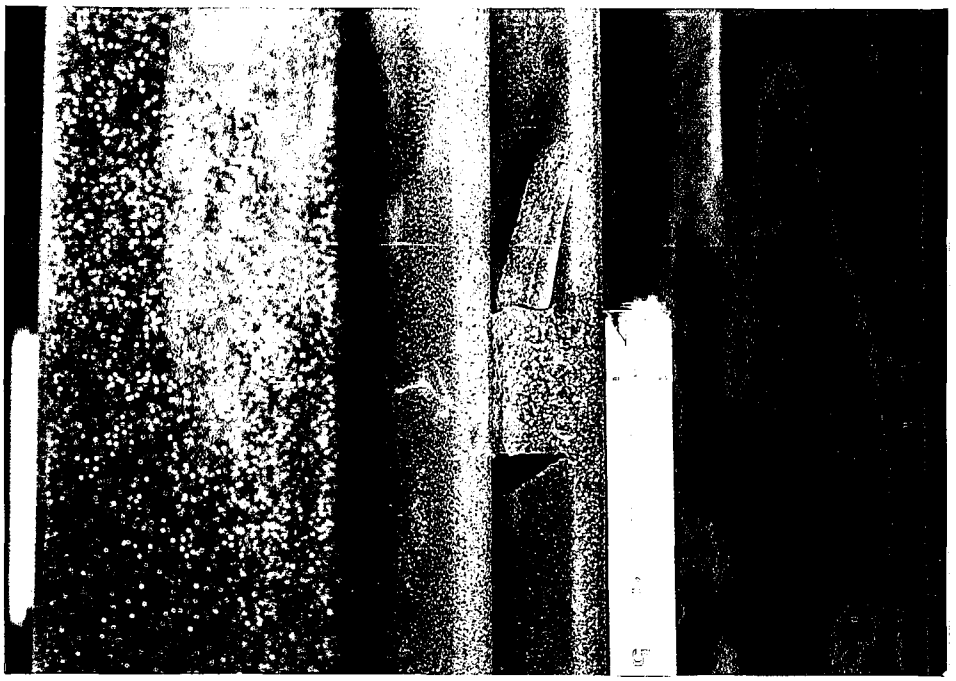

Figure 3. Filler Plate Weld Crack and Solidified Rust

The normal weathering, or corrosion, of the A588 weathering steel caused rust to build up between the double angle legs and filler plates. Built up corrosion products in restricted areas, called "pack rust", can generate pressures of up to 10 ksi (Kulicki et al. 1990). By considering an internal pressure of 10 ksi over the area between the double angle and filler plate, the force on the weld at each end of an 8 inch long filler plate is 80 kips (1/2 x 8 inches long x 2 inches wide x 10 ksi = 80 kips). The stress applied to the weld (throat area approximately 3/16 inch x 2 inches = .375 in^2) at the end of a filler plate would be approximately 200 ksi. This value is almost three times the weld capacity of 70 ksi. In a number of locations, the throat area of cracked welds was observed to be smaller than assumed above which would only serve to increase the stress on the weld. Thus, confined rust is considered to be the cause of the filler plate weld cracks in the double angle members at the tied arch span.

The weld cracks created by the "pack rust" are parallel to the applied stress on the double angles and have not propagated into the angles and pose no immediate threat to the integrity of the trusses. However, the possibility of future cracking in the tension members was a concern prior to this project. One maintenance strategy considered by the AHD was to remove the filler plates and grind out the welds. However, this option would be expensive and may be unnecessary. For tension members alone at the northbound and southbound spans it would involve removing approximately 960 filler plates.

The purpose of the project reported here was to measure the traffic loading stresses in the floortruss tension members and to address whether it is necessary to remove the filler plates from these members and grind out the welds. Based on the results of the field tests, behavior patterns and recommendations concerning the floortrusses at the arch span are presented in this report.

PROJECT OBJECTIVES

The possibility of filler plate weld cracks causing or becoming fatigue cracks in the double angle tension members of the arch span provided the motivation for this phase of the project. Field testing was the best method to determine the traffic loading stresses and overall behavior of the floortrusses and for accurately predicting the future of these cracks. The major questions this project sought to answer are listed below:

1) What are the axial stresses in the floortruss tension members?
2) Are these members experiencing bending?
3) If bending is present, what are the extreme fiber stresses very near the filler plates?
4) What is the appropriate fatigue limit for the cracked filler plate weld details?
5) Are the tensile stresses high enough to cause fatigue cracks to develop in the double angle members near the filler plate weld details?

METHODOLOGY AND SCOPE OF REPORT

The project objectives were met by use of field tests performed during the summer of 1992. Field measurements were made to determine the magnitudes of stresses in the tension members of the floortrusses at the tied arch span. The measurements were made at quarter-span and mid-span locations along the arch span with loading from trucks of known weight and with loading from the normal truck traffic crossing the bridges.

The field measurements will be compared later in this report to the fatigue limit for the filler plate weld details. Fatigue limit is the fatigue strength below which an unlimited number of cycles can be applied to a member without failure. Stresses in the filler plate

weld details of the double angle members at the tied arch span can be classified under Stress Category C (AASHTO 1991). This category applies to the base metal with longitudinal loading at fillet and groove welded attachments less than or equal to two inches in length. The allowable fatigue stress range, or fatigue limit, for a Category C detail with redundant load paths and subjected to over two million cycles is 10 ksi. Figure 4 (taken from NCHRP Report 286) illustrates the fatigue resistance of various Category C details as determined by laboratory tests (Keating and Fisher 1986). For fatigue cracking to occur in the double angle tension members very near the filler plate welds, the area around the weld details would have to experience stress ranges from traffic loading greater than 10 ksi.

Along with the comparison of the field test data to the AASHTO fatigue limit, fracture mechanics approaches were applied to draw conclusions on whether fatigue cracking will pose a problem at the tied arch span. Fracture mechanics is an applied science developed because of the occurrence of low stress fracture in high strength materials. Due to the presence of only small cracks, structures that are designed with high strength materials can fail at stresses below the maximum stress they were designed for. Fracture mechanics will be used to predict fatigue thresholds and to estimate a tolerable crack size and fatigue life for the floortruss double angle members at the tied arch span.

Descriptions of the tied arch span and test locations, instrumentation and data acquisition, and data collection and reduction methods are given in Chapters Two, Three, and Four, respectively. Test results and analyses of these results are presented in Chapter Five. Final evaluation of the potential for fatigue cracking in the double angle members is given in Chapter Six. Conclusions and recommendations are discussed in Chapter Seven.

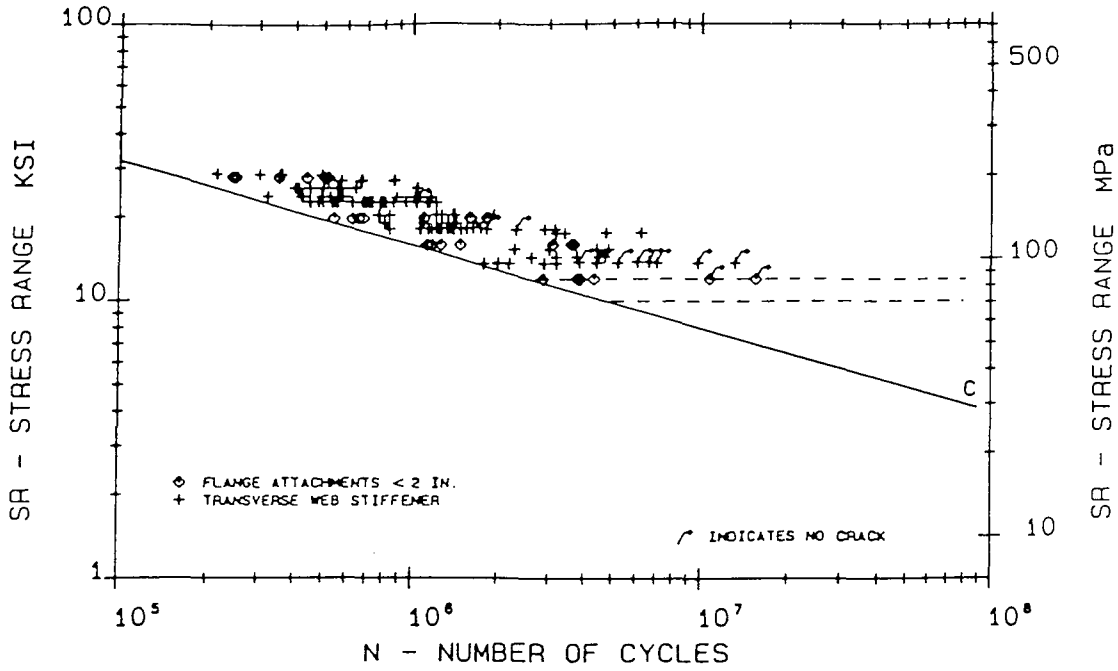

Figure 4. Fatigue Resistance of Category C Details (from Keating and Fisher 1986)

CHAPTER TWO

BRIDGE DESCRIPTION AND TEST LOCATIONS

The steel tied arch span extends 800 feet across the Mobile River, with the lowest point on the span approximately 125 feet above the water. The span consists of 16 panels, each measuring 50 feet long and 46 feet wide. Expansion joints in the deck system are located 200 feet apart at quarter points along the arch span (above the fourth, eighth, and twelfth floortrusses).

The concrete deck is supported by six lines of stringers that run parallel to the direction of traffic, as shown in Figure 5. These lines are made of four units of stringers. Each unit is made continuous between expansion joints by splices placed at points where the bending moment is small. The stringers, which rest on top of each floortruss, are braced by diaphragms that run perpendicular to the traffic flow.

Fifteen floortrusses spaced at 50 feet on centers are located transverse to the arch tie girders. The vertical, diagonal, and bottom members of each floortruss consist of double angles that contain filler plates spaced at two feet on centers. Horizontal cross-bracing is provided by T-sections arranged in an "X" configuration between floortrusses.

The tied arch span, and all the Delta Crossing Bridges, are subjected to traffic loadings from vehicles traveling to and from the port city of Mobile. A traffic history (total of northbound and southbound vehicles) for the bridges is given in Table 1.

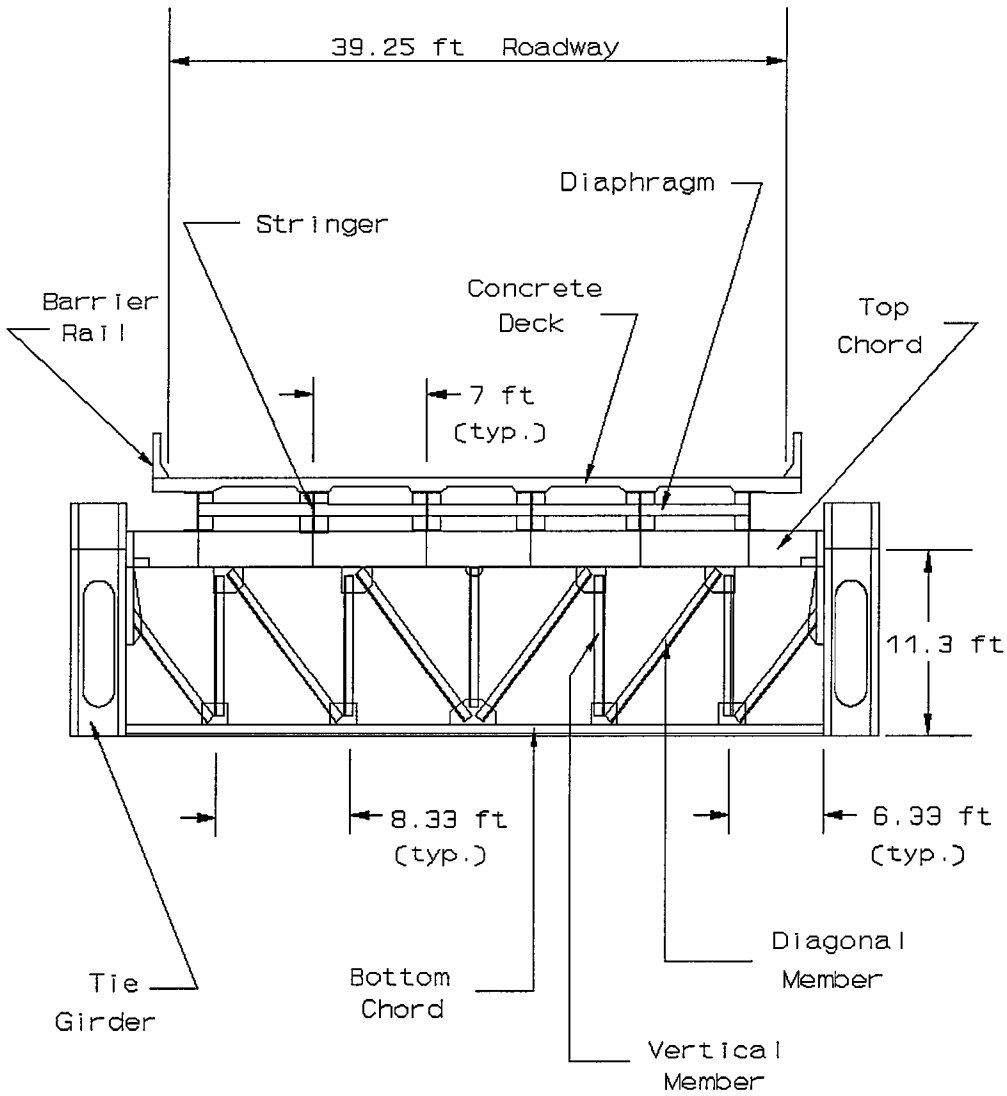

Figure 5. Typical Floortruss Section

Table 1. Traffic History of the Mobile Delta Crossing Bridges

Year	Average Daily Traffic	Percent Commercial Vehicles	Percent Heavy Vehicles	Number Heavy Vehicles
1991	13020	26	85	2877
1990	12220	26	85	2701
1989	11300	28	85	2689
1988	10490	30	85	2675
1987	10150	30	85	2588
1986	9940	30	85	2535
1985	8530	34	85	2465
1984	8410	34	85	2430
1983	8120	35	85	2416

TEST LOCATIONS

The field tests referred to in this report were performed during the months of August and September of 1992. These tests concentrated on the southbound arch span portion of the bridge. The location of the arch span in relation to the rivers and creeks below it and to the other bridges is shown in Figure 6.

The exact test locations along the arch span included floortrusses at quarter-span and mid-span. Gages were also placed on the floortruss just north of mid-span. However, this floortruss was not considered a major test location, and a discussion of this fact is presented later in this chapter. The quarter-span and mid-span locations spoken of fall in line with lower panel points L12 and L8, respectively, shown in Figure 7. Each lower panel point, and consequently floortruss, lies directly below a tie arch suspension cable.

As mentioned earlier in this chapter, the 800 foot long arch span consists of fifteen floortrusses spaced at 50 feet on centers with expansion joints in the concrete deck located at quarter points along the span. The significance of the expansions joint locations is that the top chord member size for floortrusses located below an expansion joint differs from that of all other floortrusses. That is, the geometry is the same for all fifteen floortrusses except for the top chord members. The top chord at floortrusses under expansion joints is made up of a channel and t-section. The top chord at all other floortrusses consists of a wide flange section. A typical floortruss section was illustrated in Figure 5 and corresponding member sizes are given in Table 2.

To ensure that the presence of an expansion joint and break in continuity in the floor system above a floortruss had little or no effect on the floortruss stresses, gages were placed along the neutral axis of two of the outer diagonal members of floortruss seven. This floortruss is located one panel north of the mid-span floortruss (in line with

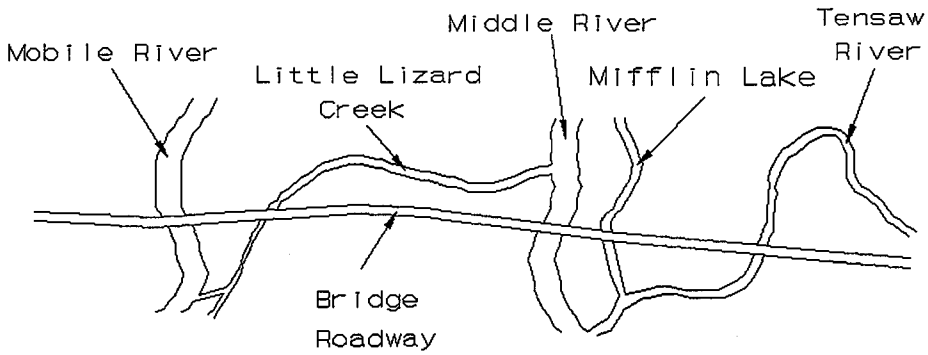

Plan View

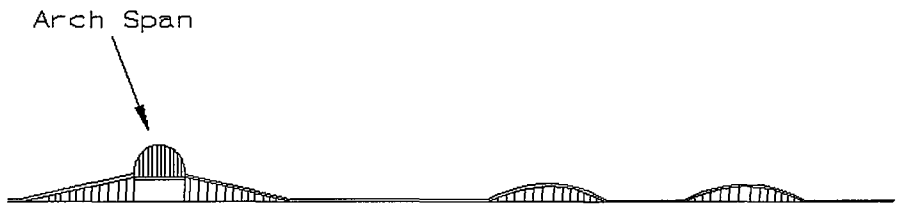

Elevation View

Figure 6. Mobile Delta River Crossing Bridges

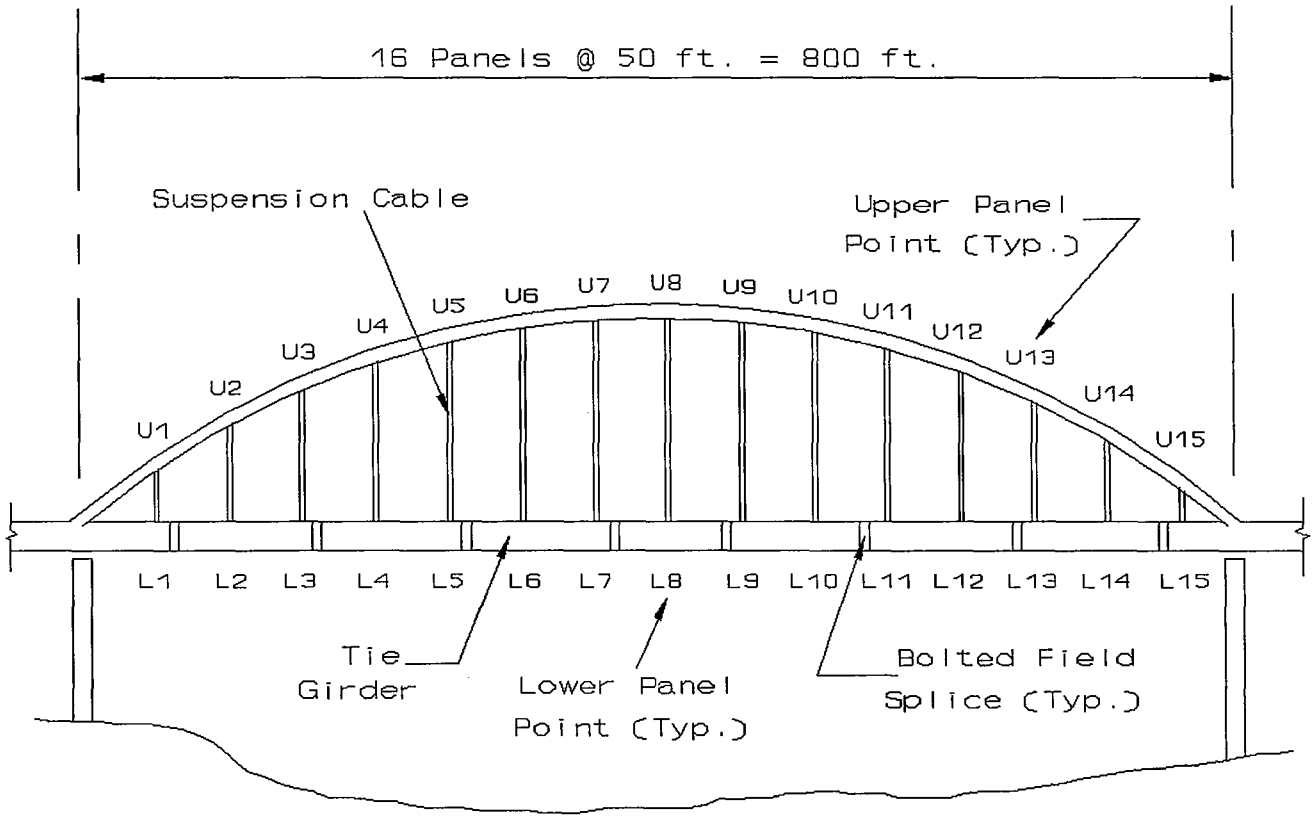

Figure 7. Elevation View of Southbound Arch Span (Looking from Northbound Lane)

Table 2. Floortruss Member Sizes

Member	Size
Stringer	W 30 X 99
Diaphragm	C 15 X 33.9
Top Chord[a]	MC 18 X 42.7 / WT 18 X 67.5 W 24 X 103
Vertical	8 X 6 X 1/2 LLBB[b]
Diagonal Interior (4) Exterior (2)	 8 X 6 X 1/2 LLBB 8 X 6 X 3/4 LLBB
Bottom Chord	8 X 6 X 3/4 SLBB[c]

[a]MC 18 X 42.7 / WT 18 X 67.5 at quarter-span & mid-span;
W 24 X 103 at all other floortrusses
[b]LLBB = double angle with long legs back to back
[c]SLBB = double angle with short legs back to back

lower panel point L9 on Figure 7) and does not have an expansion joint above it. The results of this comparison between floortrusses with different top chord member sizes are presented in Chapter Five. As expected however, the difference in stresses in the two floortrusses was minimal, and the major test locations chosen (quarter-span and mid-span) appear to be representative of all fifteen floortrusses at the arch span.

Finally, in order to differentiate between floortruss members it was necessary to adopt an identification scheme. This scheme is based on viewing the north side of the floortruss. The six bottom chord members, starting from the right, were labeled B1 through B6. Similarly, the six diagonal members were labeled D1 through D6. Figure 8 illustrates this system.

Filler Plate Weld Cracks at Test Locations

Floortrusses 4 and 8 were chosen as test locations because they were assumed to be representative of the behavior of all the floortrusses at the arch span. They were not chosen as floortrusses to be instrumented because they had the most or least filler plate weld cracks. However, it is interesting to note which filler plate welds at the two test locations were cracked.

Figure 9 shows the locations of weld cracks at floortrusses 4 and 8 and whether the cracks were near the top or bottom of the angles. The letters shown in the figure identify individual cracks and are used in Table 3 to further describe them.

The weld cracks generally occurred in the outside diagonal members at both test locations. As will be shown later in this report, the highest stressed members in the floortrusses are the outside diagonals. However, the above statements do not necessarily mean that the stresses in the double angle members are directly related to the formation of

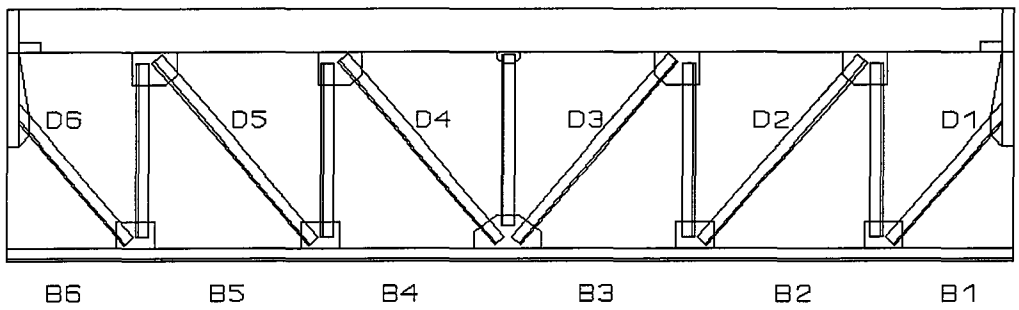

Figure 8. Identification Scheme for Floortruss Members (Looking South)

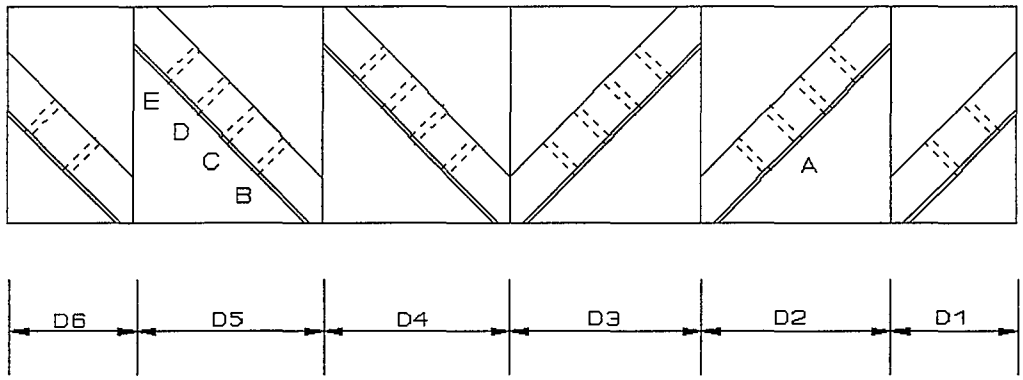

(a)

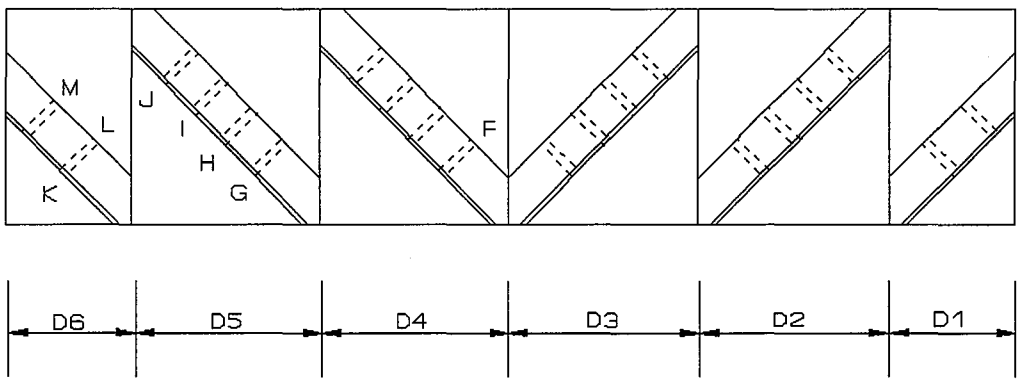

(b)

Figure 9. Existing Filler Plate Weld Crack Locations (Denoted by Letters): (a) Floortruss 4; (b) Floortruss 8 (Looking South)

Table 3. Filler Plate Weld Cracks at Test Locations

Weld Crack	Side of Filler Plate that Crack was on
Floortruss 4 (Quarter-Span)	
A	North
B	South
C	North
D	North
E	North
Floortruss 8 (Mid-Span)	
F	North
G	North
H	North
I	South
J	South
K	North
L	North
M	South

the filler plate weld cracks. As discussed in Chapter One, the weld cracks were caused by pressures generated by confined rust between the filler plates and double angle legs.

One further observation is that the majority of weld cracks in a floortruss occur in the outer diagonals perhaps because these members are subjected to more moisture that the interior members. During rainstorms, water is more likely to reach the outer members because of a two foot wide gap between the concrete deck and the arch tie girder.

CHAPTER THREE

INSTRUMENTATION AND DATA ACQUISITION

WORKING ENVIRONMENT

In order to obtain stress readings due to normal truck traffic, all computer and data acquisition equipment and supplies had to be kept beneath the bridge and out of sight of passing traffic. This was accomplished by using work platforms constructed by the Alabama Highway Department (AHD).

Two work platforms, illustrated in Figure 10, were built at each test location. The first platform, used to support the computer and data acquisition equipment, was located near the center of the T-section cross braces which span between floortrusses. Steel angles were clamped to the T-sections and aluminum planks were laid across the angles to form the work area. The second platform, used for mounting strain gages and to store supplies, was located on each side of the bottom chord of the floortruss. This platform was made of two plank sections spanning the entire length of the floortruss. Each plank was supported by placing an angle across the outer bottom chord member and the cross bracing member that connected to the bottom chord. One end of each plank section laid across the angle and the other end rested on the bridge inspection walkway (or cat-walk). The bridge inspection walkway was used to provide access from the bridge deck to the test locations. The movement of equipment from the bridge deck to test locations or from one test location to another was accomplished through the use of the AHD's bucket and

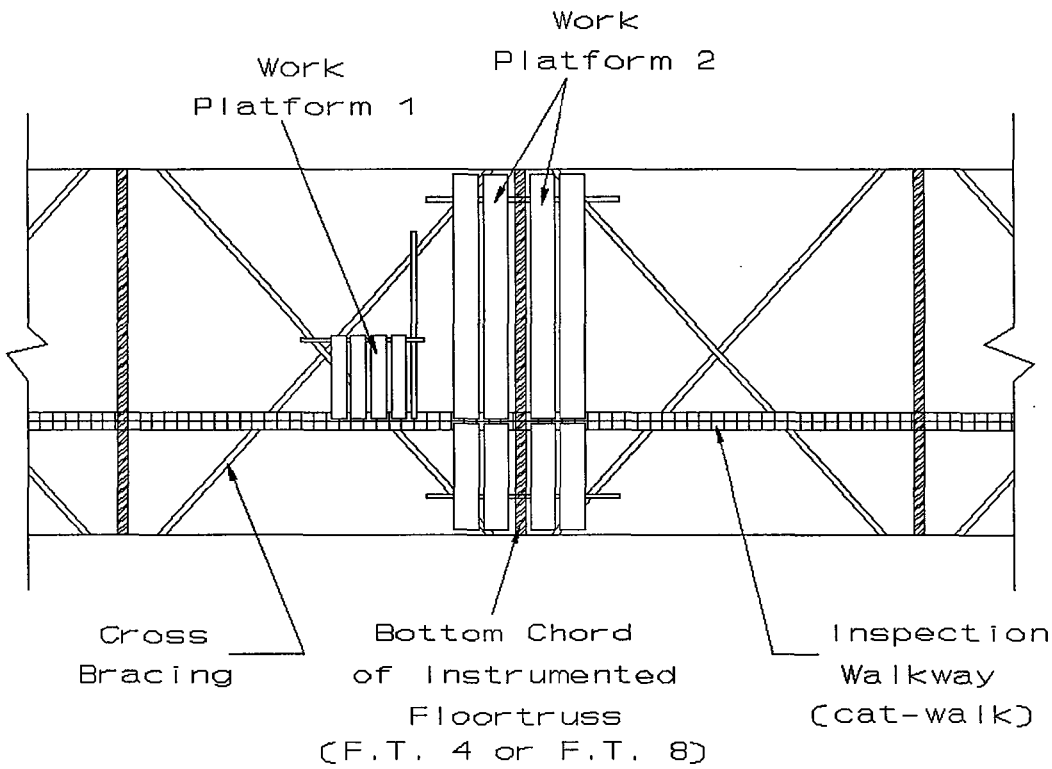

Figure 10. Plan View of Work Platforms at Floortruss Test Location

boom truck (Reach-All). This truck was also used in part of the instrumentation. Five of the six bottom chord members were gaged out of the truck's bucket. Member B6, the outer bottom member on the fast lane side of the bridge, could not be reached with the truck and was gaged from the second work area mentioned above. All diagonal members were instrumented directly from platform 2.

INSTRUMENTATION

Electrical resistance strain gages were used for measuring surface strains on the diagonal and bottom chord members. The strain gages were self temperature compensating foil gages with polyamide encapsulation and pre-attached leads. All the gages had a nominal resistance of 120 ohms. A table of gage sizes and gage factors will be presented later in this chapter. The gages used were manufactured by BLH Electronics, Inc. and Measurements Group, Inc.

The strain gages were connected to the data acquisition system through a series of two cables. Cinch connectors were first installed near each gage location using five minute epoxy. The gages were connected to the cinch connectors with light gage two lead stranded wire. Shielded cable was then used to connect the cinch connectors to the data acquisition system. The shielded cable reduced the effects of electrical noise on the data. Also, connecting the shielded cable to the cinch connectors instead of directly to the strain gages provided ease of connection and disconnection as well as enabling reuse of the shielded cable.

Thirty strain gages were mounted at each test location. Sixteen gages were placed on the bottom chord and fourteen on the diagonal members. Gages with a 1/4 inch gage length were used at all thirty gage locations at the mid-span floortruss. At quarter-span,

due to available supplies, 1/4 inch length gages were mounted on the diagonal members and 1/4 inch and 1/8 inch length gages were used on the bottom chord members.

The 16 bottom chord gage locations are shown in Figure 11. The points of interest on these members were the extreme top and bottom fibers near the filler plates. Gages were mounted three inches from the edge of the filler plates and as close as possible to the top and bottom edges of the members. Since the bottom surface of the double angle was flat, gages were mounted directly on the extreme bottom fiber of members B2, B3, B4, and B5. The bottom of member B6 could not be reached from the platform or Reach-All truck and thus a gage was placed at the neutral axis. Member B1 was gaged similarly for symmetry. The gage locations at or near the extreme bottom fiber are referred to here as gage position one on the various members. Thus, gage B21 refers to a gage on member B2 in position one, as illustrated in Figure 11.

The stresses at the extreme top fiber of the bottom members were also of interest. However, due to the curvature of the edge of the angle legs, gages could not be mounted directly on this top fiber. A gage was mounted 3/4 inch from the top edge and directly above position one. This gage location is referred to as position two. The position one and position two gage readings were used to linearly extrapolate to the unknown top fiber stress. Linear extrapolation was also used to find the extreme bottom fiber stress for members B1 and B6. Based on classical flexural theory, the strain diagram across the height of the double angle varies linearly.

A third gage was mounted on members B2, B3, B4, and B5 at 3/4 inch from the top and three inches from the filler plate edge on the member end away from gage positions one and two. Having this third gage position (referred to as position three) allowed the top and bottom extreme fiber stresses at the position three end of the bottom

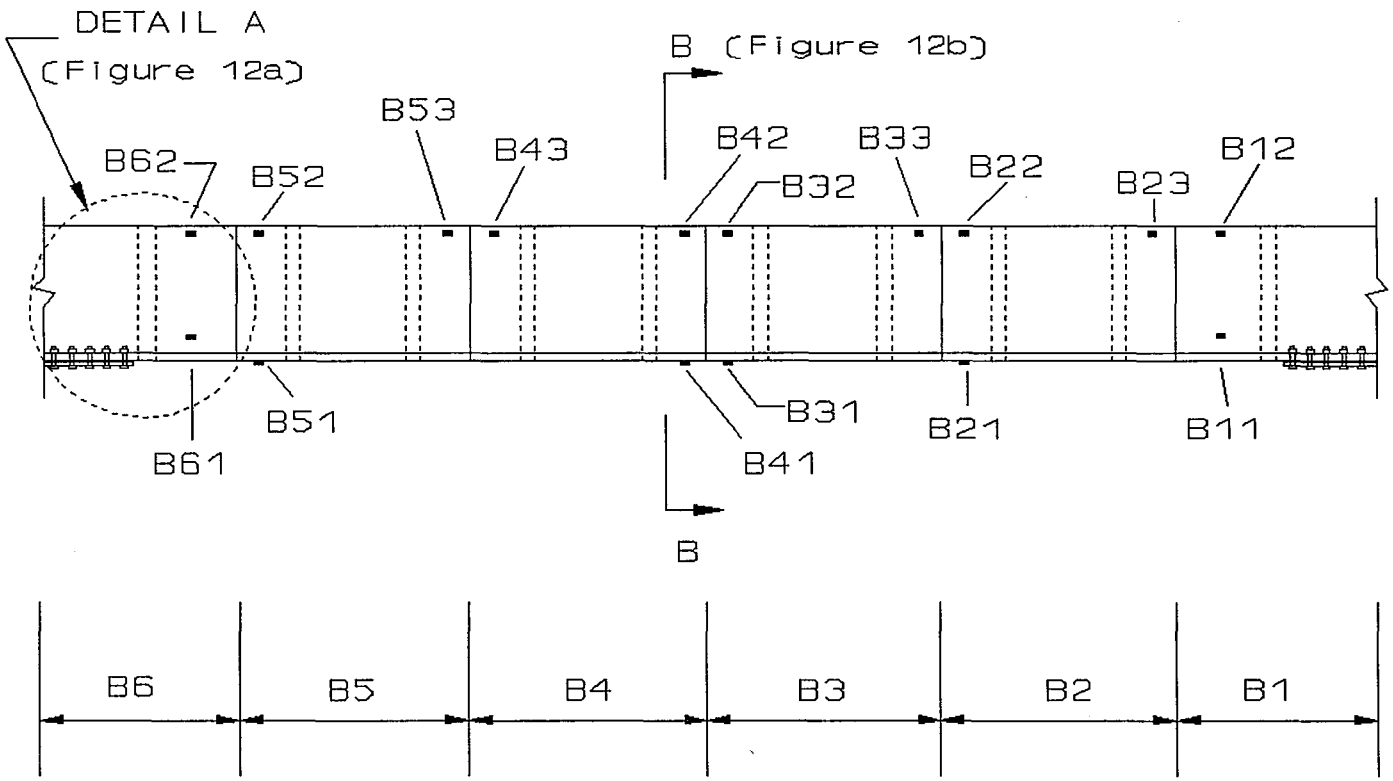

Figure 11. Gage Locations on Bottom Chord Members

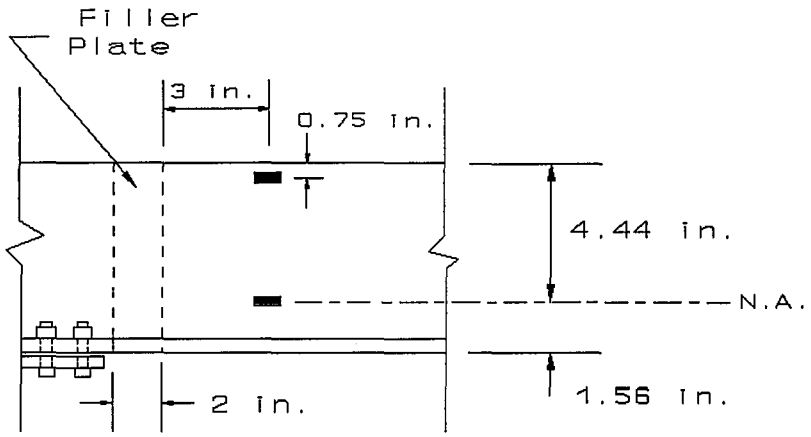

(a)

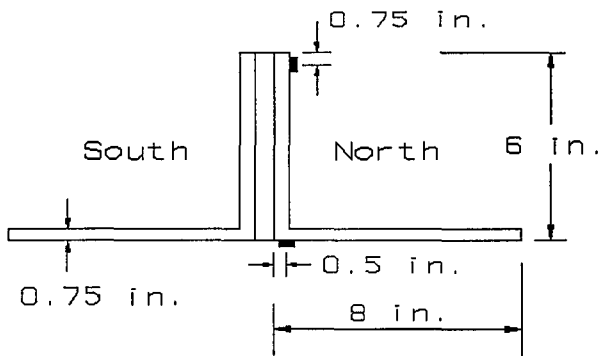

(b)

Figure 12. Bottom Chord Gage Location Details (See Figure 11) (a) Detail A; (b) Section B-B

members to be calculated. That is, the strain at the neutral axis (position one) is the same at all points along the double angle. Thus, the position one and position three gage readings were used to linearly extrapolate to the unknown top and bottom fiber stresses on the position three end of the member. Therefore, the top and bottom extreme fiber stresses at each end of members B2, B3, B4, and B5 were calculated. Figure 11 illustrates the identification system for all 16 strain gages on the bottom chord.

As stated earlier, 14 gages were mounted on the diagonal members at each test location. Photographs of some of the instrumented diagonals are shown in Figure 13. All diagonal gage positions are illustrated in Figure 14. The gage locations on these members were determined by a preliminary analysis of a typical floortruss through the use of a general planar frame analysis computer program. This analysis suggested that the highest stresses occur near the upper ends of diagonal members D2, D3, D4, and D5. The critical stress locations on the outer diagonals were not as easily located. Thus, the points of interest on the diagonal members were the extreme top and bottom fibers near the filler plates on both ends of the two outer diagonals and on the upper ends of the four interior diagonals.

For members D2, D3, D4, and D5, two gages were mounted three inches from the filler plate on the upper end. One gage was installed at the neutral axis, referred to as position one, and the second gage was located 3/4 inch from the top, called position two. Linear extrapolation was used to find the extreme top and bottom stresses above and below these two gage positions.

Three gages were mounted on the two outer diagonal members (D1 and D6). Gages were installed at positions one and two (as defined above) on the lower end, and a third gage (position three) was mounted on the upper end at three inches from the filler

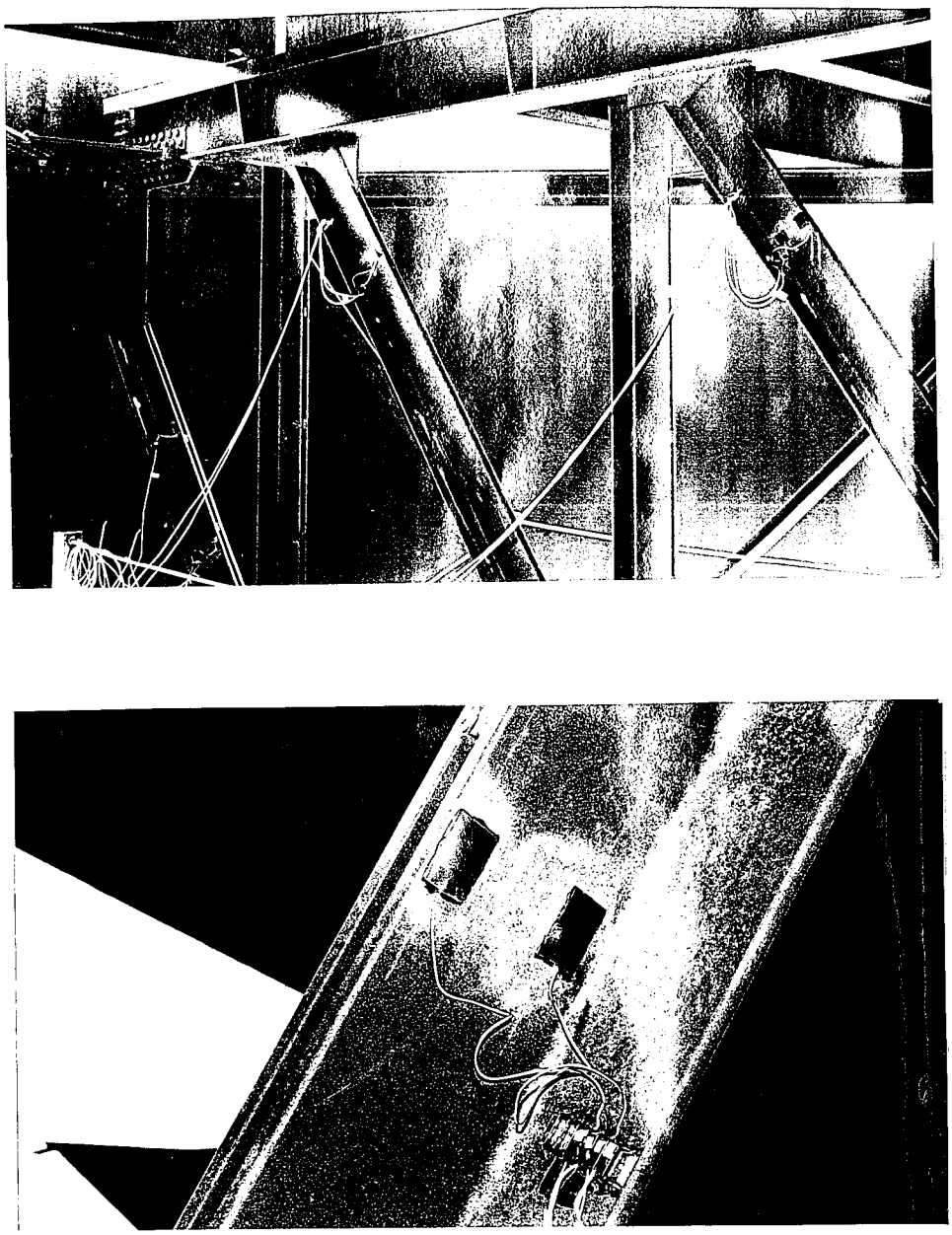

Figure 13. Instrumented Diagonal Members

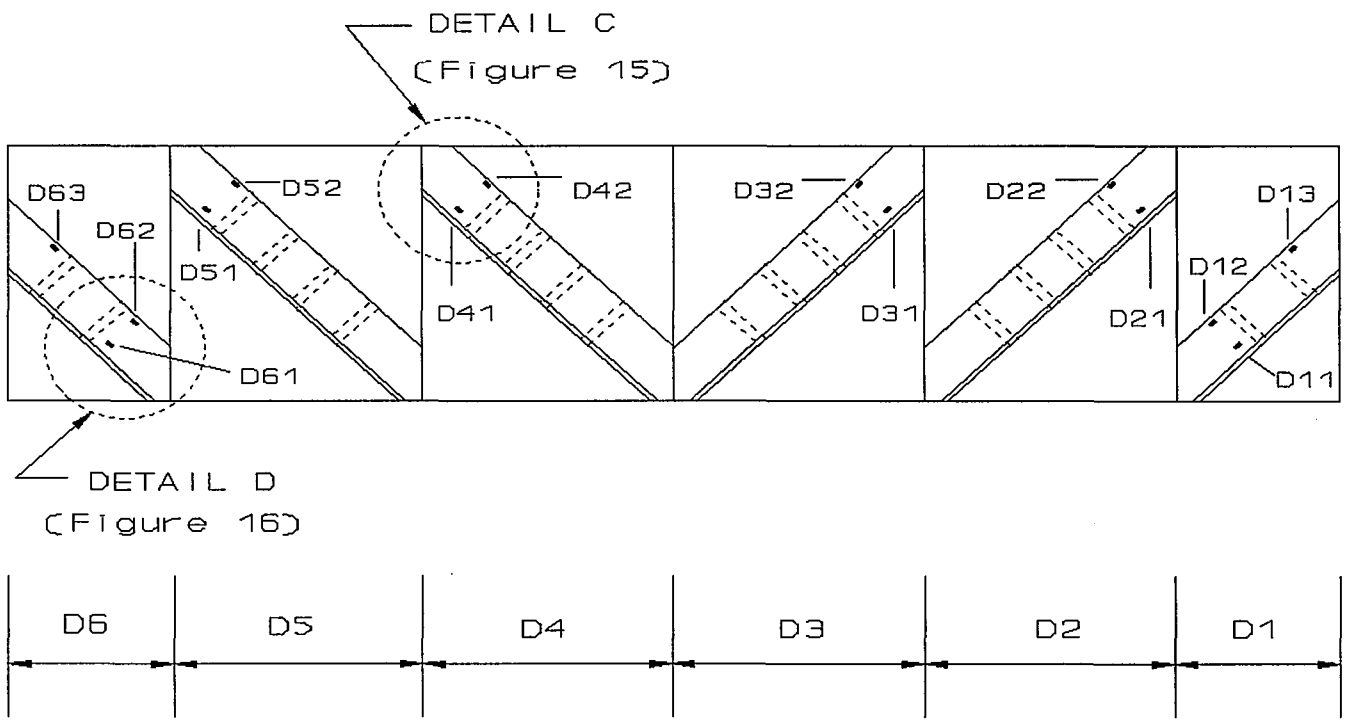

Figure 14. Gage Locations on Diagonal Members

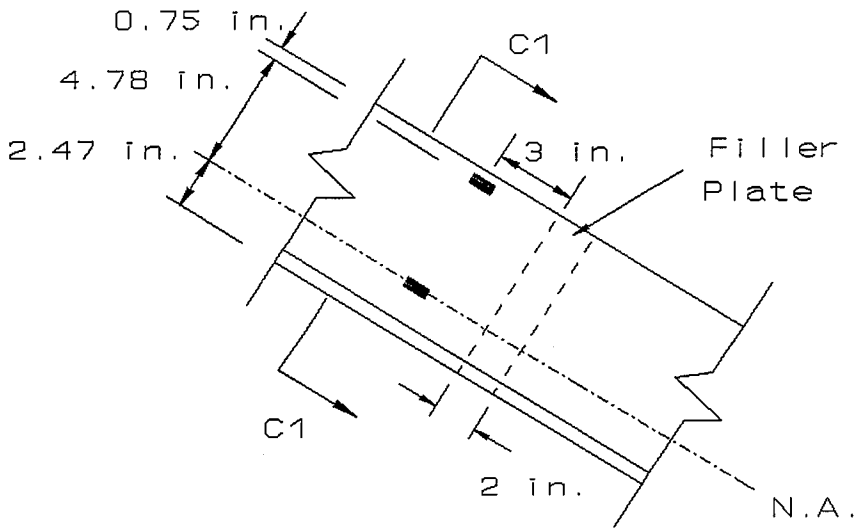

Figure 15. Gage Location Details for Members D2, D3, D4, and D5 (a) Detail C (See Figure 14); (b) Section C1-C1

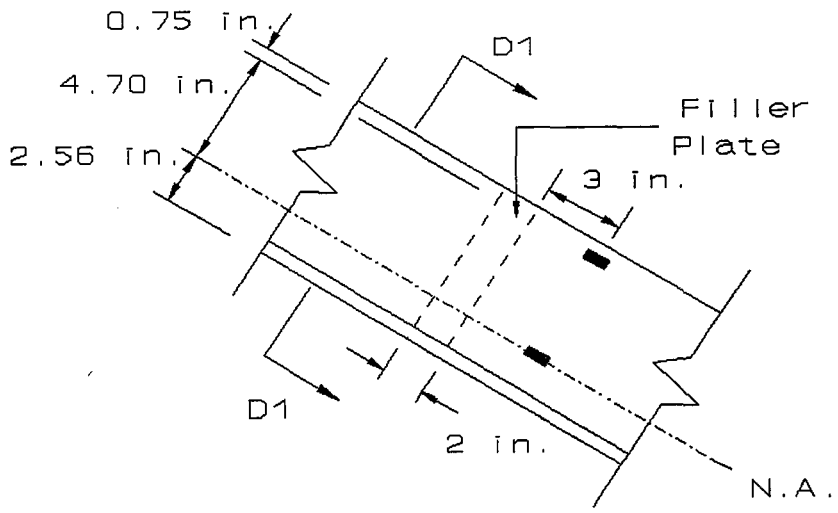

Figure 16. Gage Location Details for Members D1 and D6 (a) Detail D (See Figure 14); (b) Section B-B

plate edge and 3/4 inch from the top edge. The three gage positions enabled the top and bottom extreme fiber stresses at each end of the two outer diagonals to be calculated. The gage identification system for the diagonal members is similar to that of the bottom chord members. That is, gage D13 would refer to a gage on member D1 in position three. Figure 14 illustrated the identification system for all 14 gage positions on the diagonal members.

Tables 4 and 5 list the gage type, gage length, and gage factor for each gage installed at the quarter-span and mid-span test locations.

Strain Gage Installation

All strain gages described above were installed in the following manner. A hand held pencil bit grinder was first used to clear away rust. Next, a disk grinder, with 60 and 120 grit disks, was used to smooth the surface. Once the grinding was completed, the surface was hand sanded with 200 and 400 grit sand paper. Cross hairs representing the desired gage location were marked on the surface with a ball point pen. The surface was then degreased and cleaned with methyl ethyl ketone (MEK) and gauze pads.

After the mounting surface was prepared, the strain gage was cleaned with MEK and taped to a clean aluminum plate using cellophane tape. The gage and tape were then transferred from the aluminum plate to the appropriate mounting location. By adjusting the tape, the gage was aligned with the location marks (cross-hairs) and glued to the steel using Permabond 910 adhesive manufactured by BLH Electronics, Inc. After the adhesive dried, the tape was peeled off and the gage area was cleaned with freon purge. The gage was temporarily protected with drafting tape. Afterwards, connection wires were soldered to the gage wires and then connected to cinch connectors. Finally, the gage was

Table 4. Gages Installed on Diagonal Members

GAGE NO.[a]	D1	D12	D13	D2	D22	D3	D32	D4	D42	D5	D52	D6	D62	D63
	1			1		1		1		1		1		
Floortruss 4 (Quarter-Span)														
GAGE TYPE	1[b]	1	1	2[c]	2	1	2	1	1	1	1	1	1	2
Floortruss 8 (Mid-Span)														
GAGE TYPE	1	1	1	2	2	2	2	2	2	2	2	2	2	2

[a]Gage Numbering defined in Figure 12.

[b]1 = FAE-25-12-S6EL, 1/4 inch gage length, gage factor = 2.02 +/- 0.5 %

[c]2 = EA-06-250BG-120, 1/4 inch gage length, gage factor = 2.075 +/- 0.5 %

Table 5. Gages Installed on Bottom Chord Members

GAGE NO.[a]	B11	B12	B21	B22	B23	B31	B32	B33	B41	B42	B43	B51	B52	B53	B61	B62
Floortruss 4 (Quarter-Span)																
GAGE TYPE	1[b]	1	1	3[d]	3	1	3	3	1	3	3	1	3	3	1	1
Floortruss 8 (Mid-Span)																
GAGE TYPE	1	1	1	1	1	1	1	1	1	1	1	1	1	1	2[c]	2

[a]Gage Numbering defined in Figure 9.

[b]1 = FAE-25-12-S6EL, 1/4 inch gage length, gage factor = 2.02 +/- 0.5 %

[c]2 = EA-06-250BG-120, 1/4 inch gage length, gage factor = 2.075 +/- 0.5 %

[d]3 = EA-06-125BT-120, 1/8 inch gage length, gage factor = 2.105 +/- 0.5 %

waterproofed with an adhesive backed neoprene pad. The entire instrumentation process for each test location was completed within four to five days.

DATA ACQUISITION

All field test data was collected with a MEGADAC 3008AC dynamic data acquisition system (Technical Manual 1991). The unit, manufactured by OPTIM Electronics Corporation, is capable of recording data from multiple channels at an overall rate of 25,000 samples per second. A recording rate of 400 samples per second was used in gathering field data for the project reported here. A 486-33 MHz personal computer equipped with a compatible software package (TCS3000) was used to drive the MEGADAC. Communication between the computer and data acquisition system was provided by an IEEE-488 interface. A maximum of thirty-two channels was utilized in the tests reported here. Thirty-two strain gage channels were provided through four screw terminal blocks (STBs) with eight channels each. The STBs enabled easy connection and disconnection of the strain gage cables to and from the acquisition system. All data was recorded and temporarily stored on the personal computer hard disk. The data was backed up onto DC 2120 mini data cartridge tapes at the end of each day.

Previous field testing experience indicated problems with the electronic equipment were likely when recording data under humid conditions. Therefore it was necessary to use an environmental chamber to protect the computer and data acquisition system from the heat and humidity common in the Mobile Delta. The resulting chamber, shown in Figure 17, provided protection against the harsh field conditions and could furthermore be broken down into two sections for easy transport under the bridge. The chamber included a 4500 BTU air conditioner to provide the environment necessary for proper operation of

Figure 17. Environmental Chamber

the equipment. The computer was mounted on a padded platform in the chamber which provided protection from harmful vibration.

All electrical equipment housed in the environmental chamber was powered by an eight horsepower portable AC generator. The generator was placed on the two foot wide inspection walkway (cat-walk) underneath the bridge approximately 100 feet from each test location. Placing the generator under the bridge allowed the bridge deck to be completely clear during testing so that normal traffic patterns were not affected.

CHAPTER FOUR

DATA COLLECTION AND REDUCTION

The field tests referred to in this report were performed during late August and early September of 1992. All testing was performed between the hours of 7:00 a.m. and 8:00 p.m. Monday through Friday. The entire testing operation for one location was completed within two weeks. Site preparation and instrumentation lasted four to five days, and the remaining time was used for data collection.

After a test site was completely instrumented, the data acquisition system was setup on the first platform area discussed in Chapter Three. Transducer cables were connected to cinch connectors at the gage locations and to STBs at the data acquisition system. Next, sample runs were performed to identify defective gages and short circuits which would warrant repair. The sample run consisted of recording one or more truck crossings selected at random from the traffic and observing the measured results of all the gages. The general behavior of the floortruss was also assessed at this time, and individual gage magnitudes were recorded to help identify possible future gage malfunctions.

Initially, test data was collected using trucks of known weights and lane positions. These type of tests, performed under controlled conditions, were referred to as calibration tests. Next, data was collected under uncontrolled or random traffic conditions for trucks

of unknown weight traveling in the normal traffic stream. Data recorded in this manner was referred to as random truck data.

CALIBRATION TESTS

The calibration tests were performed to allow the structural response of the floortrusses to be investigated under known static and dynamic loading conditions. The test for each location lasted approximately three hours. Two different test trucks, one with three axles and one with five axles, were used to induce the loadings during these tests. A sand spreader and a lowboy were used as the 3-axle and 5-axle trucks, respectively. The sand spreader truck is very similar to a dump truck. Both trucks and drivers were supplied by the AHD. Axle dimensions for each truck and the variables that identify each axle are shown in Figure 18. The test trucks were loaded and weighed on AHD scales prior to each calibration test. Tables 6 and 7 list the axle weights of each truck for the two calibration tests.

To provide comparisons of stresses in member D1 to member D6, member D2 to member D5, and so on, a symmetrical loading condition was desirable. However, the existing lanes on the bridges (two traffic lanes and one emergency lane) were not symmetrical. An additional fictitious lane that was symmetrical to the fast lane was used for some calibration tests to produce symmetric loading. Figure 19 illustrates the three different lane positions utilized. The three lanes were called lanes A, B, and C. The fictitious lane was referred to as lane A. Lanes B and C were the slow and fast lanes, respectively. All of the lanes were physically identified on the deck with spray paint. Sprayed dashed lines, running the length of the span, located the wheel positions for the three lanes.

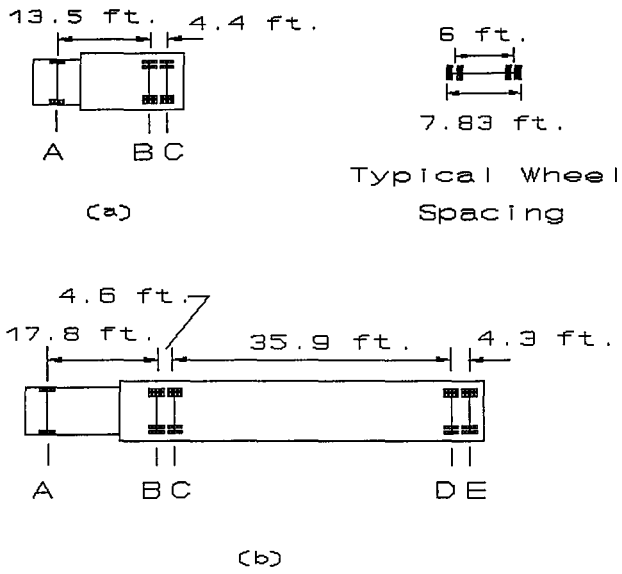

Figure 18. Plan View of Trucks Used for Calibration Tests (a) 3-Axle; (b) 5-Axle

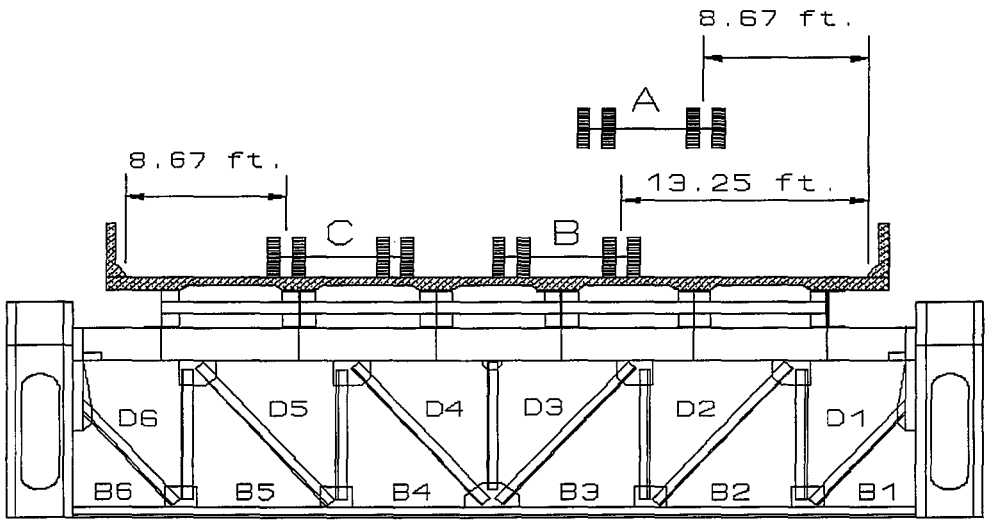

Figure 19. Test Lanes A, B, and C Used for Calibration Tests

Table 6. Calibration Truck Weights for Quarter-Span Test Location

Truck	Side[a]	Axle A (lbs)	Axle B (lbs)	Axle C (lbs)	Axle D (lbs)	Axle E (lbs)	Total (lbs)	Legal (lbs)
3-Axle	L	4,400	6,700	6,800	-----	-----		
	R	4,800	7,600	7,200	-----	-----	37,500	60,000
5-Axle	L	4,500	8,700	8,600	9,700	10,200		
	R	4,700	8,200	8,100	10,200	9,900	82,800	80,000

[a]L = Left (driver's) Side; R = Right Side

Table 7. Calibration Truck Weights for Mid-Span Test Location

Truck	Side[a]	Axle A (lbs)	Axle B (lbs)	Axle C (lbs)	Axle D (lbs)	Axle E (lbs)	Total (lbs)	Legal (lbs)
3-Axle	L	4,400	6,700	6,800	-----	-----		
	R	4,800	7,600	7,200	-----	-----	37,500	60,000
5-Axle	L	4,700	8,300	8,400	10,200	10,000		
	R	4,400	7,700	7,800	10,200	9,500	81,200	80,000

[a]L = Left (driver's) Side; R = Right Side

During the calibration tests, traffic control was provided by the AHD. At least one lane remained open to traffic at all times. Table 8 shows a typical sequence of events for a calibration test.

Four basic operations were performed during the calibration tests. These operations included balance intervals, static tests, crawl runs, and fast runs. The balance data consisted of recording measurements over a short duration of time (2 seconds) with no vehicular activity on the continuous span. The purpose here was to establish a zero live load state.

The second type of calibration operation was the static test. These tests consisted of parking the test truck in positions P1 through P7 shown in Figure 20 and recording data for approximately 2 seconds while no vehicular traffic was on the arch span. The 5-axle truck was positioned by aligning the rear axle of the front tandem over the test position as shown in Figure 21. For the 3-axle truck, the front axle of the rear tandem was aligned over the test position. Static tests were performed at all seven positions in each test lane.

The purpose of the crawl and fast runs was to determine the response at the test locations under dynamic loading. Crawl runs were made in lanes B and C. During these crawl runs, test trucks maintained a 15 mph speed over the full length of the tied arch span. Slower speeds were desirable but not possible because of the relatively long period of time required for the calibration truck to cross the span. Since one lane was open to traffic at all times, it was not possible to find long time periods when other vehicles would not cross the span with the test truck. For fast runs, the trucks were driven at normal traffic speeds, usually between 55 and 70 mile per hour. Each truck made two or three fast runs in lanes B and C. Fast runs were not made in lane A because of safety considerations.

Table 8. Typical Event Sequence for Calibration Tests

Event	Truck	Lane	Traffic Control
Balance	------	-	Lane C Open
Crawl	3-Axle	A	Lane C Open
Static	3-Axle	A	Lane C Open
Crawl	3-Axle	B	Lane C Open
Static	3-Axle	B	Lane C Open
Balance	------	-	Lane C Open
Crawl	5-Axle	A	Lane C Open
Static	5-Axle	A	Lane C Open
Crawl	5-Axle	B	Lane C Open
Static	5-Axle	B	Lane C Open
Balance	------	-	Lane C Open
Balance	------	-	Lane B Open
Crawl	3-Axle	C	Lane B Open
Static	3-Axle	C	Lane B Open
Balance	------	-	Lane B Open
Crawl	5-Axle	C	Lane B Open
Static	5-Axle	C	Lane B Open
Balance	------	-	Lane B Open
Fast Run	3-Axle	B	No Traffic Control
Fast Run	5-Axle	B	No Traffic Control
Fast Run	3-Axle	B	No Traffic Control
Fast Run	5-Axle	B	No Traffic Control
Fast Run	3-Axle	C	No Traffic Control
Fast Run	5-Axle	C	No Traffic Control
Fast Run	3-Axle	C	No Traffic Control
Fast Run	5-Axle	C	No Traffic Control

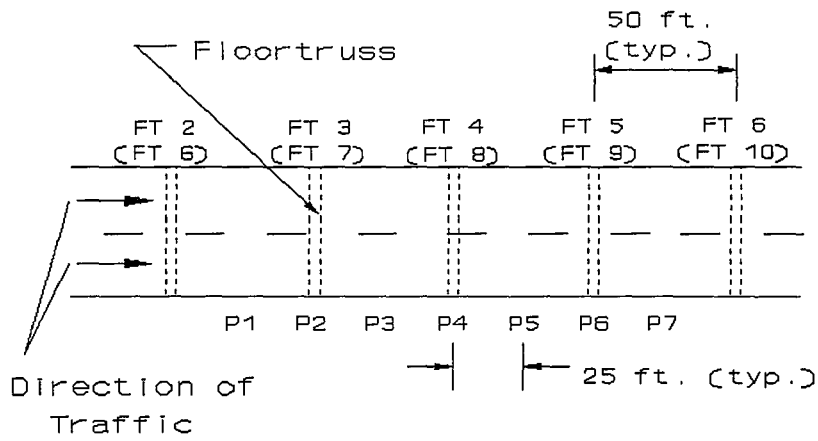

Figure 20. Plan View of Southbound Lanes with Static Calibration Truck Positions P1 through P7

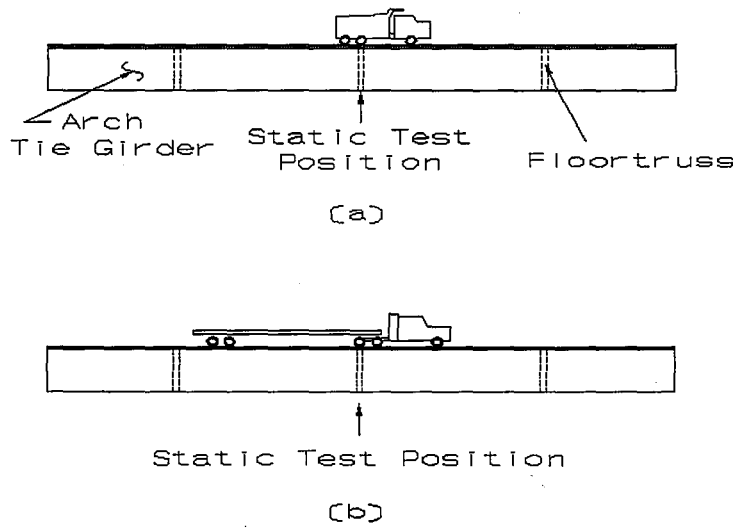

Figure 21. Alignment of Test Trucks for Static Tests (a) 3-Axle Truck; (b) 5-Axle Truck

RANDOM TRUCK TESTS

While the calibration tests provided data for known truck weights and positions, random tests allowed for observation of stresses in the floortrusses under normal traffic loading. The random truck data was used to calculate an effective constant amplitude stress range, or effective stress range, at each critical location. Effective stress ranges are explained in detail later in this chapter. In order to calculate these stress ranges accurately, 250 random trucks were recorded at each test location.

During the random tests there was no traffic control on the roadway and all data acquisition equipment was situated underneath the bridge. These actions were taken to ensure that the speeds and lane positions of the random trucks followed the normal traffic patterns. At least one person was positioned under the bridge at all times to monitor the equipment during testing.

A self triggering procedure was used to activate the data recording process during random truck testing. The data acquisition system continuously scanned a selected gage for strains that exceeded a prescribed limit. Data that was scanned in the time period of 4 seconds before and 8 seconds after the limit was exceeded was recorded. The resulting record was approximately twelve seconds in length with the majority of the truck response occurring between 4 and 8 seconds. Because truck crossings were the only data of interest, the gage limits were defined so as to prevent electronic noise and strains from light vehicles from triggering the system. Typically, a vehicle producing a maximum strain larger than 25 microstrain (0.7 ksi) in a number one gage on member D2 was required to activate the system. Approximately seven to eight hours was required to collect 250 truck crossing at each test location.

DATA REDUCTION

Data collected during a random or calibration test was initially stored on the hard disk of the computer which controlled the data acquisition system. After the test was complete, the data was transferred to mini data cartridge tapes and then erased from the hard disk to make room for more test data. Each of these tapes can store up to 120 mega bytes of data. A random test and calibration test at one location could be stored on two tapes.

The actual data reduction process did not begin until all field testing was complete and the data acquisition equipment was transported back to Auburn University. The test data stored on the mini cartridge tapes was copied onto the hard disks of several 386 and 486 personal computers, each of which was equipped with the TCS3000 software.

Strain ranges were determined from raw data from the random tests and fast run calibration tests. These strain ranges were found from records of strain versus time by using a peak-to-peak method. A typical strain range is illustrated in Figure 22. The reasoning behind the selection of this method was discussed in Volume I (Stallings et al. 1993). In the peak-to-peak method, a strain range is defined as the absolute difference between the maximum and minimum strain values. Each truck crossing created one strain range. Transform equations incorporated directly into TCS3000 calculated the maximum , minimum, and strain range values for each truck crossing. These values were read directly from the digital monitors portion of TCS3000. Strain versus time plots for selected gages and truck crossings were viewed in order to verify the integrity of the data and behavior of the floortrusses. Stress ranges were then obtained by multiplying the strain ranges by the modulus of elasticity for steel of 29,000 ksi.

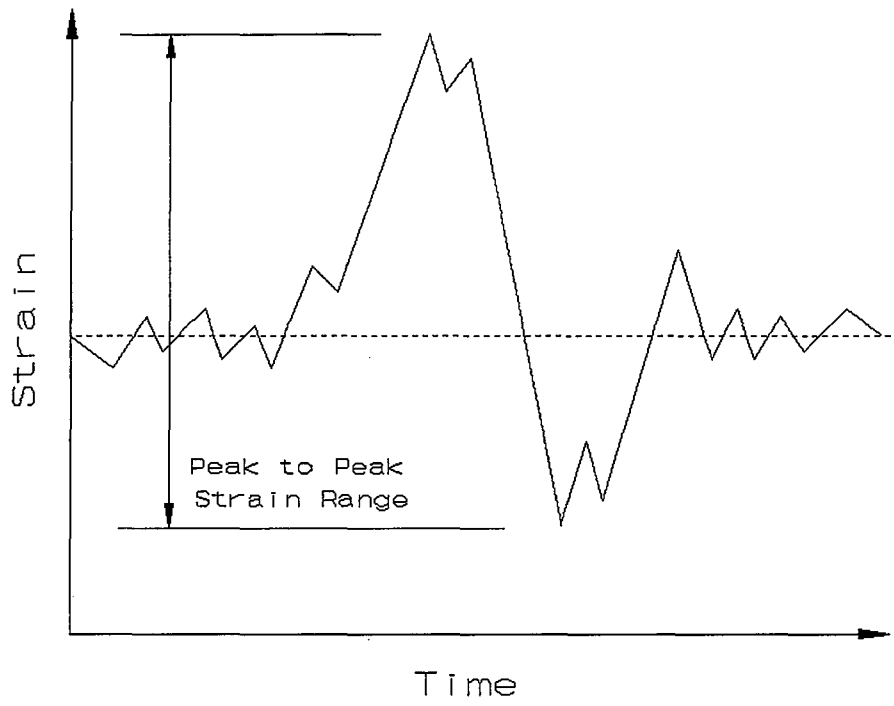

Figure 22. Illustration of Peak to Peak Method

In order to find strains due to static loading, transform equations were used to average the strain readings of the balance intervals and static tests. The static strains were averaged from each scan of the 100 scans recorded per second for approximately two seconds for each test. Balance intervals taken in sequence with the static tests were averaged for comparison with the static values. Since the balance and static measurements should result in a constant value, the accuracy of the measurements was enhanced by the averaging process, which eliminated any random stationary electronic noise. The strain value for a particular gage due to static loading was determined by finding the difference between the strain recorded during the static test and the strain recorded during the balance test. Like the random and fast run data, strains due to static loading were multiplied by 29,000 ksi to obtain stress values.

EFFECTIVE STRESS RANGE

A primary goal of reducing the variable amplitude data gathered in the field tests reported here was to determine effective stress ranges (equivalent constant amplitude stress ranges) at critical locations.

The equivalent constant amplitude stress range can be calculated from variable amplitude stress range data by the root-mean-square method (RMS) and Miner's effective stress range, also called the root-mean-cubed method (RMC). Both of these methods can be represented by

$$S_r = \left[\sum_{i=1}^{k} \frac{\left(n_i \; S_{ri}^{b}\right)}{N} \right]^{\frac{1}{b}} \qquad (1)$$

where k is the total number of stress ranges; i is the current stress range; n_i is the number of stress cycles at the ith stress range, S_{ri}; and N is the total number of cycles. The

method that the above equation represents is indicated by the value of b. That is, for Miner's effective stress range, b is related to the slope of a log-log plot for constant amplitude fatigue life data and is usually given a value of 3. The root-mean-square method uses a value of 2 for b.

Both methods have shown good correlation with experimental data (Fisher 1978, Yamada and Albrecht 1976, Fisher et al. 1989). Miner's effective stress range tends to give a larger result than the root-mean-square method (Fisher et al. 1989). Miner's method is also more theoretically based (Yamada and Albrecht 1976). The root-mean-square method has been reported to show slightly better correlation to test data but results in a less conservative value (Fisher et al. 1989). Both methods have been widely used to calculate effective stress ranges. However, because the Miner's effective stress range produces a more conservative estimate than the RMS method, it is more commonly used for making bridge fatigue life estimates. All effective stress ranges calculated for this project were Miner's effective stress ranges.

CHAPTER FIVE

TEST RESULTS AND ANALYSES

In general, the goal of the field tests was to gain an understanding of the behavior of the floortrusses at the arch span in order to make an accurate prediction about the severity and future behavior of existing filler plate weld cracks. This goal was accomplished with static tests, where test trucks were stopped on the span, and dynamic tests, where tests trucks crossed the span at normal traffic speeds. Stresses were measured at the neutral axis and extreme fibers of floortruss tension members. These measurements indicated that the most critical members were the four outer diagonals. The maximum extreme fiber stress range was approximately 20 percent higher than the axial stress range in these members. The most critical extreme fiber location on any of the members tested was on the bottom of member D2 nearest the filler plate on the upper end at floortrusses 4 and 8. The highest stress range found at these locations was 4.4 ksi.

STATIC TEST RESULTS

Plots of axial stress versus truck position resulting from the static calibration tests are shown in Figures 23 through 38. Plots are shown for members D1, D2, D5, and D6 with the 3-axle and 5-axle test trucks being parked in the slow lane and in the fast lane. As illustrated in Figure 20 in Chapter Four, the truck positions 1 through 7 were spaced

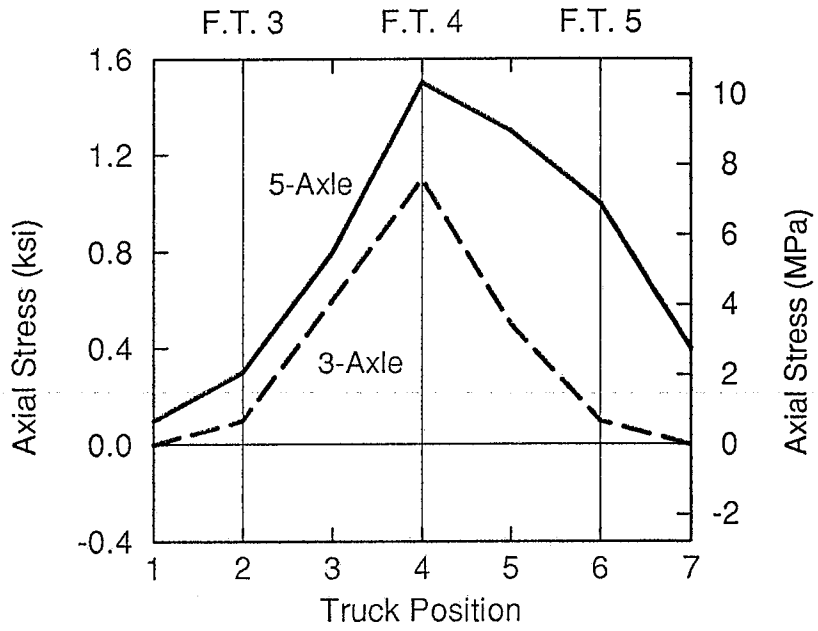

Figure 23. Axial Stress in Member D1 of Floortruss 4 with Test Trucks in Slow Lane

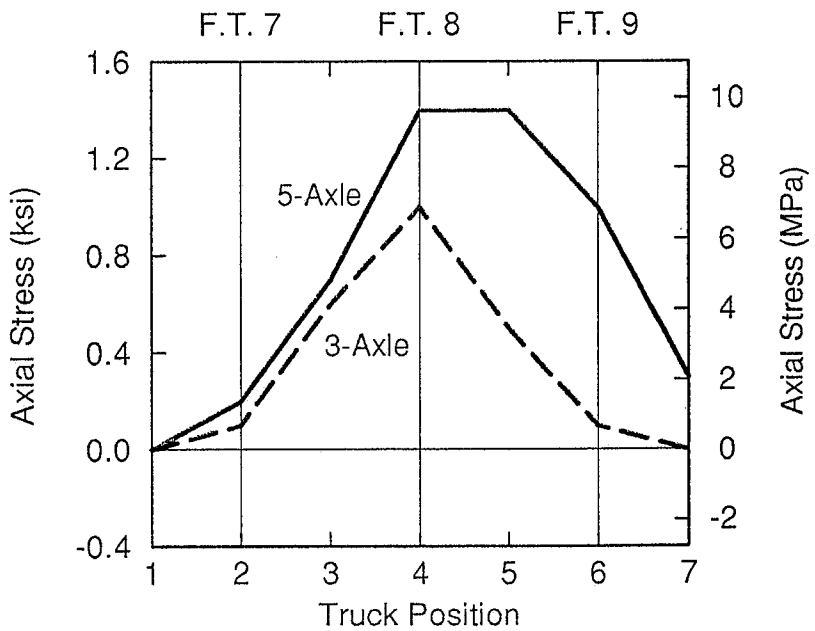

Figure 24. Axial Stress in Member D1 of Floortruss 8 with Test Trucks in Slow Lane

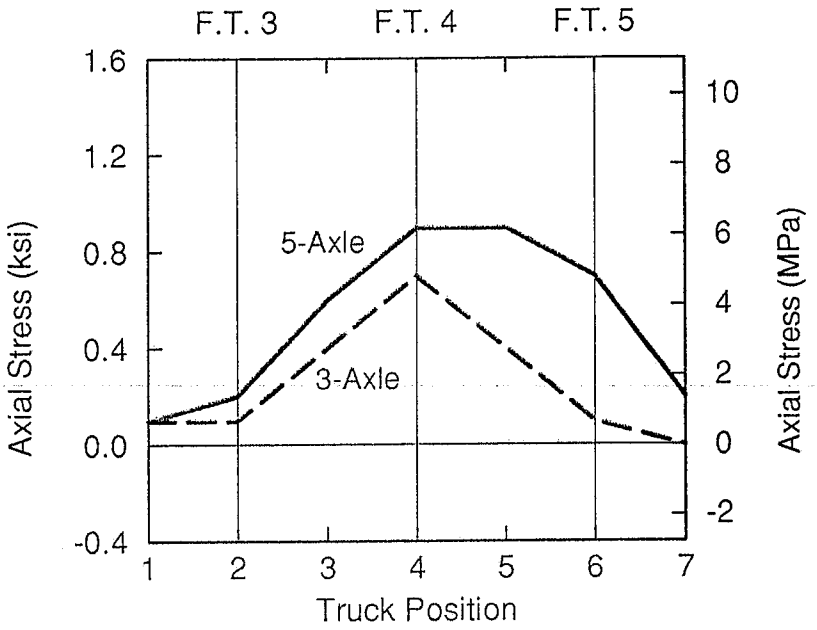

Figure 25. Axial Stress in Member D1 of Floortruss 4 with Test Trucks in Fast Lane

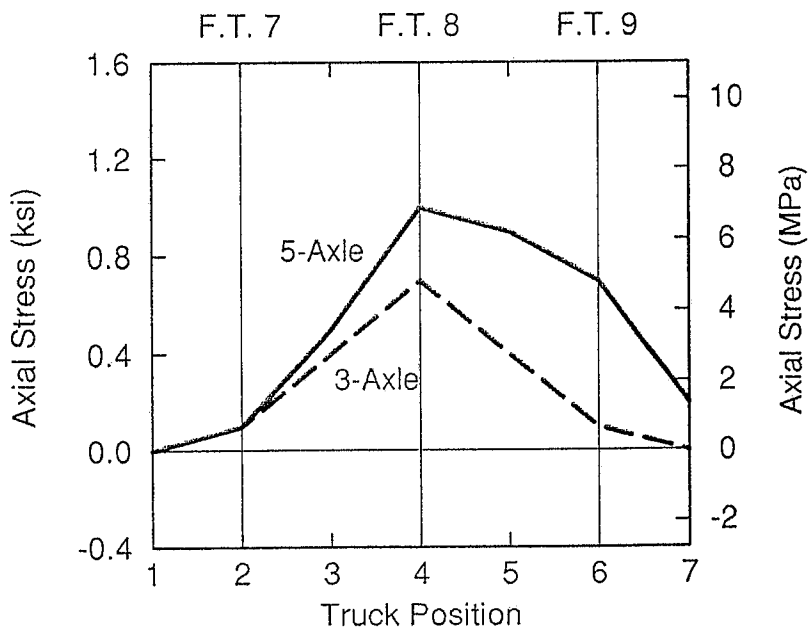

Figure 26. Axial Stress in Member D1 of Floortruss 8 with Test Trucks in Fast Lane

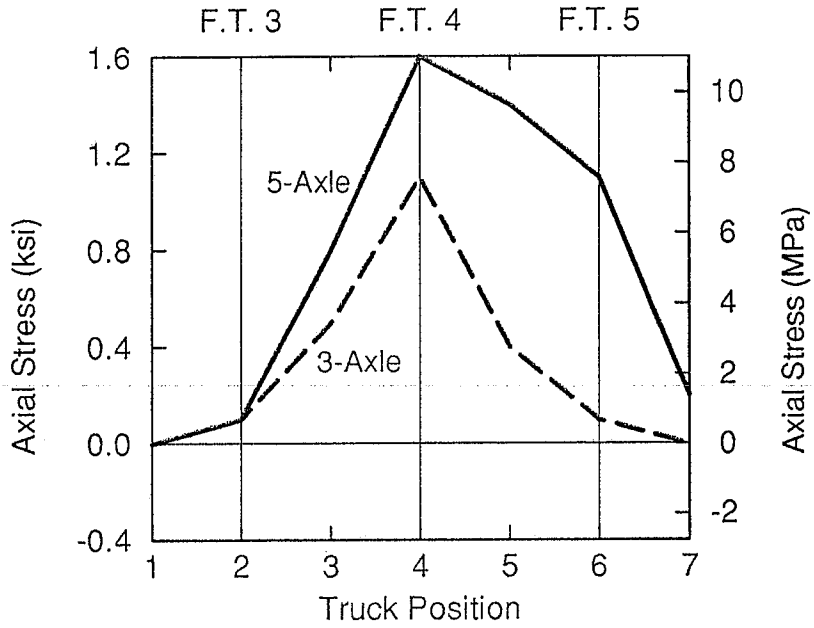

Figure 27. Axial Stress in Member D2 of Floortruss 4 with Test Trucks in Slow Lane

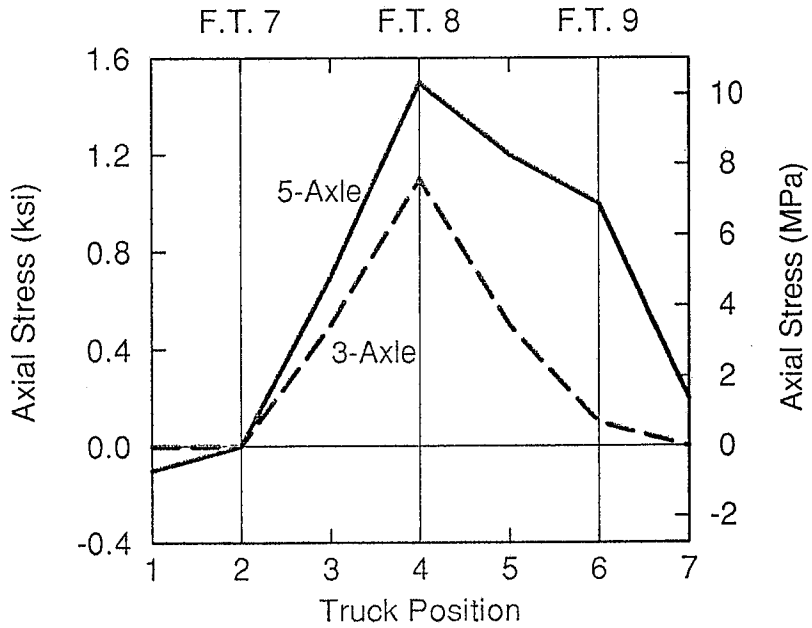

Figure 28. Axial Stress in Member D2 of Floortruss 8 with Test Trucks in Slow Lane

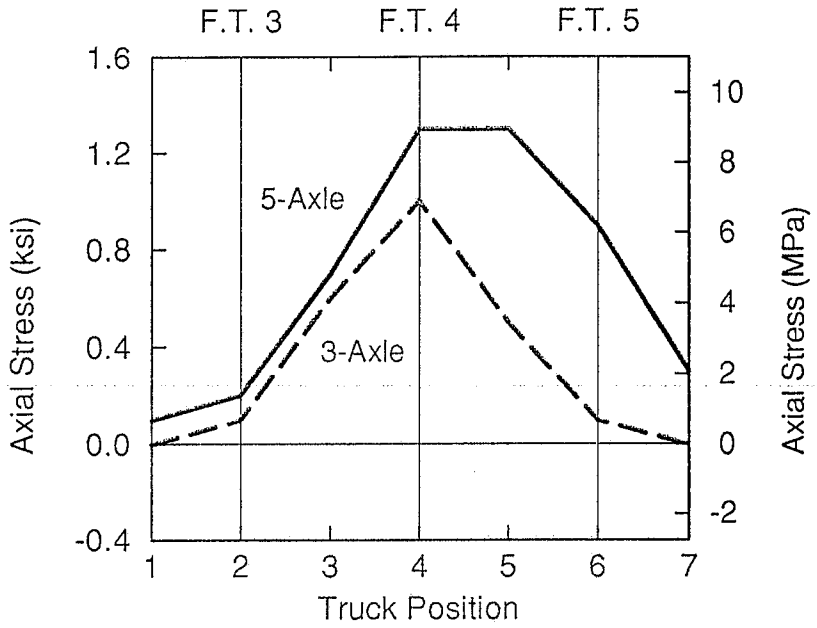

Figure 29. Axial Stress in Member D2 of Floortruss 4 with Test Trucks in Fast Lane

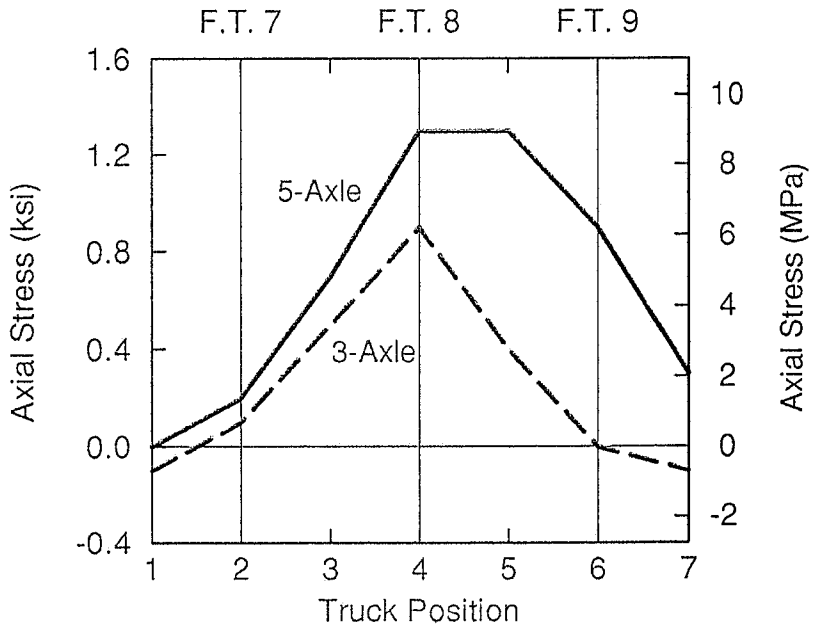

Figure 30. Axial Stress in Member D2 of Floortruss 8 with Test Trucks in Fast Lane

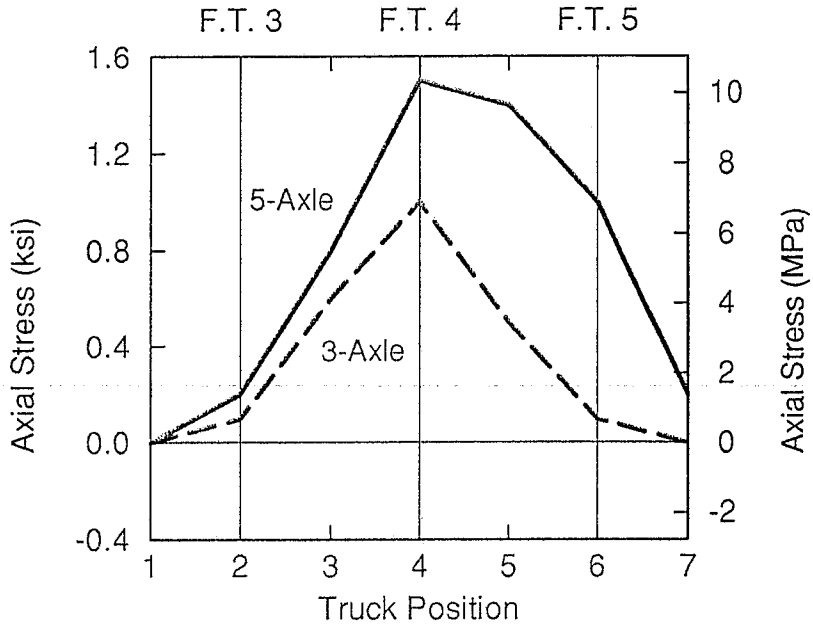

Figure 31. Axial Stress in Member D5 of Floortruss 4 with Test Trucks in Slow Lane

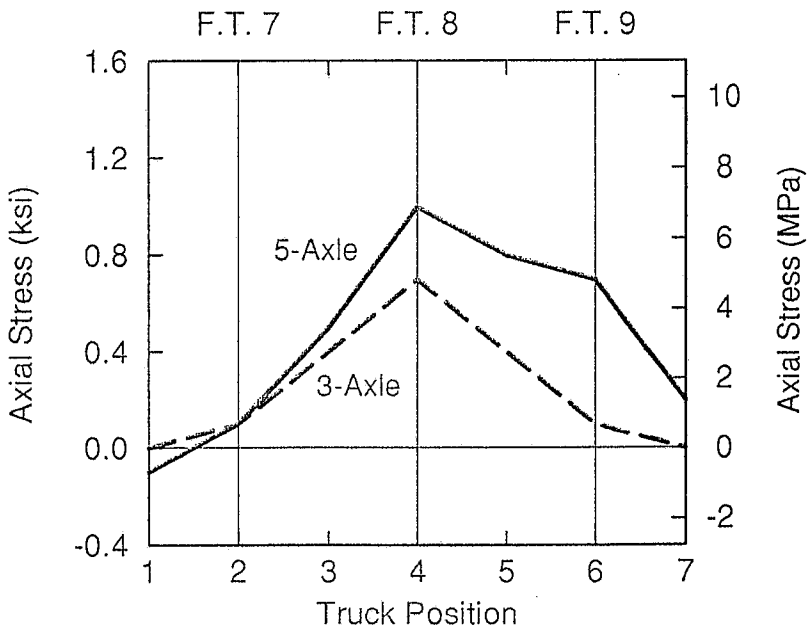

Figure 32. Axial Stress in Member D5 of Floortruss 8 with Test Trucks in Slow Lane

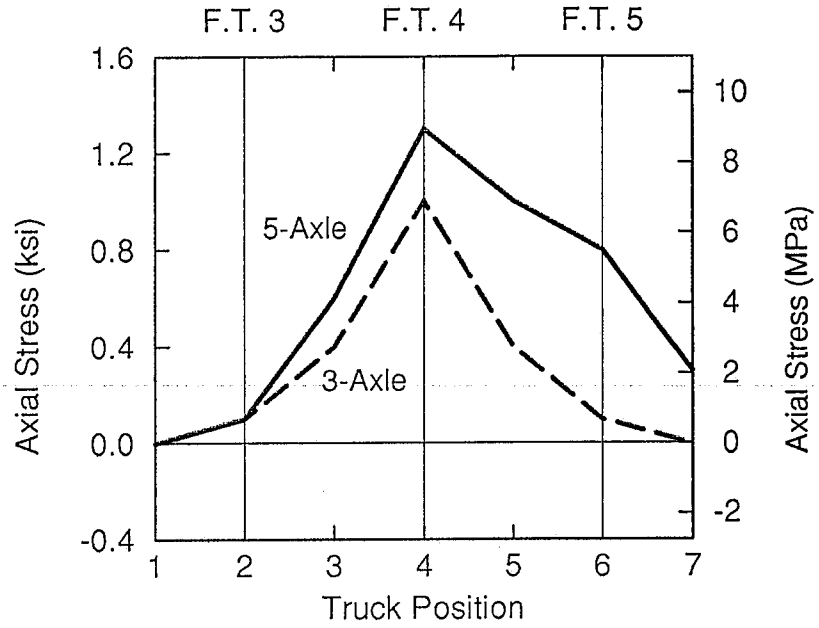

Figure 33. Axial Stress in Member D5 of Floortruss 4 with Test Trucks in Fast Lane

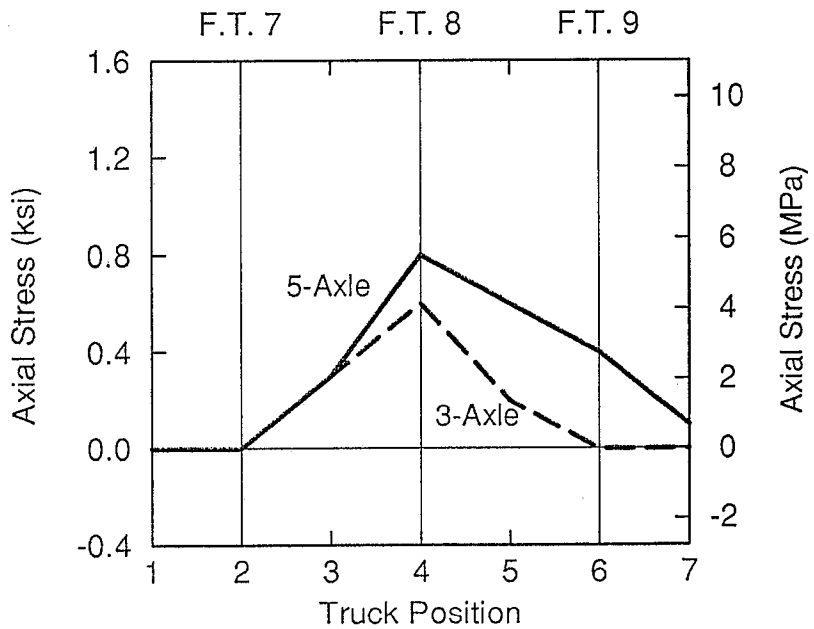

Figure 34. Axial Stress in Member D5 of Floortruss 8 with Test Trucks in Fast Lane

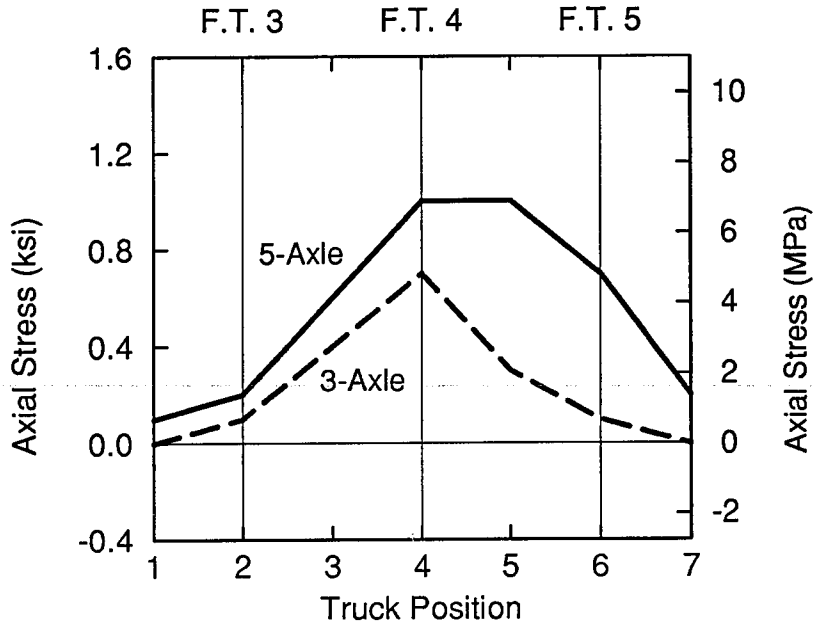

Figure 35. Axial Stress in Member D6 of Floortruss 4 with Test Trucks in Slow Lane

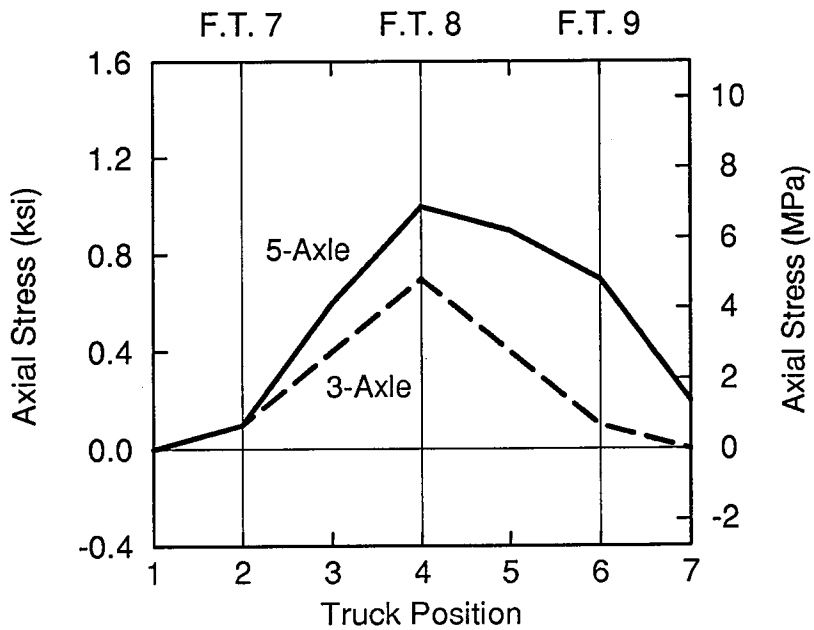

Figure 36. Axial Stress in Member D6 of Floortruss 8 with Test Trucks in Slow Lane

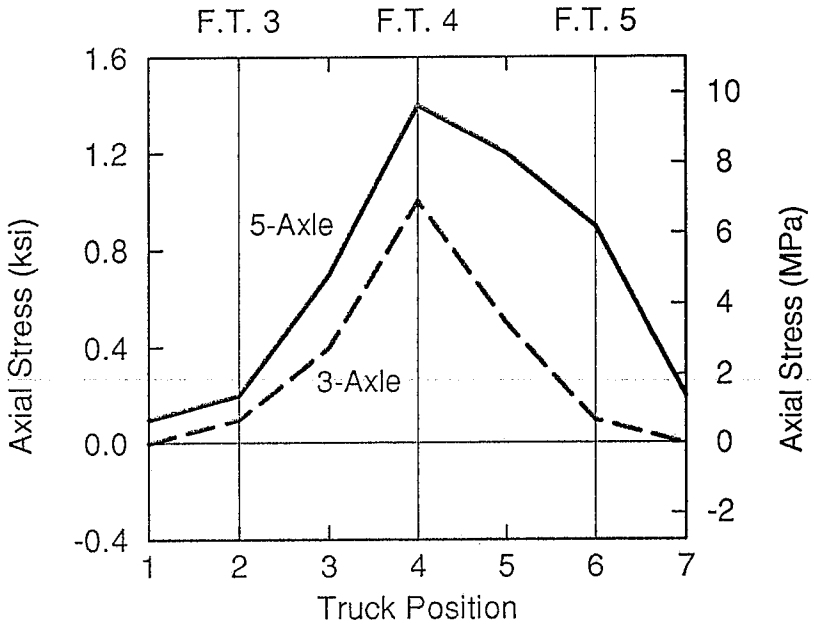

Figure 37. Axial Stress in Member D6 of Floortruss 4 with Test Trucks in Fast Lane

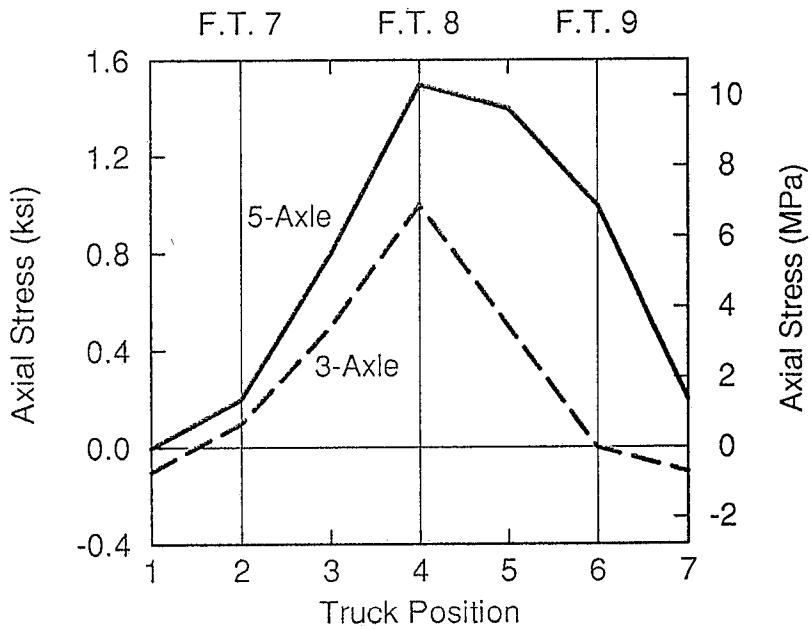

Figure 38. Axial Stress in Member D6 of Floortruss 8 with Test Trucks in Fast Lane

evenly at 25 ft. intervals along the bridge. A test truck parked directly over a gaged floortruss would be located at position 4.

The largest axial stresses in members D1, D2, and D6 due to static loading occurred when the test trucks were parked over the side of the floortruss on which the members were located. That is, test trucks parked in the slow lane produced the greatest stresses in members D1 and D2, and test trucks parked in the fast lane produced the largest stresses in member D6. However, the axial stress in member D5 was largest when the test trucks were parked in the slow lane. These results are logical considering the locations of the traffic lanes relative to the diagonals as shown in Figure 19 in Chapter Four.

The plots in Figures 23 through 38 involving the 3-axle truck rise to a single peak where the test truck is positioned over the gaged floortruss. These plots are characteristic of an influence line for a single concentrated load and results because the 3-axle truck is relatively short. The plots for the 5-axle truck are always above those for the 3-axle truck and tend to drop off slower for positions after position 4. The stresses due to the 5-axle truck are larger because the gross vehicle weight is larger. The plots fall off slowly because the truck is long and the rear axles of the trailer remain close to the instrumented floortruss for several positions after position 4.

The largest axial stress produced in any one member during a static test was 1.6 ksi. This stress was measured in member D2 at floortruss 4 when the 5-axle test truck was parked in the slow lane directly over floortruss 4 (Figure 27). The maximum static stresses measured for each of the outer diagonal members (D1, D2, D5, and D6) ranged from 0.6 ksi to 1.6 ksi.

Symmetry of Static Stresses

The geometry and member sizes of the floortrusses at the tied arch span are symmetric about the mid-span of the floortrusses. However, the slow and fast traffic lanes are not symmetric about the floortruss mid-span. In order to check the symmetry of the floortrusses, a fictitious lane was used. This lane, called lane A, was symmetric about the floortruss mid-span with the fast lane (lane C) as discussed and illustrated in Figure 19 in Chapter Four.

Table 9 lists the axial stresses in members D1, D2, D5, D6, B3, and B4 due to the test trucks being parked directly over the gaged floortruss. If symmetry holds, then for symmetric loadings the axial stresses in member D1 should equal those in member D6, member D2 stresses should equal member D5 stresses, and so on. For example, the axial stress in member D2 due to the 5-axle truck in Lane A was 1.3 ksi. The axial stress in member D5 due to the 5-axle truck in Lane C was also 1.3 ksi. The stresses listed in Table 9 for corresponding members, like D2 and D5, are the same or very close. Small differences in the stresses can be attributed to typical experimental error in the measurements, which is estimated to be approximately plus or minus 0.15 ksi (5 $\mu\epsilon$). Some differences may be due to a passing vehicle either entering or exiting the arch span during the static test. As mentioned earlier, the bridge was not closed to traffic during the static calibration tests. The only significant deviations from symmetry in the measured stresses were between members D2 and D5 of floortruss 8. The stresses measured in member D2 were typically 0.3 to 0.5 ksi higher than those in member D5. The reason for these differences is not known.

Another important point can be made about the overall symmetry of the measured stresses. To obtain results as in Table 9 provides confidence that the gage installations,

Table 9. Static Axial Stresses for Test Trucks Parked Directly Over the Gaged Floortruss

D6 (ksi)	D5 (ksi)	B4 (ksi)	B3 (ksi)	D2 (ksi)	D1 (ksi)
Floortruss 4 (Quarter-Span)					
5-Axle Truck in Lane C			5-Axle Truck in Lane A		
1.4	1.3	0.9	0.9	1.3	1.7
5-Axle Truck in Lane A			5-Axle Truck in Lane C		
1.0	1.5	0.2	0.2	1.3	0.9
3-Axle Truck in Lane C			3-Axle Truck in Lane A		
1.0	1.0	0.8	0.8	1.0	1.4
3-Axle Truck in Lane A			3-Axle Truck in Lane C		
0.7	1.0	0.2	0.3	1.0	0.7
Floortruss 8 (Mid-Span)					
5-Axle Truck in Lane C			5-Axle Truck in Lane A		
1.5	0.8	0.9	0.9	1.3	1.9
5-Axle Truck in Lane A			5-Axle Truck in Lane C		
1.0	1.0	0.3	0.3	1.3	0.9
3-Axle Truck in Lane C			3-Axle Truck in Lane A		
1.0	0.6	0.8	0.8	1.0	1.3
3-Axle Truck in Lane A			3-Axle Truck in Lane C		
0.8	0.8	0.3	0.3	0.9	0.7

wiring, data acquisition equipment, and data reduction processes were all operating properly.

DYNAMIC TEST RESULTS

As was the case with the static tests, the highest stresses due to dynamic loading were the four outer diagonal members and the two inner bottom chord members. Typical strain records for members D1, D2, and B3 are shown in Figures 39 through 41. These figures illustrate plots of microstrain at the neutral axis versus time for 3-axle and 5-axle test truck fast runs in the slow lane.

Several distinct patterns are evident from these strain records. For plots involving the short 3-axle test truck, the continuous data line for all three members in question had a single peak. For plots involving the longer 5-axle test truck, the continuous data lines contained two peaks. As pointed out in the Static Test Results section, the distance between the front and rear axles of the 3-axle test truck is so short that the truck acts similar to a point load, thus producing a single peak. The two peaks present in strain records produced by the 5-axle truck are due to the front and rear tandem of wheels crossing the instrumented floortruss.

Another observation is the amount of sign reversal in strains as the test truck crosses the arch span. For members D1 and D2 at floortrusses 4 and 8 subjected to the 3-axle truck (Figures 39a, 39b, 40a, and 40b), the strain values are essentially all tensile. For the same members subjected to the 5-axle truck (Figure 39c, 39d, 40c, and 40d), there is a change in sign at floortruss 4 after the truck crosses the instrumented floortruss. Figures 39c and 40c show the continuous data lines approaching (-10) microstrain between 8 and 10 seconds. Strain ranges for these type of plots would equal the

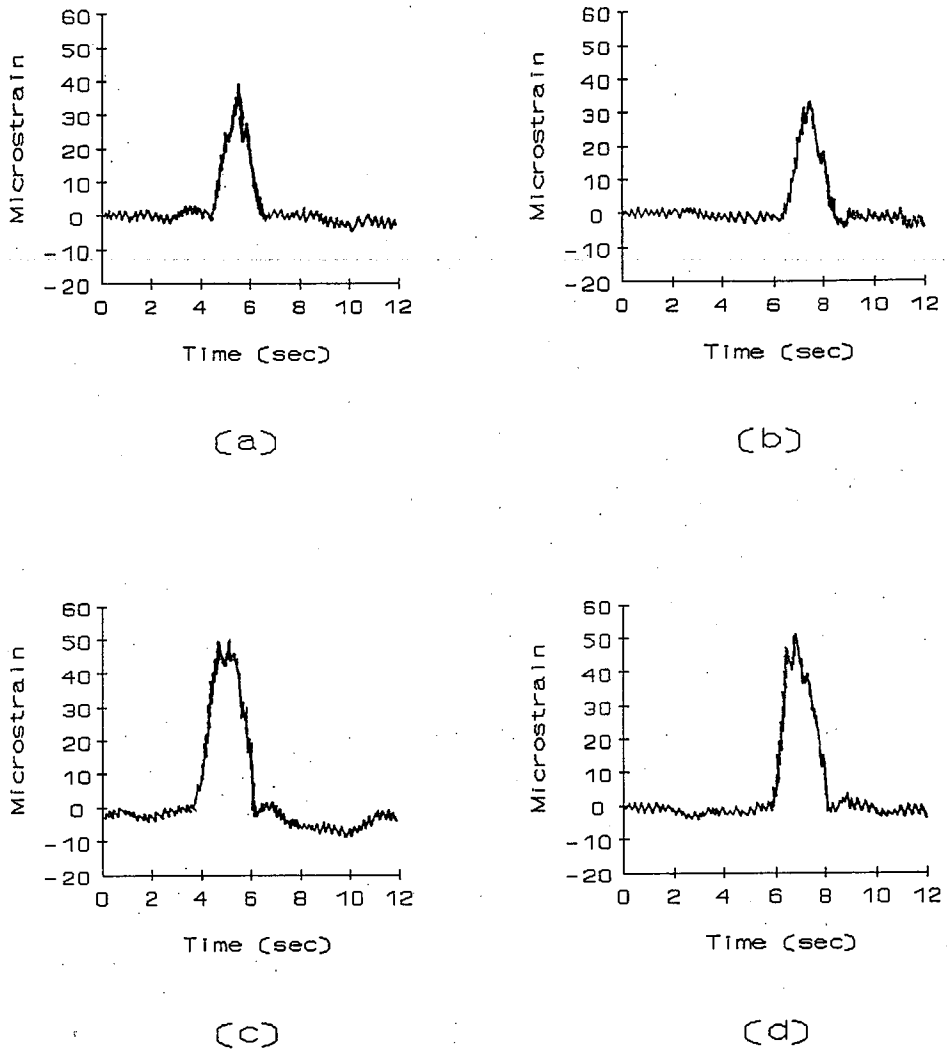

Figure 39. Typical Axial Strain Records for Member D1 Due to Test Truck Fast Runs in the Slow Lane: (a) 3-Axle at Floortruss 4; (b) 3-Axle at Floortruss 8; (c) 5-Axle at Floortruss 4; (d) 5-Axle at Floortruss 8

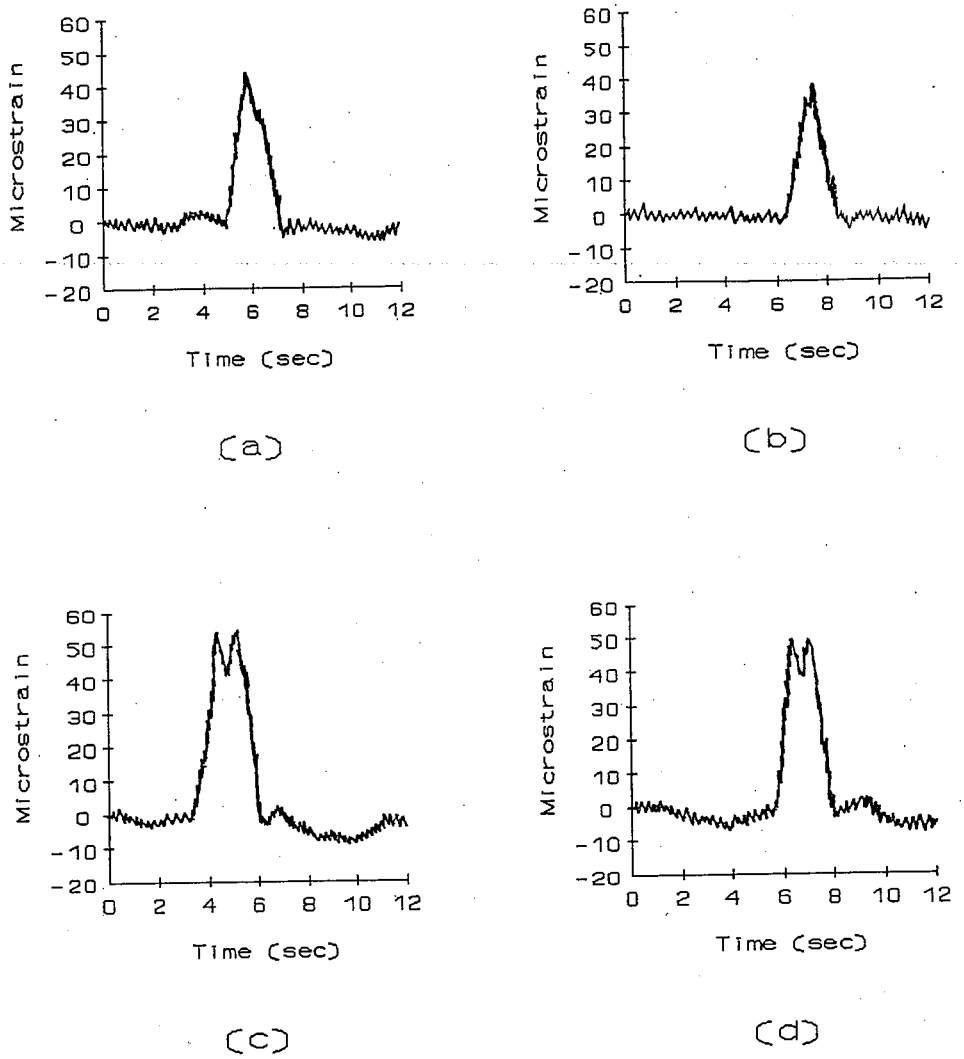

Figure 40. Typical Axial Strain Records for Member D2 Due to Test Truck Fast Runs in the Slow Lane: (a) 3-Axle at Floortruss 4; (b) 3-Axle at Floortruss 8; (c) 5-Axle at Floortruss 4; (d) 5-Axle at Floortruss 8

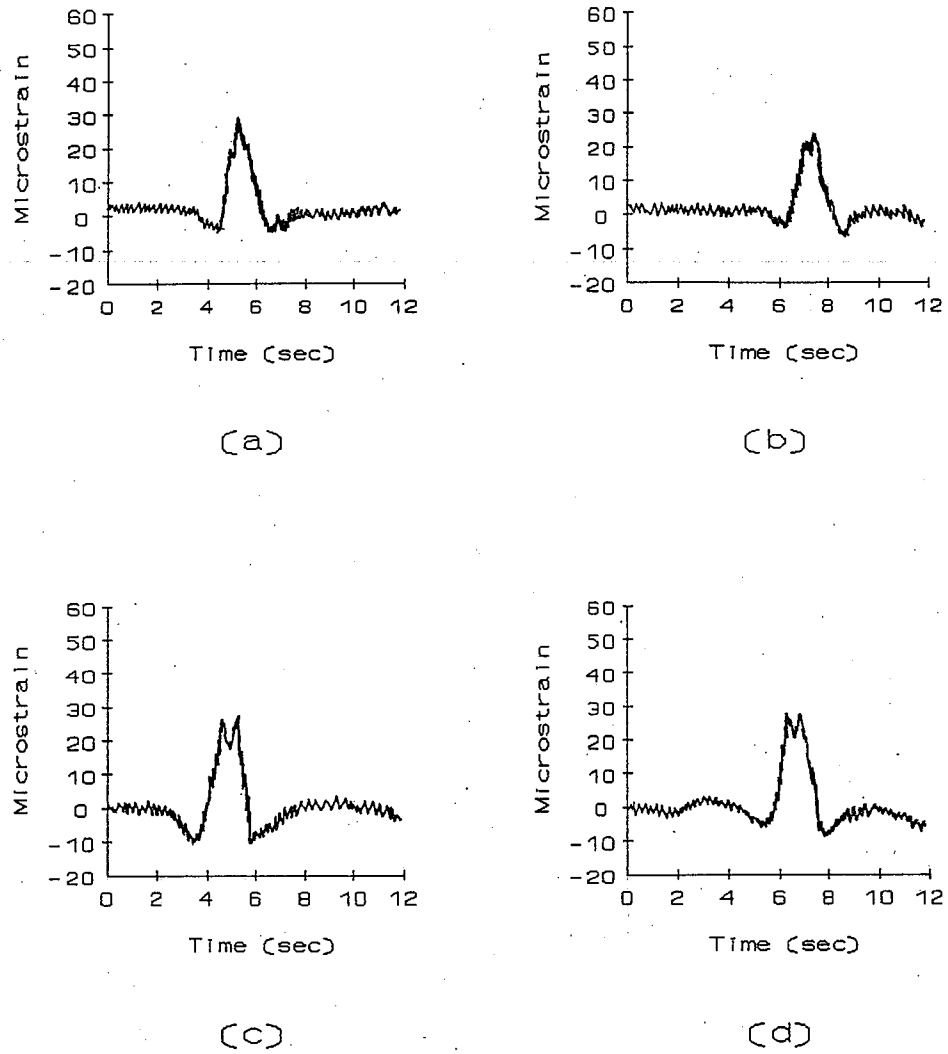

Figure 41. Typical Axial Strain Records for Member B3 Due to Test Truck Fast Runs in the Slow Lane: (a) 3-Axle at Floortruss 4; (b) 3-Axle at Floortruss 8; (c) 5-Axle at Floortruss 4; (d) 5-Axle at Floortruss 8

difference between the maximum microstrain and minimum microstrain, as was illustrated in Figure 22 in Chapter Four. As will be shown throughout this chapter, dynamic stress ranges found at floortruss 4 were consistently higher than those found at floortruss 8. Part of this difference in the outer diagonals is due to the increase in stress range because of the compressive stresses present after a truck passes floortruss 4. Later in this chapter, measured stresses are compared to stresses calculated from a structural analysis computer program. For this comparison, any compressive strain values present after the truck passes the instrumented floortruss are ignored. That is, maximum stresses, not stress ranges, from the field tests are compared to the calculated dynamic stresses.

For member B3 at floortrusses 4 and 8 subjected to the 3-axle and 5-axle test trucks (Figure 41), compressive strains were present immediately before and after the truck crossed the instrumented floortruss. The largest sign reversal of axial strain in member B3 was found at floortruss 4 due to dynamic loading from the 5-axle test truck (Figure 41c).

Strain records like the ones discussed above were use to determine strain ranges, which were converted to stress ranges. Figures 42 through 45 illustrate the relative magnitudes of the axial stress ranges in the floortruss members when a truck crosses the arch span. Axial stress ranges produced by the 5-axle and 3-axle test truck traveling in the slow lane and the fast lane at floortrusses 4 and 8 are shown. Regardless of what lane the truck was in, the four outer diagonals exhibited the highest stress ranges. Of the bottom chord members, B3 and B4 were the only members that were consistently in tension. However, the axial stress range magnitudes of these two members were generally lower than the lowest axial stress ranges of any of the four outer diagonals. The outer bottom chord members (B1, B2, B5, and B6) exhibited tensile and compressive

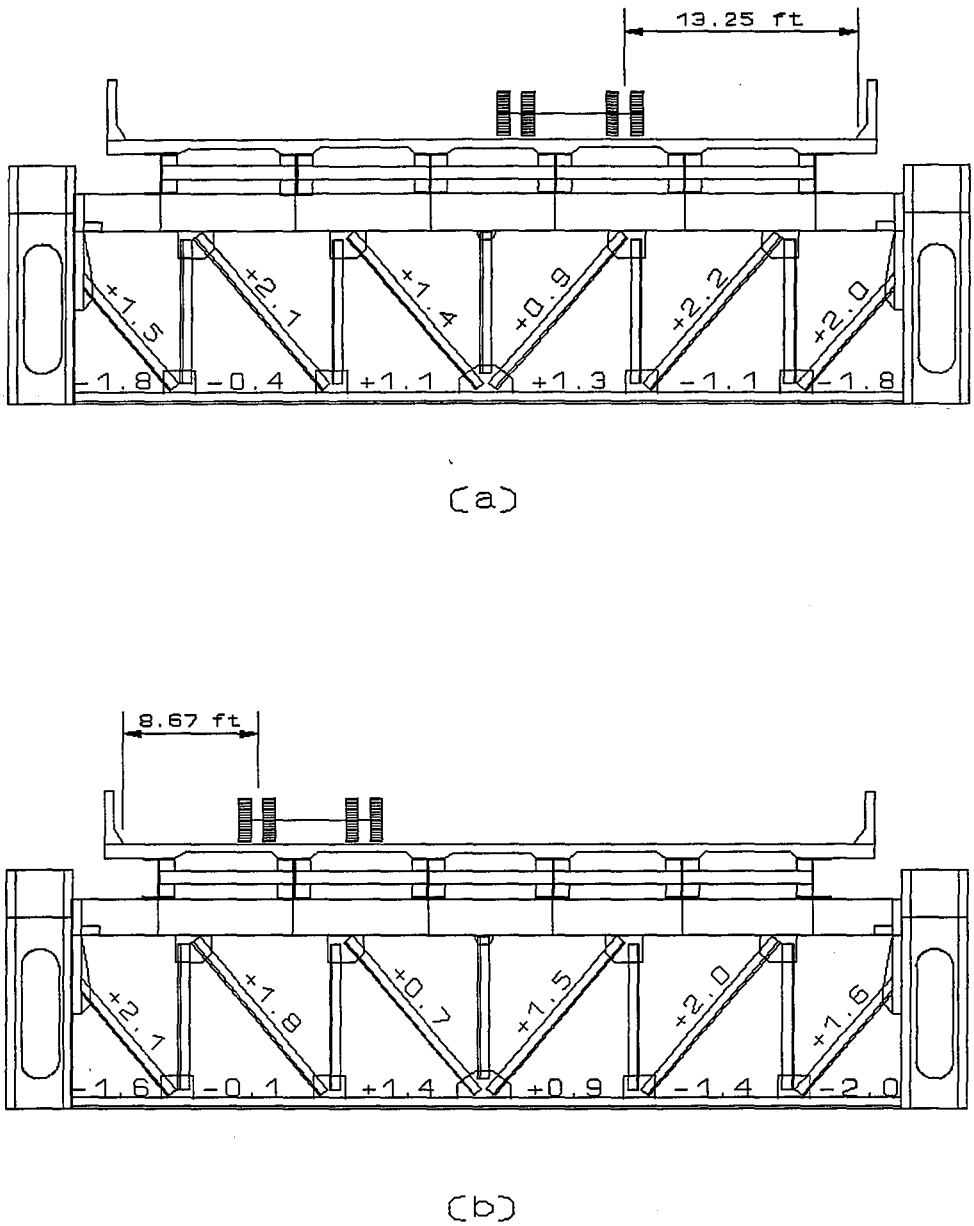

Figure 42. Axial Stress Ranges (ksi) in Floortruss 4 Due to 5-Axle Test Truck: (a) Truck in Slow Lane at 53 mph; (b) Truck in Fast Lane at 53 mph

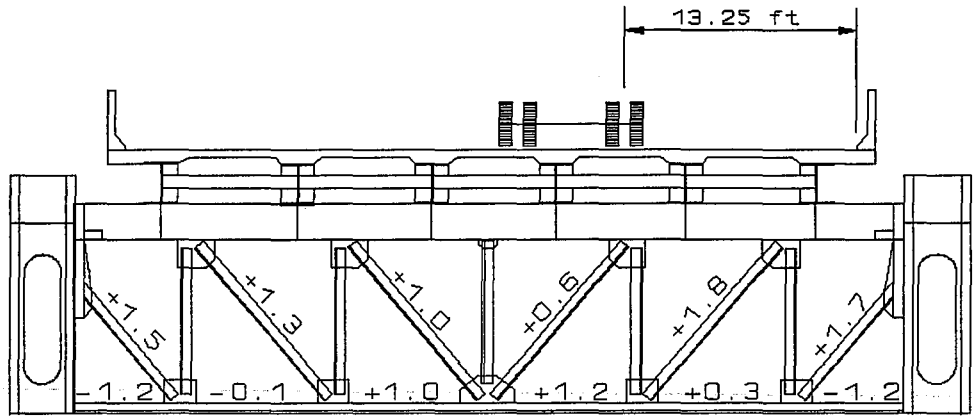

(a)

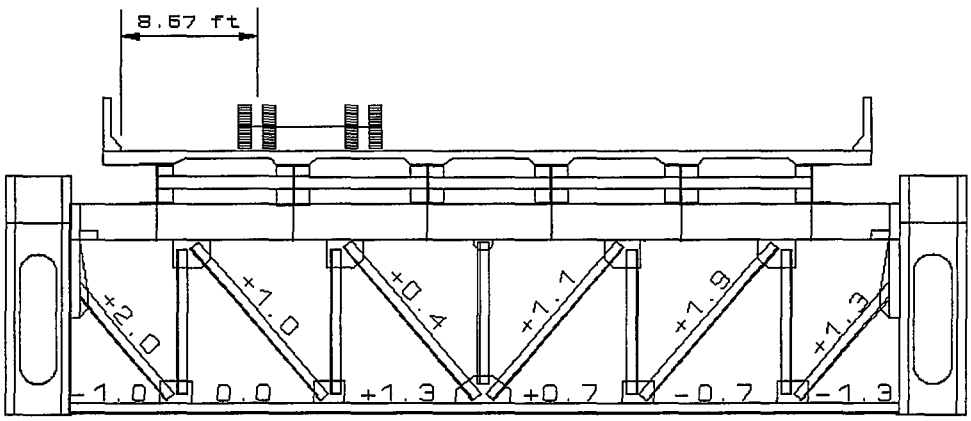

(b)

Figure 43. Axial Stress Ranges (ksi) in Floortruss 8 Due to 5-Axle Test Truck: (a) Truck in Slow Lane at 53 mph; (b) Truck in Fast Lane at 53 mph

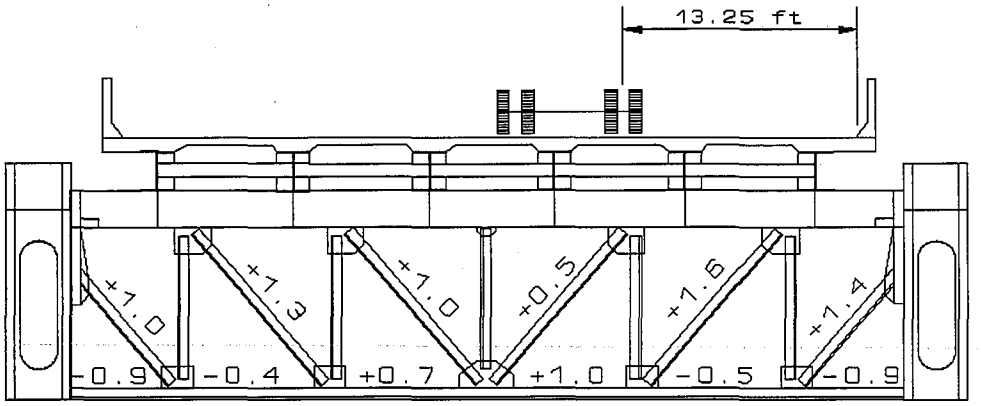

(a)

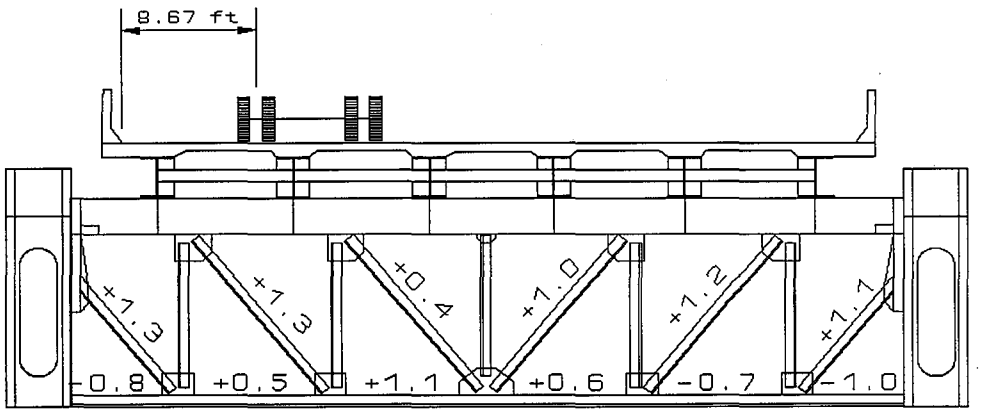

(b)

Figure 44. Axial Stress Ranges (ksi) in Floortruss 4 Due to 3-Axle Test Truck: (a) Truck in Slow Lane at 50 mph; (b) Truck in Fast Lane at 55 mph

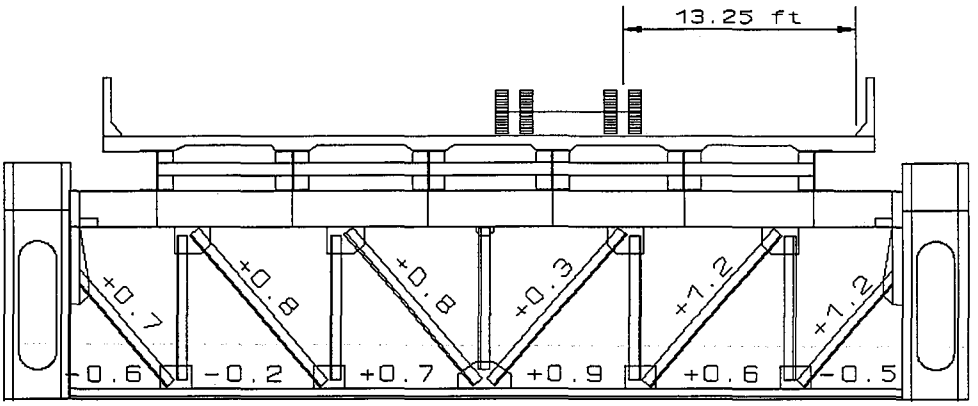

(a)

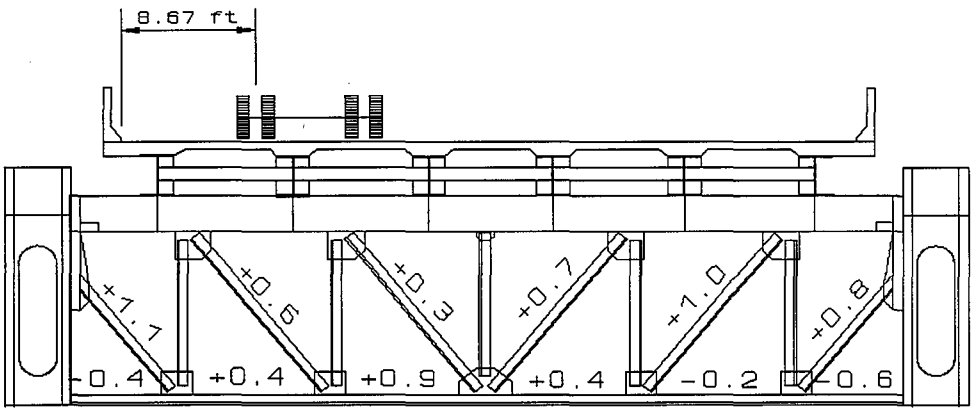

(b)

Figure 45. Axial Stress Ranges (ksi) in Floortruss 8 Due to 3-Axle Test Truck: (a) Truck in Slow Lane at 50 mph; (b) Truck in Fast Lane at 55 mph

stresses. But these members were generally in compression. The largest axial stress range produced by any of the fast run calibration tests was 2.2 ksi. This stress range was found in member D2 at floortruss 4 when the 5-axle test truck was traveling in the slow lane (Figure 42a). Axial stress ranges produced by the 3-axle test truck traveling in the slow and fast lanes at floortrusses 4 and 8 were similar in pattern but smaller in magnitude than those produced by the 5-axle test truck. The observations and patterns from the fast run calibration tests discussed above are very similar to those found from the random test data, which will be discussed in a later section.

Fast run calibration data used in plots later in this chapter are given in Tables 10 through 13. This calibration data will be used for comparison to random truck data.

Impact

Impact effect can be viewed as the difference between stresses produced by static loading and the maximum stresses produced by dynamic loading. This effect is presented in Table 14 through comparisons between static and dynamic axial stresses in the four outer diagonals (D1, D2, D5, and D6). The static stresses were due to the 5-axle test truck being parked directly over the gaged floortruss in the slow lane. The dynamic stresses were produced by 5-axle test truck fast runs in the slow lane. The difference in stresses was greatest at floortruss 8. For all eight members in question, the maximum dynamic stresses were only slightly higher than the static stresses. In most cases the difference between the static and dynamic values was approximately the same magnitude as the estimated level of precision of the measurements (0.15 ksi). The important observation from Table 14 is that the increase in stress due to impact is not consistently larger than the AASHTO impact fraction value of 0.29.

Table 10. Axial and Maximum Extreme Fiber Stress Ranges due to 3-Axle Test Truck Fast Runs in the Slow Lane

Member	Axial Stress Range (ksi)		Maximum Extreme Fiber Stress Range (ksi)	
	FT 4	FT 8	FT 4	FT 8
D1	1.4	1.2	1.6	1.2
D2	1.6	1.2	1.7	1.3
D3	0.5	0.3	1.1	0.7
D4	1.0	0.8	1.2	1.1
D5	1.3	0.8	1.5	0.8
D6	1.0	0.7	1.3	0.9
B3	1.0	0.9	1.4	1.0
B4	0.7	0.7	1.1	1.1

Table 11. Axial and Maximum Extreme Fiber Stress Ranges due to 3-Axle Test Truck Fast Runs in the Fast Lane

Member	Axial Stress Range (ksi)		Maximum Extreme Fiber Stress Range (ksi)	
	FT 4	FT 8	FT 4	FT 8
D1	1.1	0.8	1.6	0.9
D2	1.2	1.0	1.4	1.0
D3	1.0	0.7	1.2	0.8
D4	0.4	0.3	1.1	0.8
D5	1.3	0.6	1.6	0.9
D6	1.3	1.1	1.6	1.3
B3	0.6	0.4	0.9	0.7
B4	1.1	0.9	1.2	1.0

Table 12. Axial and Maximum Extreme Fiber Stress Ranges due to 5-Axle Test Truck Fast Runs in the Slow Lane

Member	Axial Stress Range (ksi)		Maximum Extreme Fiber Stress Range (ksi)	
	FT 4	FT 8	FT 4	FT 8
D1	2.0	1.7	2.2	1.9
D2	2.2	1.8	2.2	1.8
D3	0.8	0.5	1.5	1.0
D4	1.2	0.9	1.5	1.2
D5	1.7	1.1	1.9	1.2
D6	1.3	1.2	1.7	1.7
B3	1.1	1.0	1.5	1.3
B4	0.9	0.8	1.2	1.2

Table 13. Axial and Maximum Extreme Fiber Stress Ranges due to 5-Axle Test Truck Fast Runs in the Fast Lane

Member	Axial Stress Range (ksi)		Maximum Extreme Fiber Stress Range (ksi)	
	FT 4	FT 8	FT 4	FT 8
D1	1.6	1.3	1.7	1.5
D2	2.0	1.9	2.0	1.9
D3	1.2	1.0	1.4	1.2
D4	0.6	0.3	1.0	0.9
D5	1.5	0.9	1.8	1.0
D6	1.7	1.7	2.1	1.9
B3	0.8	0.6	1.0	1.1
B4	1.2	1.1	1.3	1.3

Table 14. Impact Effect of 5-Axle Test Truck in Slow Lane

Member	Static Axial Stress (ksi)	Maximum Dynamic Axial Stress (ksi)	Percent Diff.
Floortruss 4 (Quarter-Span)			
D1	1.5	1.5	0
D2	1.6	1.7	6
D5	1.5	1.6	7
D6	1.0	1.1	10
Floortruss 8 (Mid-Span)			
D1	1.4	1.6	14
D2	1.5	1.6	7
D5	1.0	1.2	20
D6	1.0	1.3	30

COMPARISON OF RESULTS FROM FLOORTRUSSES 4, 7, AND 8

One of the most significant, and expected, similarities between the two primary test locations (floortrusses 4 and 8) was the location of the highest stressed members. For each of these floortrusses, outside diagonal members D1, D2, D5, and D6 and inside bottom members B3 and B4 experienced the greatest tensile stresses. The vertical members and top chord members were in compression and are of no concern in this report.

As mentioned in Chapter Two, the member sizes for all fifteen floortrusses at the arch span are identical except for the top chords. Floortrusses 4, 8, and 12, which are located under expansion joints, each have a top chord made up of a channel and a T-section while the top chord of all other floortrusses consists of a wide flange section. Axial stresses in members D1 and D2 of floortrusses 4, 7, and 8 will be compared to determine the effect, if any, of the expansion joints and different top chord sizes. It should be noted that it would be most appropriate to compare floortruss 7 to floortruss 8 only since these two floortrusses are side by side at only fifty feet apart. However, the stresses in all three floortrusses will be presented to illustrate the similar behavior between them. It should also be pointed out that because of the expansion joints above floortrusses 4 and 8, the portion of the bridge between these floortrusses can be thought of as a continuous beam with four equal spans. And for this system, if there is a difference in the amount of load carried by the floortrusses it should be most apparent in the first interior supports (floortrusses 5 and 7).

The similarities in stresses at floortrusses 4, 7, and 8 are evident for the static calibration tests. Figures 46 and 47 illustrate plots of axial stress versus truck position for members D1 and D2 with the 5-axle test truck in each traffic lane. Results for static truck

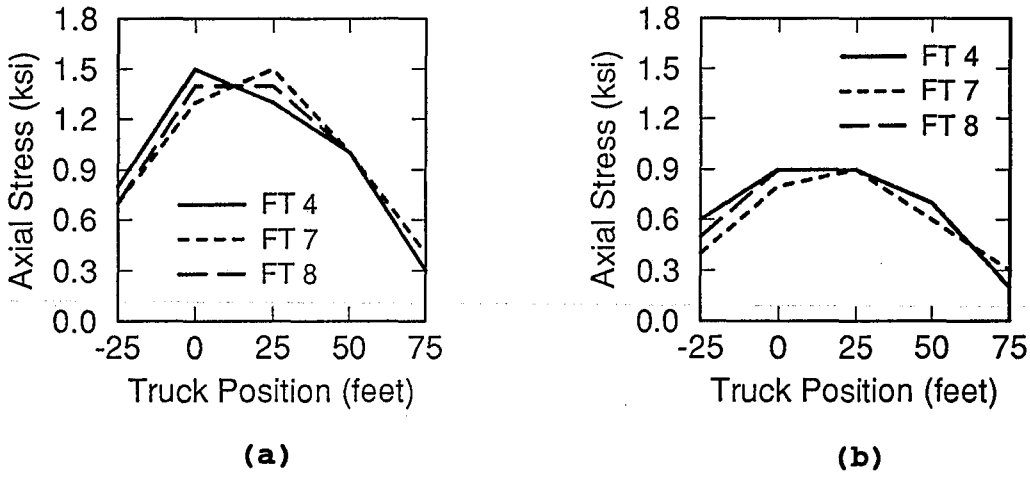

Figure 46. Static Axial Stress in Member D1 from 5-Axle Truck: (a) Truck in Slow Lane; (b) Truck in Fast Lane

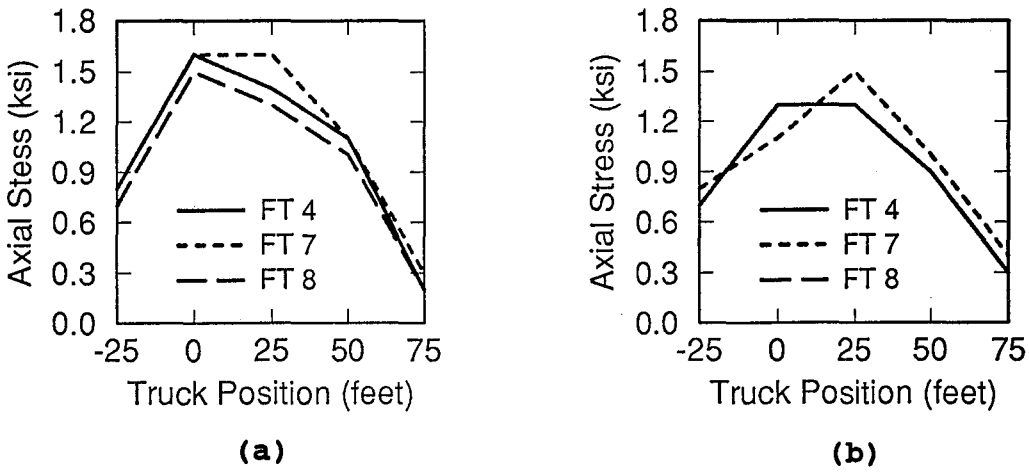

Figure 47. Static Axial Stress in Member D2 from 5-Axle Truck: (a) Truck in Slow Lane; (b) Truck in Fast Lane

positions are shown in these plots. A truck position of (-25) feet implies that the 5-axle truck was parked 25 feet north (traffic direction is southbound) of the gaged floortruss. The gaged floortruss is labeled as position 0 and the other three positions are located 25, 50, and 75 feet south of the gaged floortruss.

These plots show that there was 0.2 ksi or less difference between the three floortrusses for all test positions except one. The exception was for the position 25 feet south of the instrumented floortruss shown in Figure 47a where the difference between the stresses in diagonal 2 of floortrusses 7 and 8 is 0.3 ksi. These differences are not considered significant since the expected level of accuracy in the experimental measurements is approximately plus or minus 0.15 ksi.

Although the maximum differences are not large, the results from floortruss 7 do show an interesting trend. A common result from the static calibration tests shown in Figures 46 and 47 is that when the test truck was parked 25 feet south of the three gaged floortrusses, the stresses in floortruss 7 were always equal to or slightly greater than the stresses in floortrusses 4 and 8. This trend is probably an indication of the effect of having continuous stringers over floortruss 7, as mentioned earlier in this section.

Tables 15 and 16 list the stress ranges at the neutral axis of members D1 and D2 due to 5-axle and 3-axle calibration fast runs. The stress ranges due to both test truck fast runs at floortruss 7 generally fell between the stress ranges at floortrusses 4 and 8, with the greatest stress ranges found at floortruss 4. However, the difference between the axial stress ranges at floortruss 7 and floortruss 8 are minimal and in some cases nonexistent. For example, when the 5-axle truck is traveling in the fast lane (lane C), there is no difference between the floortruss 7 and floortruss 8 stress ranges in members D1 and D2.

Table 15. Stress Ranges at the Neutral Axis of Members D1 and D2 for 5 Axle Test Truck

Floortruss	Truck in Lane B		Truck in Lane C	
	D1 (ksi)	D2 (ksi)	D1 (ksi)	D2 (ksi)
4	2.0	2.2	1.6	2.0
7	2.0	2.1	1.3	1.9
8	1.7	1.8	1.3	1.9

Table 16. Stress Ranges at the Neutral Axis of Members D1 and D2 for 3-Axle Test Truck

Floortruss	Truck in Lane B		Truck in Lane C	
	D1 (ksi)	D2 (ksi)	D1 (ksi)	D2 (ksi)
4	1.4	1.6	1.1	1.2
7	1.3	1.5	0.8	1.1
8	1.2	1.2	0.8	1.0

Table 17. Effective Stress Ranges at the Neutral Axis of Members D1 and D2 (Based on 250 Random Trucks)

Floortruss	D1 (ksi)	D2 (ksi)
4	1.7	1.9
7	1.6	1.8
8	1.5	1.6

The effective stress ranges at the neutral axis of members D1 and D2 due to random truck data are listed in Table 17. As was the case with the fast run data, the highest effective stress ranges were found at floortruss 4 and the lowest at floortruss 8. Also, the effective stress ranges in members D1 and D2 are only 7 percent and 13 percent higher, respectively, at floortruss 7 than floortruss 8.

The objective of this part of the results chapter was to ensure that the expansion joints and difference in top chord size, and in essence the break in continuity in the floor system, did not significantly affect the stresses in floortrusses 4 and 8. The expansion joints appear to reduce the stresses in these two floortrusses due to static loading at one particular test position. Stresses due to static loading at the other four test positions, random truck traffic, and fast run calibrations are slightly reduced or do not change in floortrusses below an expansion joint. Based on the tests discussed above, the overall difference in stresses in members D1 and D2 between floortrusses 7 and 8 is minimal. The presence of an expansion joint above a floortruss did not significantly affect the stresses in the floortruss. Thus, the two major test locations (floortruss 4 and floortruss 8) appear to be representative of all fifteen floortrusses at the arch span.

As mentioned several times above, the overall behavioral patterns of floortrusses 4 and 8 were very similar. The stresses measured in static tests at each location agree very well, but the stress ranges due to the test trucks and random truck traffic were consistently higher at floortruss 4 than floortruss 8. The difference in stress ranges, which was generally around 20 percent, was found to result from compression in the members before and after a truck crossed floortruss 4. This compression was most likely caused by relative displacements between the tie girders at each end of the floortruss.

COMPARISON OF AXIAL AND EXTREME FIBER STRESS RANGES

Among the project objectives given in Chapter One was to determine if the floortruss tension members were experiencing bending, and if so, to determine the extreme fiber stresses very near the filler plates. The answer to the first of these questions can be found in Figures 48 through 63. The figures, each of which show data points for 250 random truck crossings from the normal traffic stream, illustrate the relationship between axial stress range and maximum extreme fiber stress range for all six diagonal members and the two inner bottom members at floortrusses 4 and 8. The stresses in the outside bottom members (B1, B2, B5, and B6) were close to zero or even compressive and will not be investigated further.

If a tension member experienced no bending, a plot of maximum extreme fiber stress range versus axial stress range would simply be a straight line with a one to one slope. This line is shown as a dashed line in all of the plots mentioned above. Also, "best-fit" lines with their respective slopes are drawn through the random truck data points. The slopes represent the difference in maximum stress range and axial stress range. For example, in Figure 48, the maximum extreme fiber stress range for member D1 at floortruss 4 is 23 percent higher than the axial stress range, as a result of bending. All the members shown in these figures exhibited some level of bending.

As stated earlier in this chapter, the highest stressed diagonal members were D1, D2, D5, and D6. The amount of bending in these members was less than the bending in the interior diagonals, D3 and D4. For the four highest stressed diagonals at floortruss 4, the extreme fiber stress ranges were 20 percent higher on average than the axial stress ranges. And at floortruss 8, there was an average difference of 15 percent between the extreme fiber stress range and axial stress range for members D1, D2, D5, and D6. The

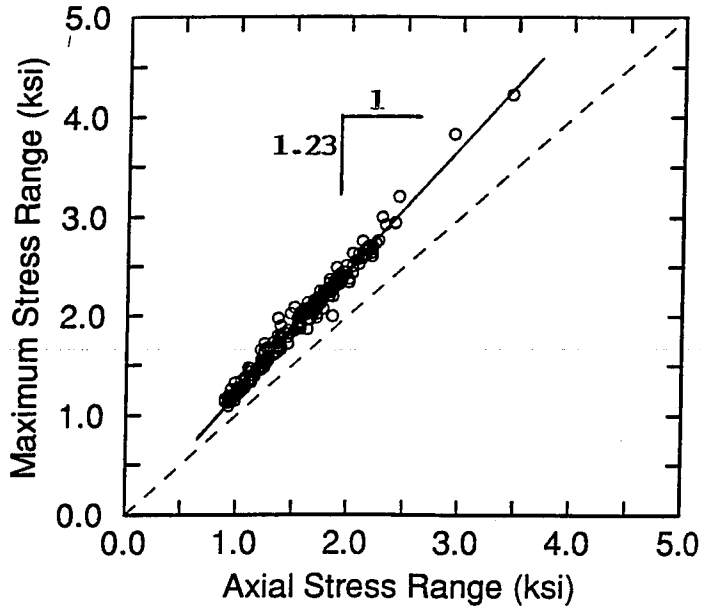

Figure 48. Maximum Extreme Fiber Stress Range Versus Axial Stress Range for Member D1 at Floortruss 4

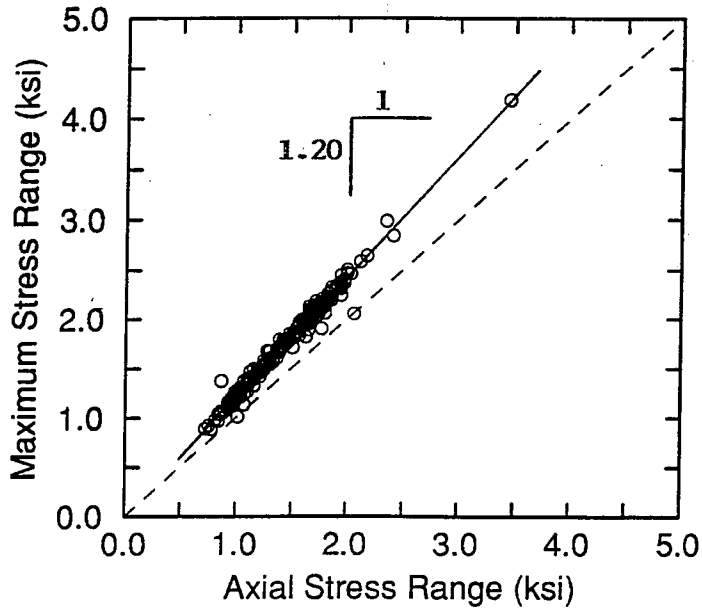

Figure 49. Maximum Extreme Fiber Stress Range Versus Axial Stress Range for Member D1 at Floortruss 8

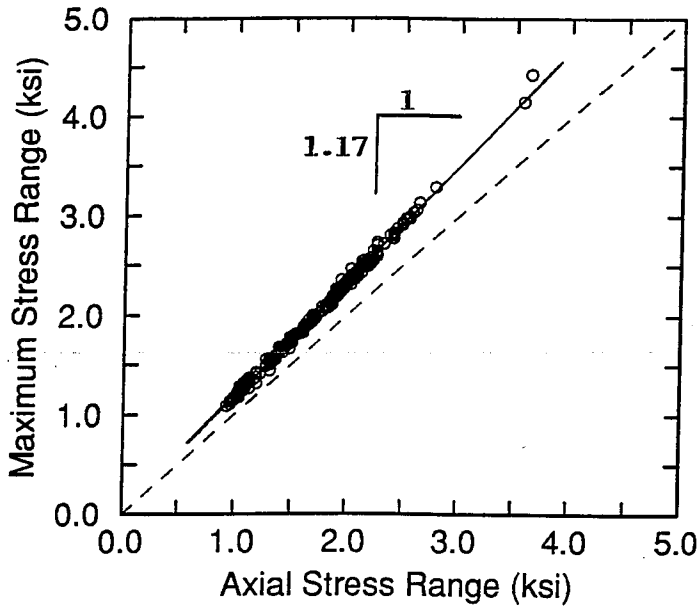

Figure 50. Maximum Extreme Fiber Stress Range Versus Axial Stress Range for Member D2 at Floortruss 4

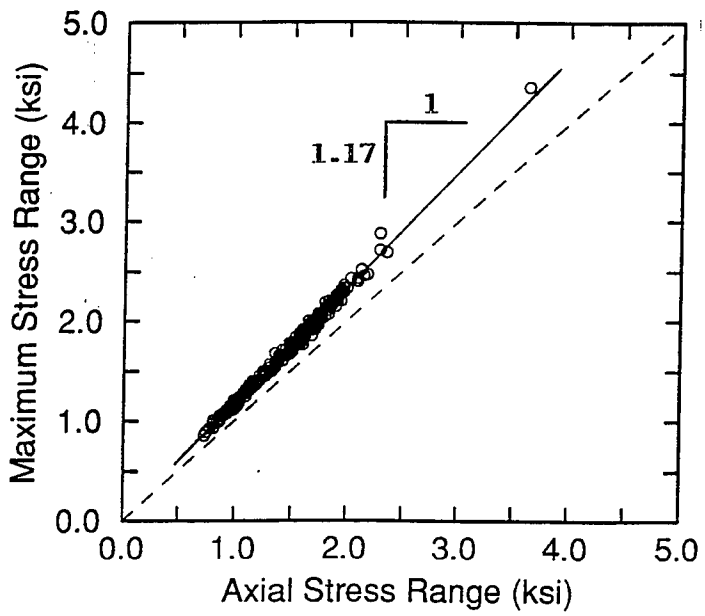

Figure 51. Maximum Extreme Fiber Stress Range Versus Axial Stress Range for Member D2 at Floortruss 8

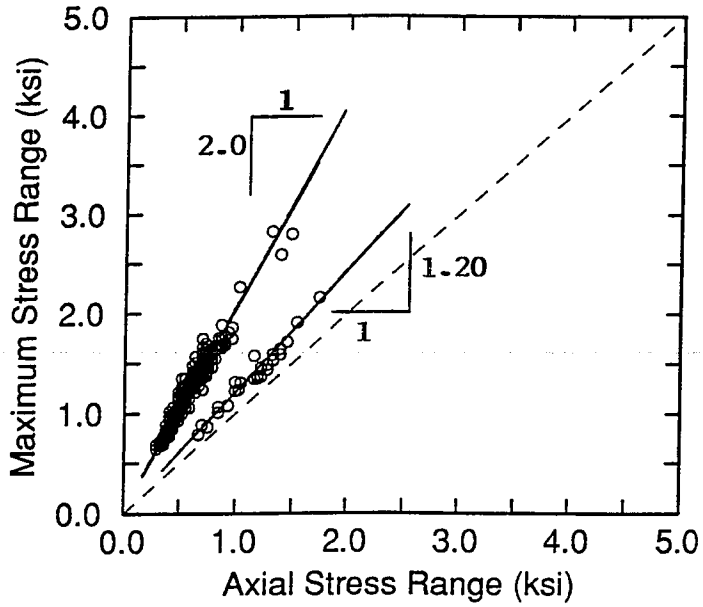

Figure 52. Maximum Extreme Fiber Stress Range Versus Axial Stress Range for Member D3 at Floortruss 4

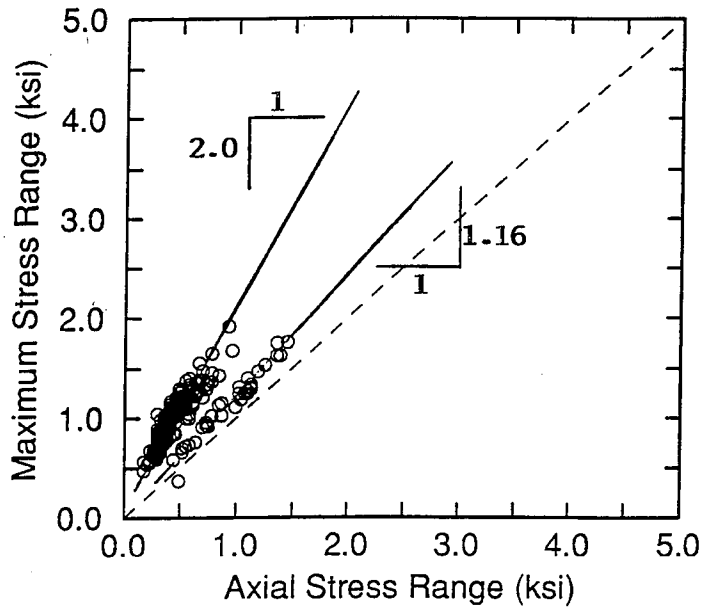

Figure 53. Maximum Extreme Fiber Stress Range Versus Axial Stress Range for Member D3 at Floortruss 8

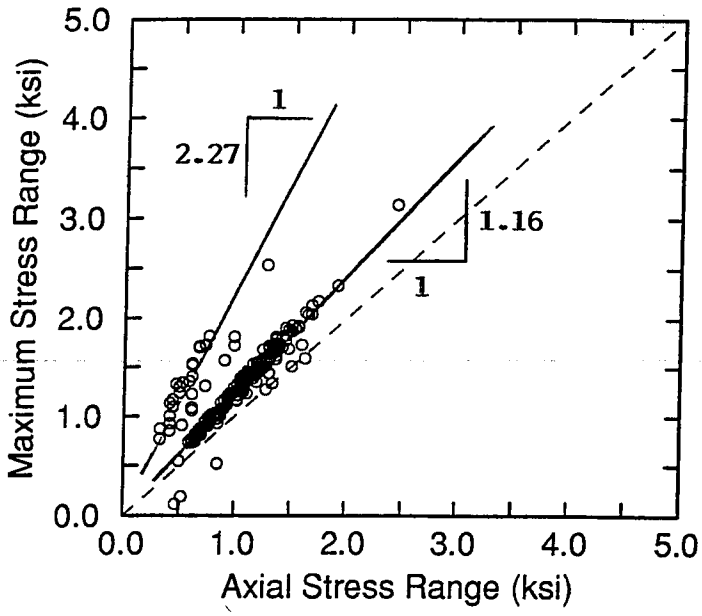

Figure 54. Maximum Extreme Fiber Stress Range Versus Axial Stress Range for Member D4 at Floortruss 4

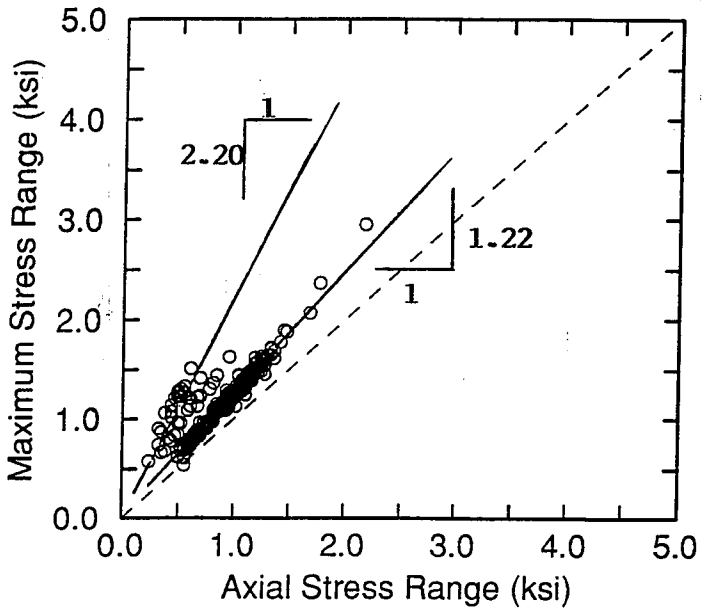

Figure 55. Maximum Extreme Fiber Stress Range Versus Axial Stress Range for Member D4 at Floortruss 8

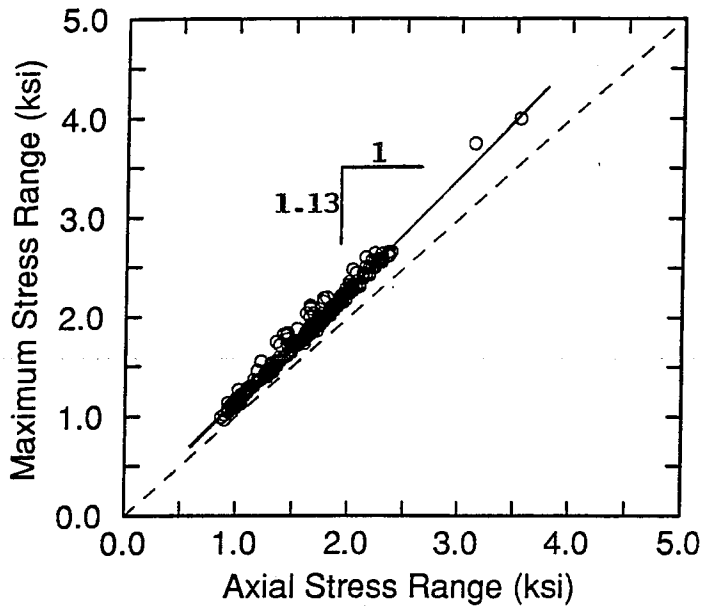

Figure 56. Maximum Extreme Fiber Stress Range Versus Axial Stress Range for Member D5 at Floortruss 4

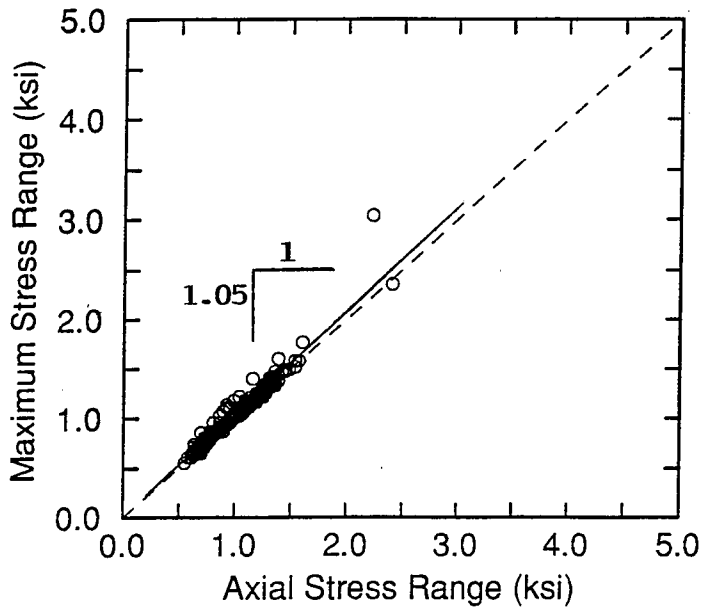

Figure 57. Maximum Extreme Fiber Stress Range Versus Axial Stress Range for Member D5 at Floortruss 8

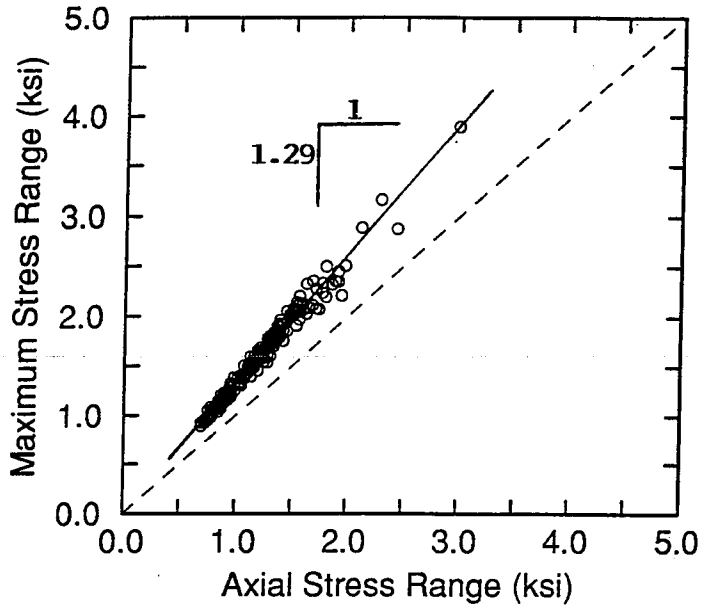

Figure 58. Maximum Extreme Fiber Stress Range Versus Axial Stress Range for Member D6 at Floortruss 4

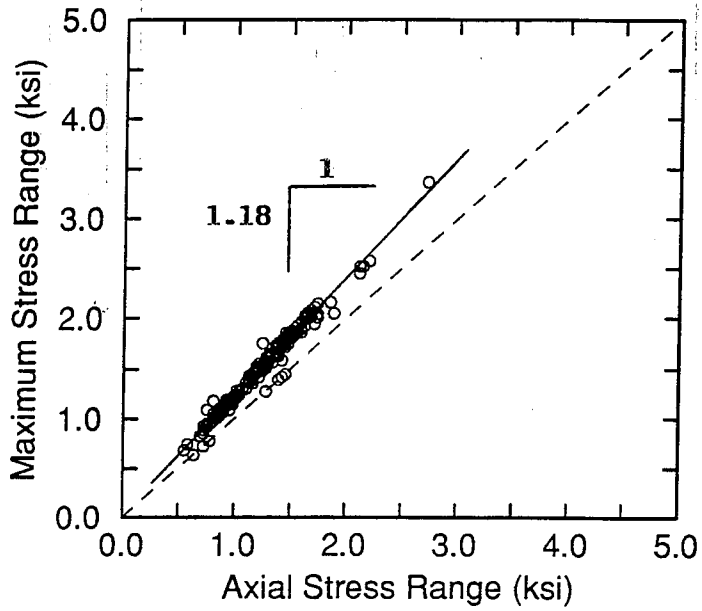

Figure 59. Maximum Extreme Fiber Stress Range Versus Axial Stress Range for Member D6 at Floortruss 8

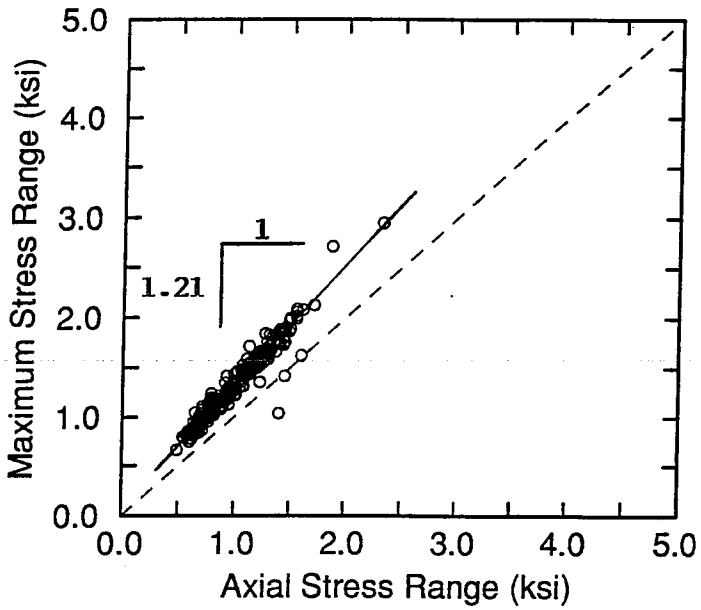

Figure 60. Maximum Extreme Fiber Stress Range Versus Axial Stress Range for Member B3 at Floortruss 4

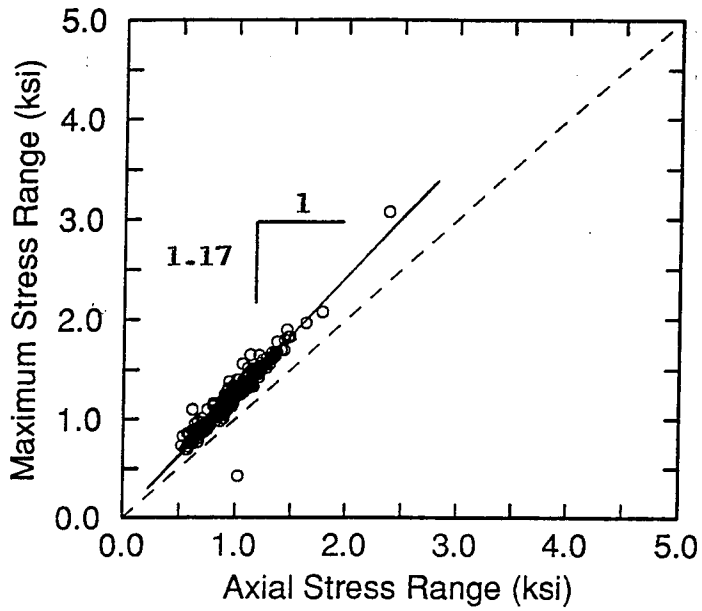

Figure 61. Maximum Extreme Fiber Stress Range Versus Axial Stress Range for Member B3 at Floortruss 8

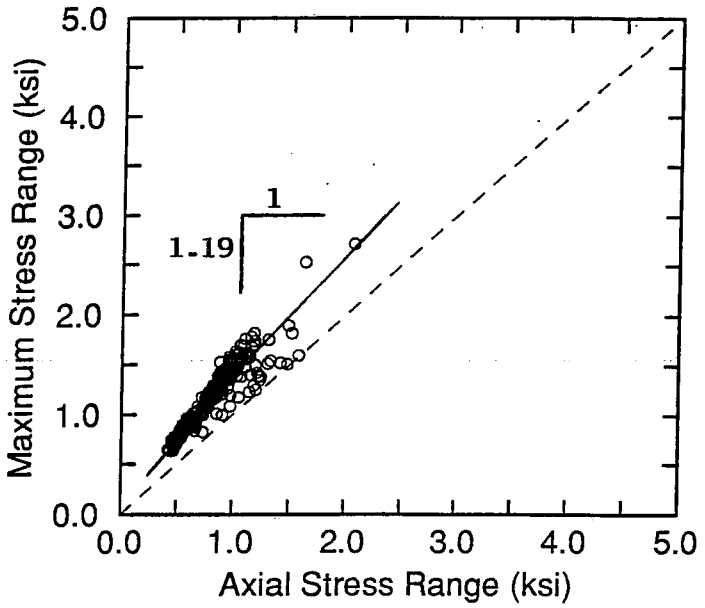

Figure 62. Maximum Extreme Fiber Stress Range Versus Axial Stress Range for Member B4 at Floortruss 4

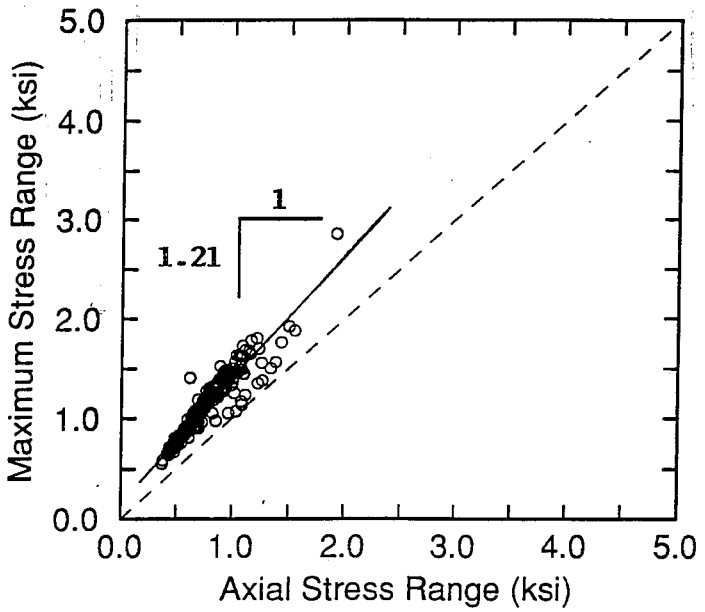

Figure 63. Maximum Extreme Fiber Stress Range Versus Axial Stress Range for Member B4 at Floortruss 8

data points, or random trucks, for each of these four diagonals at floortrusses 4 and 8 plotted along relatively straight lines. Thus, the weight of the truck or lane a truck was traveling in during the random tests did not have an effect on percentage increase in stress due to bending in the higher stressed members.

Conversely, the data points for members D3 and D4 at floortrusses 4 and 8 form two distinct lines. For member D3 (Figures 52 and 53), most of the random trucks fall along the line with the greater slope. The majority of trucks on the road travel in the slow lane. Thus, a fair assumption would be to say the line with the most data points denotes trucks traveling in the slow lane, and the line with less data points denotes trucks in the fast lane. This reasoning is justified based on a detailed investigation in the next section of this chapter.

For member D4 (Figures 54 and 55), the same patterns discussed above are present except the line passing through the majority of data points has the smallest slope. Assuming as before that the line with the most data points signifies trucks traveling in the slow lane, the greatest amount of bending in an inner diagonal member is therefore due to a truck traveling over that particular member. The locations of lanes B and C were shown in Figure 19 in Chapter Four. Lane B (slow lane) is located almost directly over D3 and Lane C (fast lane) is located over the left half of D4 and the right half of D5. Based on the line of data points with the greatest slope, the extreme fiber stress ranges for D3 and D4 can be over 100 percent greater than the axial stress ranges. However, the combined magnitudes are significantly smaller than the stresses in the outside diagonal members.

The highest stressed bottom chord members are B3 and B4. The extreme fiber stresses in each of these members at floortrusses 4 and 8 are an average of 20 percent higher than the axial stress ranges (Figures 60 through 63). These two inner members

would certainly be regraded as critical for the bottom chord. However, for the entire floortruss, the stresses in B3 and B4 are small relative to the diagonal members, and thus these two bottom members are not considered critical.

SIGNIFICANCE OF LANE POSITION

As mentioned briefly in the previous section, the lane in which a truck is traveling has an effect on the stress ranges and level bending of the interior diagonal members. The effect of lane position is investigated for all diagonals and bottom members B3 and B4 at both test locations in Figures 64 through 79. These figures illustrate how stress ranges from test trucks of known weight and lane position compare to random truck data.

For the exterior diagonal members (D1, D2, D5, and D6) shown in Figures 64 through 67 and Figures 72 through 75, respectively, the test truck data points fall in line with the random data. All data for test trucks in the slow lane and fast lane fall in a straight line indicating that lane position does not affect the percentage of bending. The 5-axle test truck produced the highest stress ranges in the four diagonals. More specifically, in member D1 (Figures 64 and 65), the greatest stress ranges occurred when the 5-axle truck was traveling in the slow lane, which is located above the member D1. Similarly, in member D6, (Figures 74 and 75), the greatest stress ranges occurred when the 5-axle truck was traveling in the fast lane, which is located above member D6. The lighter 3-axle test truck produced the smallest stress ranges in all four diagonals. The test truck data points involving the 3-axle truck also fall in a line with the random data indicating that truck weight does not affect the percentage of bending stress.

The percentage of total stress due to bending in the interior diagonals (D3 and D4) appears to be directly related to the lane in which a truck travels. Two distinct lines of

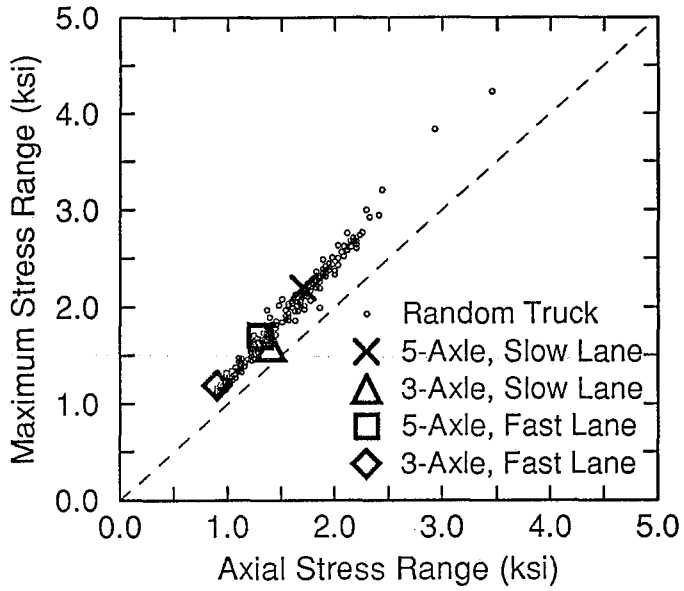

Figure 64. Maximum Extreme Fiber Stress Range Versus Axial Stress Range Due to Test Trucks and Random Truck Traffic for Member D1 at Floortruss 4

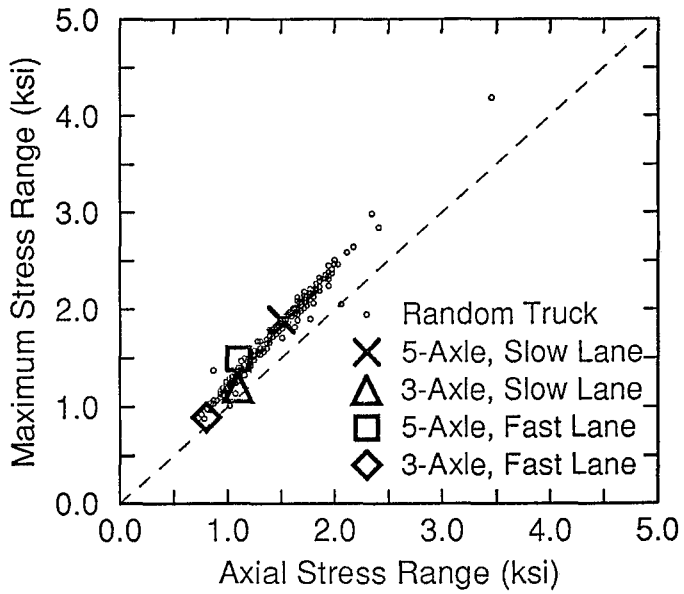

Figure 65. Maximum Extreme Fiber Stress Range Versus Axial Stress Range Due to Test Trucks and Random Truck Traffic for Member D1 at Floortruss 8

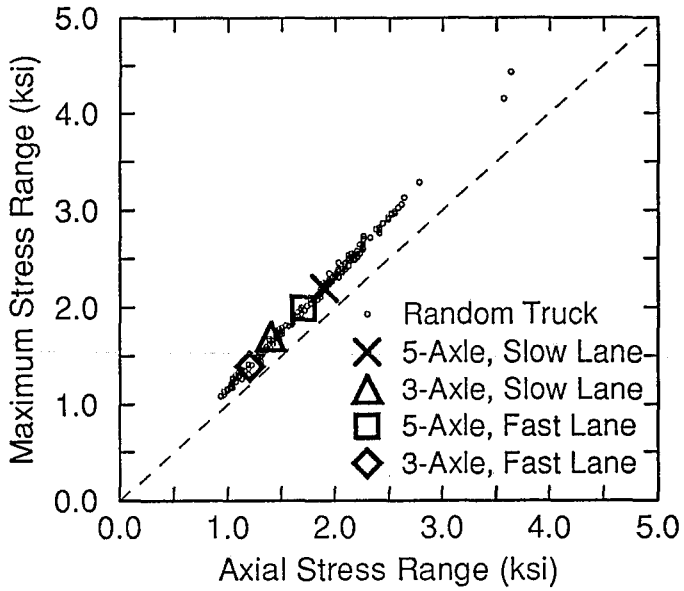

Figure 66. Maximum Extreme Fiber Stress Range Versus Axial Stress Range Due to Test Trucks and Random Truck Traffic for Member D2 at Floortruss 4

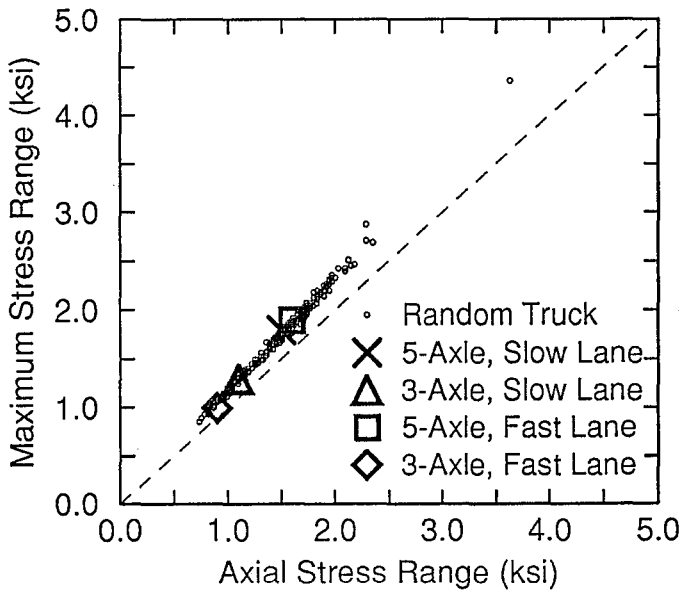

Figure 67. Maximum Extreme Fiber Stress Range Versus Axial Stress Range Due to Test Trucks and Random Truck Traffic for Member D2 at Floortruss 8

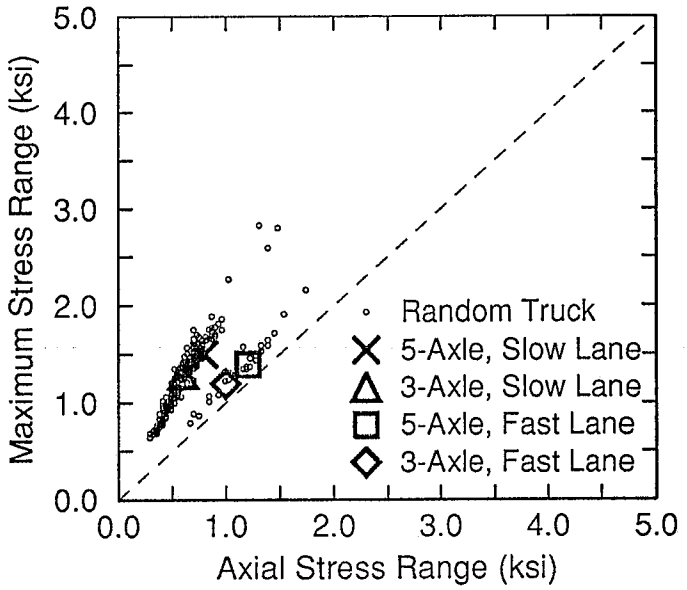

Figure 68. Maximum Extreme Fiber Stress Range Versus Axial Stress Range Due to Test Trucks and Random Truck Traffic for Member D3 at Floortruss 4

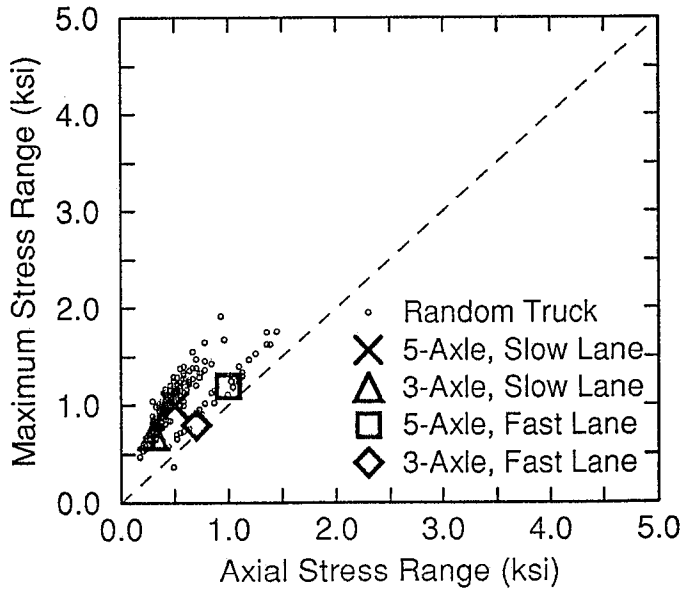

Figure 69. Maximum Extreme Fiber Stress Range Versus Axial Stress Range Due to Test Trucks and Random Truck Traffic for Member D3 at Floortruss 8

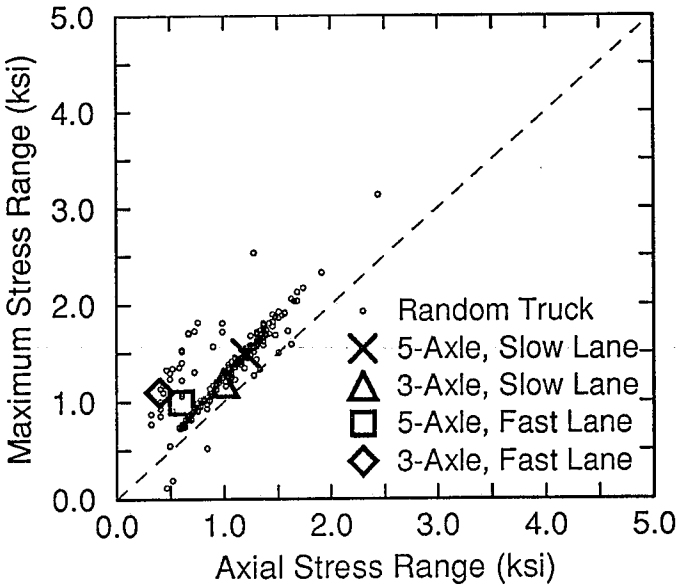

Figure 70. Maximum Extreme Fiber Stress Range Versus Axial Stress Range Due to Test Trucks and Random Truck Traffic for Member D4 at Floortruss 4

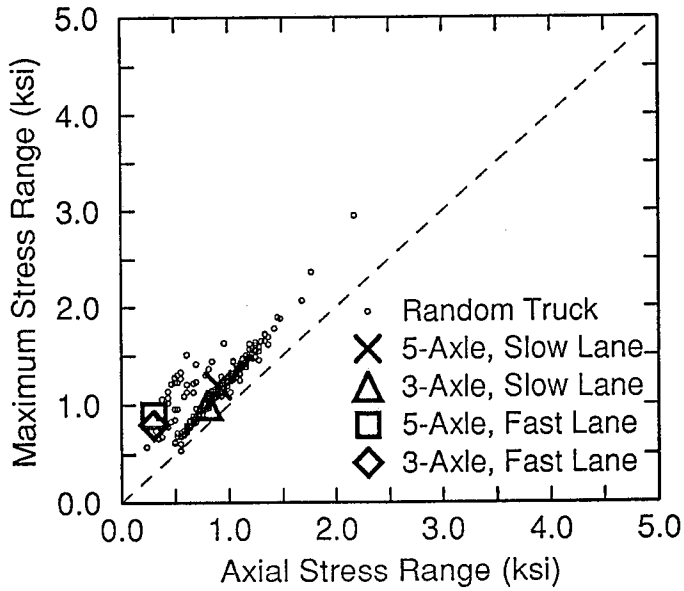

Figure 71. Maximum Extreme Fiber Stress Range Versus Axial Stress Range Due to Test Trucks and Random Truck Traffic for Member D4 at Floortruss 8

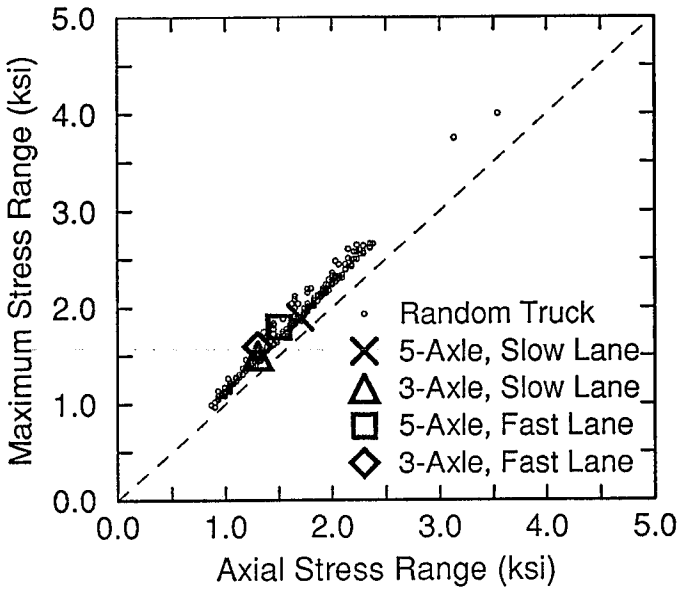

Figure 72. Maximum Extreme Fiber Stress Range Versus Axial Stress Range Due to Test Trucks and Random Truck Traffic for Member D5 at Floortruss 4

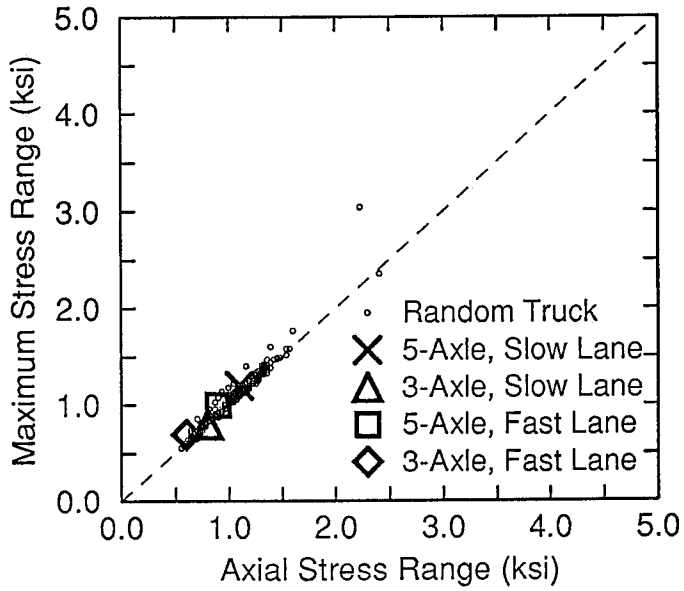

Figure 73. Maximum Extreme Fiber Stress Range Versus Axial Stress Range Due to Test Trucks and Random Truck Traffic for Member D5 at Floortruss 8

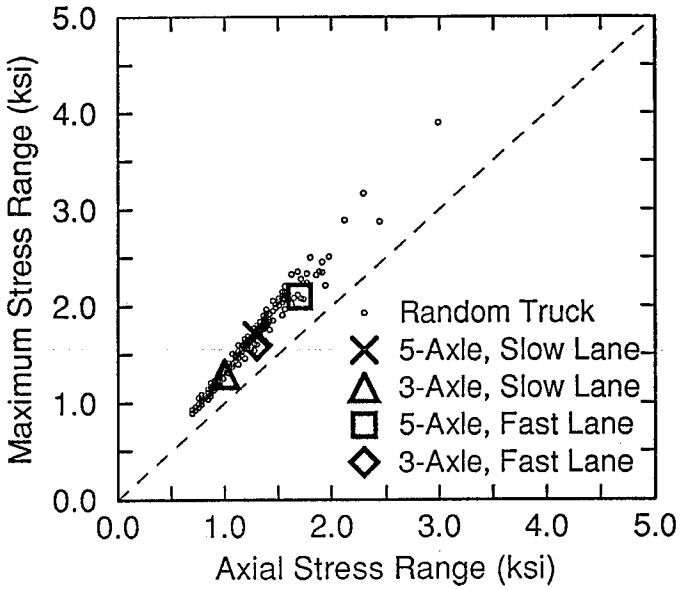

Figure 74. Maximum Extreme Fiber Stress Range Versus Axial Stress Range Due to Test Trucks and Random Truck Traffic for Member D6 at Floortruss 4

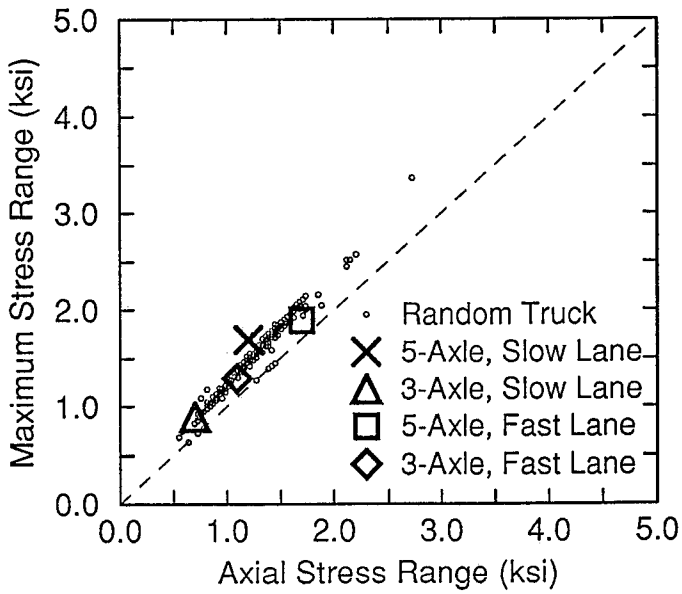

Figure 75. Maximum Extreme Fiber Stress Range Versus Axial Stress Range Due to Test Trucks and Random Truck Traffic for Member D6 at Floortruss 8

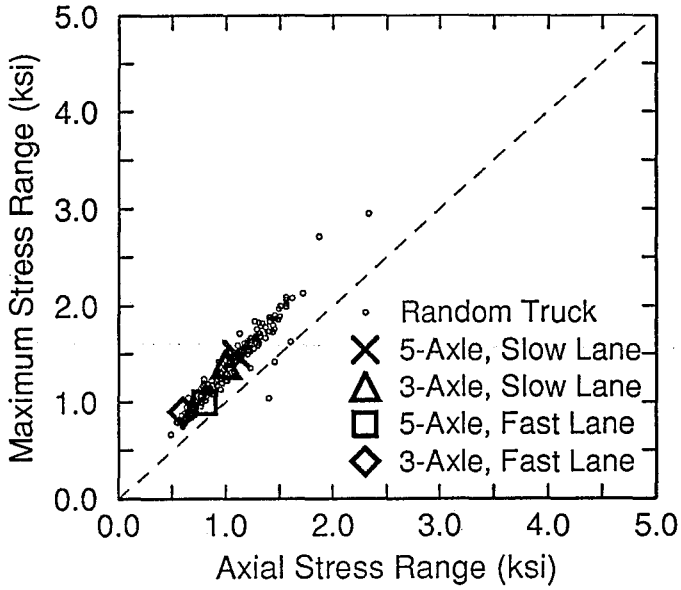

Figure 76. Maximum Extreme Fiber Stress Range Versus Axial Stress Range Due to Test Trucks and Random Truck Traffic for Member B3 at Floortruss 4

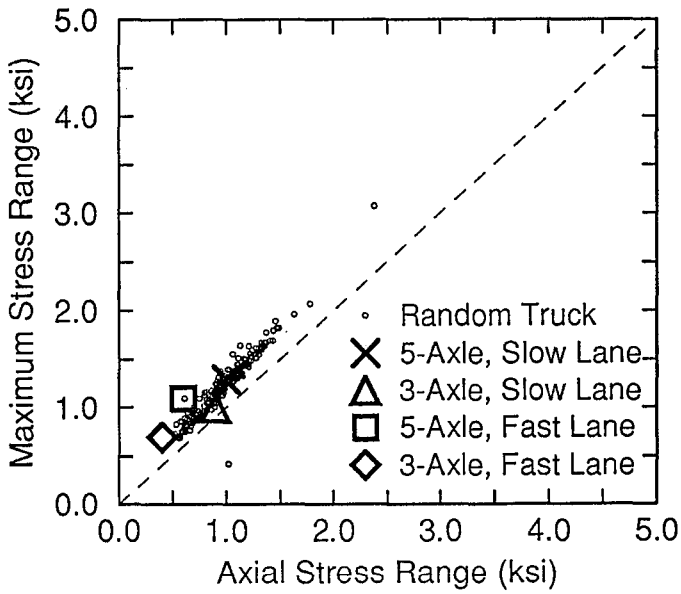

Figure 77. Maximum Extreme Fiber Stress Range Versus Axial Stress Range Due to Test Trucks and Random Truck Traffic for Member B3 at Floortruss 8

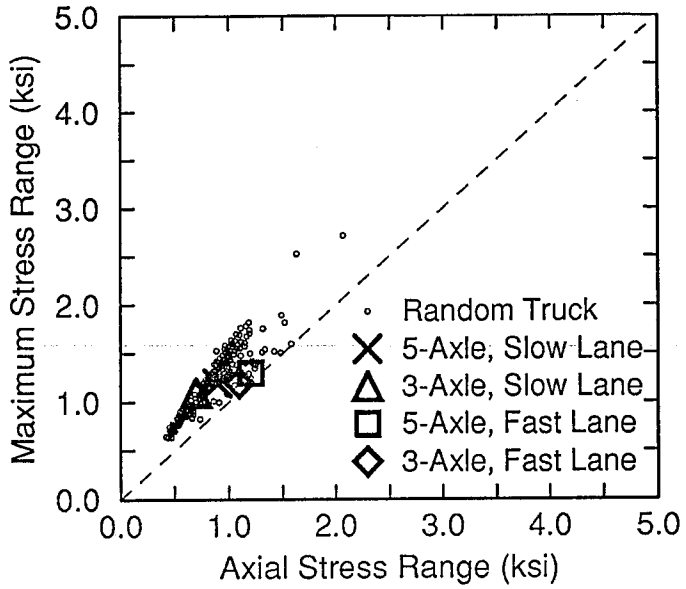

Figure 78. Maximum Extreme Fiber Stress Range Versus Axial Stress Range Due to Test Trucks and Random Truck Traffic for Member B4 at Floortruss 4

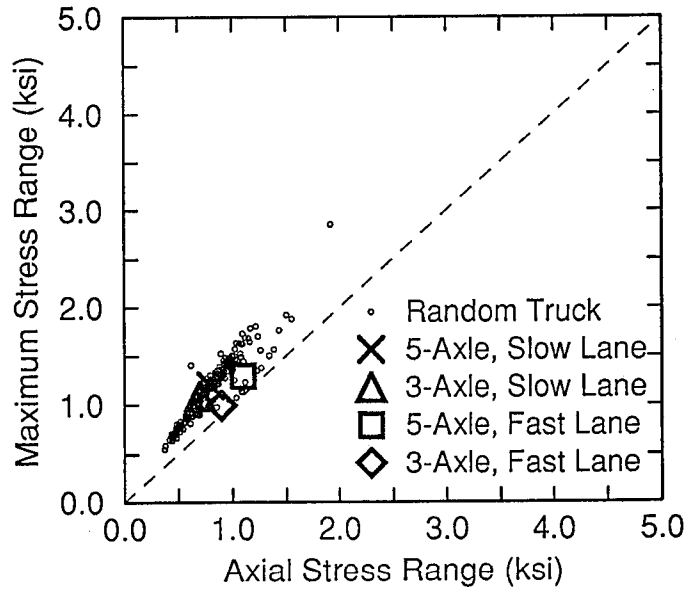

Figure 79. Maximum Extreme Fiber Stress Range Versus Axial Stress Range Due to Test Trucks and Random Truck Traffic for Member B4 at Floortruss 8

data points are shown in Figures 68 through 71. All four plots show the calibration test trucks in the slow lane plotted in one data line and test trucks in the fast lane plotted in the other.

For member D3 at floortruss 4 and 8 (Figures 68 and 69), data points for test trucks in the slow lane plot along the line with the most random data points. For member D4 at floortrusses 4 and 8 (Figures 70 and 71), this same pattern is present. Therefore, trucks traveling in the slow lane, which is located over the diagonal 3 side of the floortruss, cause the most bending in member D3. Similarly, trucks traveling in the fast lane, which is located over the diagonal 4 side of the floortruss, cause the most bending in member D4.

Finally, for the two interior bottom members (B3 and B4), the random data points and calibration truck data points are closely bunched (Figures 76 through 79). For member B4, test trucks in the slow lane tend to line up with the majority of random data points and test trucks in the fast lane fall in a separate line with a small number of random trucks. However, the difference between these two lines of points is minimal. Thus, lane position and truck weight do not significantly affect the stress ranges and bending in members B3 and B4.

COMPARISON OF RESULTS FROM FIELD TESTS AND STRUCTURAL ANALYSES

Stresses in the floortruss members were found through the use of a general planar frame analysis computer program. The load cases investigated in the calculation of these stresses included static loading by the test trucks positioned directly over the gaged floortruss and dynamic loading due to test truck fast runs. The objective of calculating

stresses in the floortruss members was to compare them to the measured stresses from the field tests in order to help further understand the behavior and patterns of the arch span floor system.

In calculating the floortruss stresses, the portion of the concrete deck over the instrumented floortruss and three floortrusses on either side of the instrumented floortruss was modeled in the longitudinal direction as two continuous beams with four supports each. The supports represented the floortrusses. Point loads representing the wheels of the test trucks were positioned (as shown in Figure 21 in Chapter Four) above the support denoting the instrumented floortruss. The reaction found at this support was assumed to be the total weight carried by the instrumented floortruss due to a test truck being parked directly over the floortruss. The concrete deck above the instrumented floortruss was then modeled in the transverse direction as a continuous beam with six supports. The six stringers located below the deck and above the top chord were represented by the supports. The vertical reactions at each support, with the signs reversed, were used as point loads acting on top of the top chord of the floortruss. Calculated stresses due to static loading were found using loading as described above in a rigid frame analysis of the floortruss. Stresses due to fast run loading were found by increasing the static loads by an impact factor. All point loads were multiplied by a factor of 1.29 to allow for dynamic or impact effects (AASHTO 1991).

Tables 18 through 21 compare calibration axial stresses in the four most critical members at floortrusses 4 and 8 to axial stresses found in the same members from the computer analysis. The stresses in these two tables are due to static loadings from the 3-axle and 5-axle test trucks being parked directly over the gaged floortruss. A distinct pattern is evident from this comparison. The greatest differences between the measured

Table 18. Comparison of Measured and Calculated Static Axial Stresses due to 5-Axle Truck in Slow Lane over the Gaged Floortruss

Member	Calculated Stresses (ksi)	Meas. Stresses Floortruss 4 (ksi)	Meas. Stresses Floortruss 8 (ksi)
D1	1.4	1.5	1.4
D2	2.2	1.6	1.5
D5	1.6	1.5	1.0
D6	1.1	1.0	1.0

Table 19. Comparison of Measured and Calculated Static Axial Stresses due to 5-Axle Truck in Fast Lane over the Gaged Floortruss

Member	Calculated Stresses (ksi)	Meas. Stresses Floortruss 4 (ksi)	Meas. Stresses Floortruss 8 (ksi)
D1	0.9	0.9	1.0
D2	1.2	1.3	1.3
D5	2.0	1.3	0.8
D6	1.8	1.4	1.5

Table 20. Comparison of Measured and Calculated Static Axial Stresses due to 3-Axle Truck in Slow Lane over the Gaged Floortruss

Member	Calculated Stresses (ksi)	Meas. Stresses Floortruss 4 (ksi)	Meas. Stresses Floortruss 8 (ksi)
D1	1.1	1.1	1.0
D2	1.7	1.1	1.1
D5	1.3	1.0	0.7
D6	0.9	0.7	0.7

Table 21. Comparison of Measured and Calculated Static Axial Stresses due to 3-Axle Truck in Fast Lane over the Gaged Floortruss

Member	Calculated Stresses (ksi)	Meas. Stresses Floortruss 4 (ksi)	Meas. Stresses Floortruss 8 (ksi)
D1	0.7	0.7	0.7
D2	0.9	1.0	0.9
D5	1.6	1.0	0.6
D6	1.4	1.0	1.0

stresses and calculated stresses for the static tests were found in members D2 and D5 when the test trucks were parked over these members. That is, in Table 18, for the 5-axle truck parked in the slow lane directly over the gaged floortruss, the stresses found in members D1, D5, and D6 from the structural analysis and from the calibration tests were very similar. However, the calculated stresses found in member D2 were 50 percent and 60 percent higher at floortrusses 4 and 8, respectively, than the calibration stresses. Similarly, in Table 19, the measured and calculated stresses found were very similar in members D1, D2, and D6. The calculated stresses found in member D5 were 77 percent and 188 percent higher at floortrusses 4 and 8, respectively, than the measured stresses. Similar patterns were also present for static tests involving the 3-axle test truck (Tables 20 and 21). The difference in stresses in all the cases discussed above may be due to the way the floortrusses were modeled in the computer analysis. Several simplifying assumptions were made, and these types of assumptions generally lead to more conservative results.

As mentioned earlier in this section, the loads used in modeling the dynamic cases were simply static loads increased by an impact factor. Thus, the results from the computer analysis were stresses and not stress ranges. For a fair comparison with dynamic cases, the calculated stresses were compared to field test maximum stresses instead of stress ranges.

Like the static loading comparisons, the calculated axial stresses due to dynamic loading found from the structural analysis were consistently higher than the measured maximum axial stresses found from the calibration fast runs (shown in Tables 22 through 25). In each table, for three of the four members in question, the structural analysis stresses and calibration stresses were reasonably close. The greatest difference

Table 22. Comparison of Measured and Calculated Dynamic Axial Stresses due to 5-Axle Truck in Slow Lane

Member	Calculated Stresses (ksi)	Meas. Stresses Floortruss 4 (ksi)	Meas. Stresses Floortruss 8 (ksi)
D1	1.9	1.5	1.6
D2	2.7	1.7	1.6
D5	2.1	1.6	1.2
D6	1.4	1.1	1.4

Table 23. Comparison of Measured and Calculated Dynamic Axial Stresses due to 5-Axle Truck in Fast Lane

Member	Calculated Stresses (ksi)	Meas. Stresses Floortruss 4 (ksi)	Meas. Stresses Floortruss 8 (ksi)
D1	1.1	1.0	1.2
D2	1.5	1.5	1.7
D5	2.5	1.3	1.0
D6	2.3	1.5	1.7

Table 24. Comparison of Measured and Calculated Dynamic Axial Stresses due to 3-Axle Truck in Slow Lane

Member	Calculated Stresses (ksi)	Meas. Stresses Floortruss 4 (ksi)	Meas. Stresses Floortruss 8 (ksi)
D1	1.5	1.2	1.2
D2	2.2	1.3	1.2
D5	1.7	1.2	0.9
D6	1.1	0.8	0.9

Table 25. Comparison of Measured and Calculated Dynamic Axial Stresses due to 3-Axle Truck in Fast Lane

Member	Calculated Stresses (ksi)	Meas. Stresses Floortruss 4 (ksi)	Meas. Stresses Floortruss 8 (ksi)
D1	0.9	0.8	0.8
D2	1.2	1.1	1.0
D5	2.0	1.2	0.7
D6	1.8	1.2	1.2

due to loading in the slow lane occurred in member D2. Similarly, the greatest difference due to loading in the fast lane occurred in member D5. The differences between the structural analysis stresses and dynamic calibration stresses are larger than the differences involving the static calibration stresses. It should be noted that part of the difference between the test and analysis values results from applying an impact fraction of 0.29 to the analysis results. The impact fraction of 0.29 is generally greater than that observed as illustrated in Table 14.

The highest axial stress found from the computer analysis was 2.7 ksi. This maximum value was found in member D2, which was also the member where the largest measured axial stress was found. The value of 2.7 ksi was due to dynamic loading from the 5-axle test truck in the slow lane, as shown in Table 22. Assuming that the extreme fiber stress is 20 percent larger than the axial stress, as was the case with the field test stresses at floortruss 4, the maximum extreme fiber stress estimate from the computer analysis is 3.2 ksi. Increasing this maximum stress by an additional 20 percent to account for compression before and after the truck crosses the floortruss, the estimated stress range due to a 5-axle truck in the slow lane is 3.8 ksi.

CHAPTER SIX

EVALUATION OF POTENTIAL FOR FATIGUE CRACKING

CRITICAL EXTREME FIBER LOCATIONS

As stated previously, the highest stressed members due calibration test trucks were the four outer diagonals (D1, D2, D5, and D6). This pattern is reaffirmed by the random truck traffic results given in Table 26. The maximum extreme fiber effective stress ranges for all six diagonal members and the two inner bottom members (B3 and B4) are listed in this table. The particular extreme fiber location on each member that was subjected to the greatest stress is also given. Based on the results of Table 26, the random data results, and the fast run calibration results, the four most critical locations of floortrusses 4 and 8 are clearly the extreme fibers of members D1, D2, D5, and D6. These critical locations are shown in Figure 80. Stress ranges in these four members at the four critical points are compared to fatigue limits, or thresholds, in the following sections.

COMPARISONS WITH AASHTO FATIGUE LIMITS

Maximum stress ranges in the four critical members based on the field test measurements are shown in Table 27. These stress ranges can be thought of as "worst case" values. That is, they represent load cases that cause the highest possible stress ranges at any point in the floortrusses.

Table 26. Effective Stress Ranges at Extreme Fiber Locations

Extreme Fiber Location	Effective Stress Range (ksi)	
	Floortruss 4	Floortruss 8
Top of D1 at Lower End	2.1	1.9
Bottom of D2 at Upper End	2.2	1.8
Bottom of D3 at Upper End	1.4	1.1
Bottom of D4 at Upper End	1.4	1.3
Bottom of D5 at Upper End	2.0	1.2
Top of D6 at Lower End	1.7	1.6
Bottom of B3 on East Side	1.2	1.1
Bottom of B4 on West Side	1.0	1.0

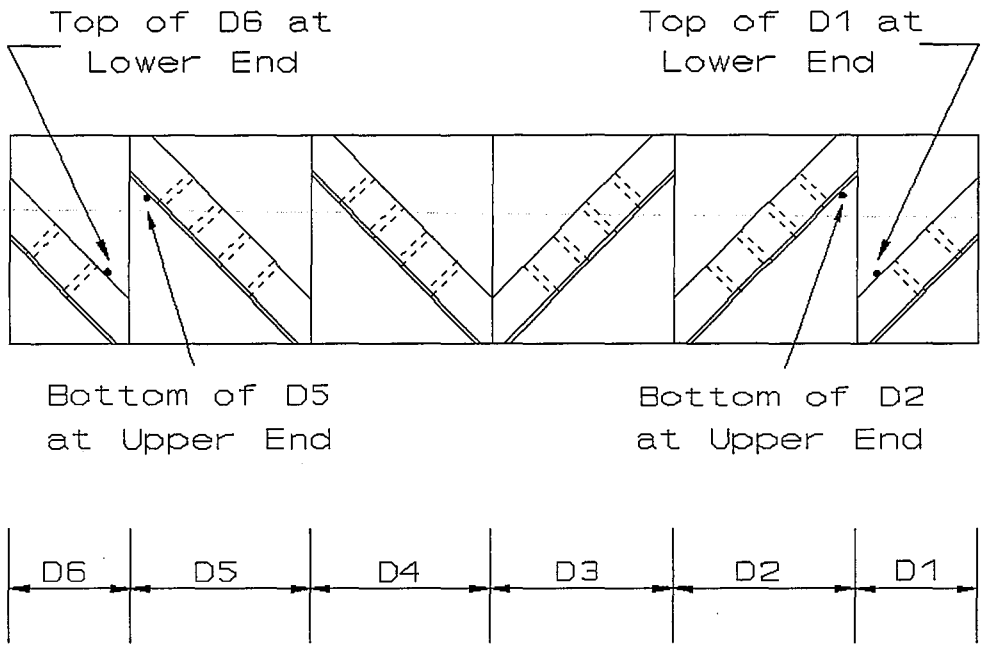

Figure 80. Critical Extreme Fiber Locations at Floortrusses 4 and 8 (Looking South)

Table 27. Maximum Stress Ranges at Extreme Fiber Critical Locations

Test	D1* (ksi)	D2* (ksi)	D5* (ksi)	D6* (ksi)
Floortruss 4 (Quarter-Span)				
Max Random	4.2	4.4	4.0	3.9
5-Axle, Lane B	2.2	2.2	1.9	1.7
5-Axle, Lane C	1.7	2.0	1.8	2.1
Lanes B+C	3.9	4.2	3.7	3.8
Floortruss 8 (Mid-Span)				
Max Random	4.2	4.4	3.0	3.4
5-Axle, Lane B	1.9	1.8	1.2	1.7
5-Axle, Lane C	1.5	1.9	1.1	1.9
Lanes B+C	3.4	3.7	2.3	3.6

* Locations shown in Figure 80.

Two fully loaded trucks traveling side by side across the arch span could be viewed as a worst case scenario. This load case is investigated in Table 27 by adding together the stress ranges due to the 5-axle test truck traveling in Lane B (slow lane) and in Lane C (fast lane). Note that the weight of the 5-axle test truck, as was shown in Tables 6 and 7 in Chapter Five, was approximately the same as the legal weight limit for the vehicle. A "Max. Random" stress range value in Table 27 represents the highest stress range found from the 250 random truck crossings taken during field testing. By inspection of Table 27, it is seen that the "Lanes B+C" values are slightly less than the maximum random stress ranges for all but one case. This observation suggests that the bridge is subjected to some side by side crossings by heavy trucks. The highest stress range recorded at any extreme fiber location at either test location was 4.4 ksi. This value was found during random testing at the bottom of member D2 at floortrusses 4 and 8.

The maximum recorded stress range of 4.4 ksi is slightly less than the fatigue limit of 5 ksi which at the time of design applied to the Category E welded connections that exist at each end of the double angle members. Hence, the actual stress conditions that exist in the floortruss members do not appear to be worse than assumed in the design process.

The filler plate welds as designed (before cracking) are a Category C detail and have a fatigue limit of 10 ksi. Visual inspection of the welds at a number of connections where cracking has not occurred did not reveal any problems that would reduce the fatigue limit for those details. Thus, fatigue cracking at those details is not a problem.

After the filler plate welds have cracked (failed) due to pack rust as discussed in Chapter One, the details do not clearly fall into an AASHTO fatigue category. A judgement about the conditions existing after a filler plate weld cracks suggests that

failure of the weld does not significantly reduce the fatigue strength of the double angle. Specifically, the fatigue strength is not believed to be less than that of the Category E details at the ends of each member. When the weld cracks, the stress concentration effect of the change in cross section at the filler plate is eliminated. A new stress concentration is created by the rough surface of the broken weld. However, because the throat of the filler plate welds was initially very small, the roughened area is small and does not appear to create a stress concentration that is worse than the original uncracked condition. The effects of the surface roughness are also reduced somewhat by the normal weathering that occurs in a relatively short time after the welds break. Hence, there does not appear to be a significant risk of fatigue cracking at locations where the filler plate welds have failed.

A limited number of the cracked filler plate welds have been repaired by field welding. In most cases the repair welds appear sound, and the repairs can be considered as a Category C detail. Thus, they do not pose a problem. However, undercut occurred at the ends of some of the repair welds. This condition is discussed further in the following sections.

FRACTURE MECHANICS APPROACHES

The previous section suggests that fatigue cracking in the double angle tension members at the tied arch span is not a problem. Further assurance of this fact can be gained from observations and estimations made using fracture mechanics. This approach will be used to predict fatigue thresholds and to estimate a tolerable crack size and fatigue life for the floortruss double angle members at the tied arch span.

Several factors that affect the susceptibility of a member to brittle fracture are temperature, material toughness, crack size, crack shape, applied stress, and yield stress. The applied stress, crack size, crack shape and orientation can be described by a single parameter called the stress intensity factor, K_I. The type fatigue crack of greatest interest here is a crack that might form at the extreme fiber of the back-to-back legs of the double angles. This type crack can be classified as an edge crack, as illustrated in Figure 81. The corner crack, also illustrated in Figure 81, represents a less critical condition.

For the edge crack geometry, the stress intensity factor can be described by:

$$K_I = 1.12\sigma\sqrt{\pi a} \qquad (2)$$

where a = crack length and σ = applied stress. For simplicity, the applied stress is taken as the extreme fiber stress and no stress gradient correction is made to account for bending.

Fatigue Threshold for Uncracked Double Angle

Notches in structural members can cause high stress concentrations to be present near the notch tip. The material element at the notch tip is subjected to the maximum stress from cyclic loads. This material element is likely to be the origin of fatigue crack initiation.

Some of the filler plates with weld cracks in floortrusses at the arch span were re-welded to the double angles. This process created small indentions, or undercut, in the edge of the angle at the end of the new weld. In estimating a fatigue threshold for an uncracked double angle, this indention will be considered a notch with a radius (ρ) between 0.01 inches and 0.05 inches and depth of 1/8 inch, as shown in Figure 82.

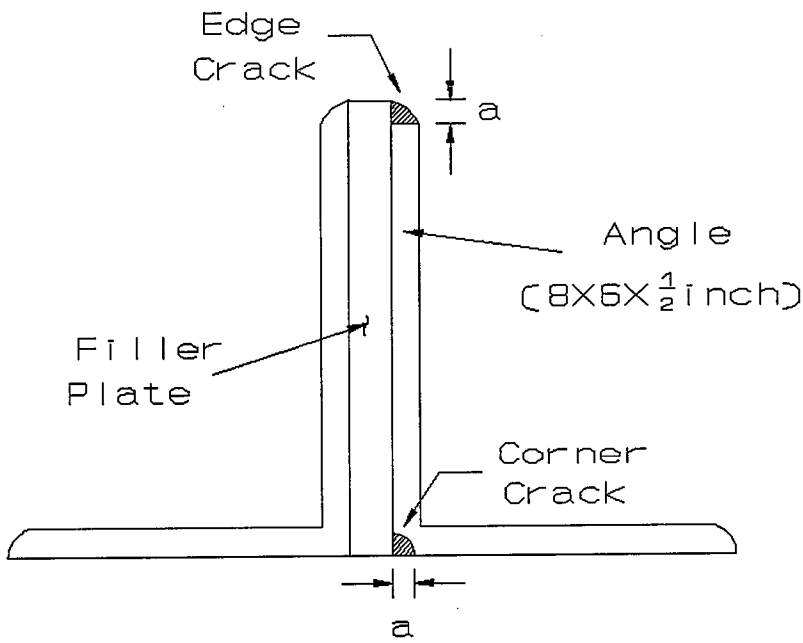

Figure 81. Possible Fatigue Crack Locations

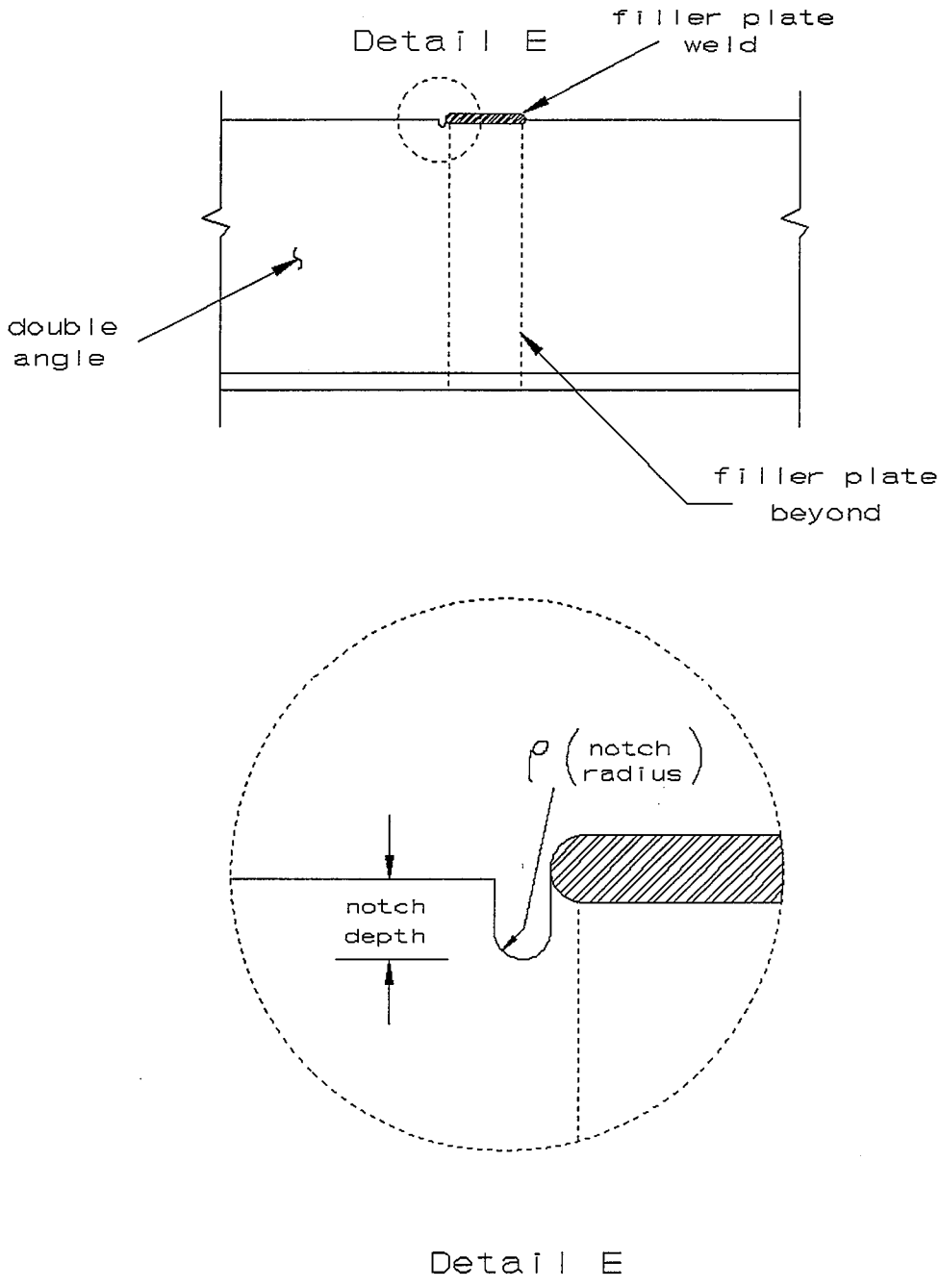

Figure 82. Assumed Notch Geometry at End of Weld

Barsom and Rolfe (1987) present data that indicate the following relationship can be used to estimate the fatigue-crack-initiation threshold for steels with yield strengths between approximately 40 and 140 ksi. The relationship is

$$\frac{\Delta K_I}{(\sigma_{ys})^{\frac{2}{3}}\sqrt{\rho}} = 5 \qquad (3)$$

where ΔK_I is in ksi$\sqrt{in}$, σ_{ys} is the yield strength in ksi, and ρ is in inches. For the base metal yield strength of 50 ksi, a fatigue-crack-initiation threshold $(\Delta K_I/\sqrt{\rho})_{th}$ of approximately 70 ksi results from equation (3).

Dividing both sides of equation (2) by $\sqrt{\rho}$ gives

$$\left(\frac{\Delta K_I}{\sqrt{\rho}}\right)_{th} = \frac{1.12\Delta\sigma\sqrt{\pi a}}{\sqrt{\rho}} \qquad (4)$$

The threshold for an uncracked double angle found using equation (4) ranges from 10 ksi to 22 ksi. Hence, these thresholds indicate that the notched double angle weld details can experience stress ranges up to 10 ksi without fatigue cracking. It is interesting to note that the lowest threshold estimate of 10 ksi matches the fatigue limit of the AASHTO Category C.

Fatigue Threshold for Cracked Double Angle

Barsom and Rolfe (1987) also present data that can be used to estimate a fatigue threshold for a member with a sharp tip crack. The threshold represents the stress range that can be applied without propagating the crack. The fatigue threshold for a cracked body is dependent upon the stress ratio, R, and is given by:

$$\Delta K_{th} = 6.4(1-0.85R) \quad ksi\sqrt{in} \qquad (5)$$

The stress ratio is the ratio of minimum stress to maximum stress. The minimum stress for the floortruss members is due to dead load only. Dead load includes the weight of the concrete deck and stringers (based on a tributary length of 50 feet) plus the weight of one floortruss. Maximum stress is equal to the stress due to truck crossings plus dead load stress. For an outer diagonal member, the dead load stress is 6.3 ksi. The Miner's effective stress range is 2.2 ksi, and 2.2 ksi is representative of stress range produced by the calibration trucks. Thus, the maximum live load stress was conservatively taken as 2.2 ksi which resulted in a maximum stress of 8.5 ksi and a stress ratio of 0.74.

As stated earlier, numerous welds between the filler plates and double angles cracked and completely fractured, but there were no cracks in any of the double angles. However, it is common in fatigue analysis to assume a crack appears, or initiates, as a worst case possibility. In the following discussion an 1/8 inch deep edge crack is assumed to initiate. Based on a stress ratio of 0.74, the fatigue threshold stress intensity factor range given by equation (5) is 2.4 ksi$\sqrt{in}$. Substituting the above stress intensity factor range and the crack length (1/8 inch) into equation (2) yields a fatigue stress range threshold of 3.4 ksi. Stress ranges below 3.4 ksi will not cause the assumed 1/8 inch crack to propagate. However, some stress ranges experienced by the double angle members exceed the threshold so an 1/8 inch deep crack could be expected to propagate slowly. The rate of growth of such a crack is discussed in a later section.

Maximum Tolerable Crack Size

Another interesting estimation is the maximum crack size that can be tolerated without propagation. Using equation (2), the maximum tolerable crack size based on a

maximum random stress range of 4.4 ksi and a stress intensity factor range of 2.4 ksi$\sqrt{in}$ is 3/32 inches. Cracks less than or equal to 3/32 inches in length will not propagate under a maximum stress range of 4.4 ksi.

Fatigue Life Estimate

A fatigue crack of 1/8 inch length exceeds the fatigue crack propagation threshold, as indicated above. It is important to estimate the length of time needed for this crack to become easily visible and reach a length required to cause brittle fracture of the double angle.

The absolute minimum fracture toughness for a double angle member is estimated to be 25 ksi$\sqrt{in}$, based on the AASHTO Guide Specifications for Fracture Critical Non-Redundant Steel Bridge Members (1991). At this toughness level, the crack length required to cause brittle fracture is 1.4 inches. Also, it is considered here that a crack length of 1/2 inch would be easily visible.

In determining the time required for an 1/8 inch crack to grow to a length of 1/2 inch (and longer), a fatigue crack growth rate relationship is required. Barsom and Rolfe (1987) suggest that fatigue crack growth in steel bridges can be described by the Paris Power Law:

$$\frac{da}{dn} = 3.6 \; X \; 10^{-10} \; (\Delta K_I)^{3.0} \qquad (6)$$

where da = change in crack length, dn = change in number of cycles, and ΔK_I = stress intensity factor range based on the Miner's effective stress range. Equations (2) and (6) can be used to determine the number of cycles required to grow an edge crack in the double angle to a specified crack length. The number of cycles can be converted to a

number of years. Based on AHD statistics (see Table 1 in Chapter Two), the I-65 Mobile Delta Crossing Bridges are subjected to approximately 3000 heavy vehicles per day (northbound and southbound). Thus, 1500 trucks (cycles) per day cross the southbound arch span, or 547,500 cycles per year.

Based on the fatigue crack growth principles discussed above, for the worst case Miner's effective stress range of 2.2 ksi it would take approximately 140 years at the current traffic volume for an 1/8 inch edge crack to grow to a visible length of 1/2 inch. An additional 50 years would be required for the 1/2 inch crack to reach a length of 1 inch. Finally, 20 more years would be needed for the 1 inch crack to reach a critical length of 1.4 inches, which could cause brittle fracture of the double angle. Based on the above results, 25 bridge inspections (50 years) will be performed in the time required for a visible 1/2 inch crack to reach a less than critical 1 inch length. This number of bridge inspections is obviously ample time to spot a fatigue crack in a double angle member. The traffic volume values (from Table 1) used in the fatigue life calculations discussed above are based on traffic history up to 1991. Extrapolations to account for future increases in traffic volume were not performed since the calculated fatigue lives are very long.

CHAPTER SEVEN

CONCLUSIONS AND RECOMMENDATIONS

SUMMARY AND CONCLUSIONS

The objective of this part of the fatigue cracking evaluation project was to use field testing to evaluate the stress conditions and potential of fatigue cracking at the tied arch span of the I-65 Mobile Delta Crossing Bridges. The concern here was due to the possibility of fatigue cracks developing in the floortruss tension members from existing filler plate weld cracks. The weld cracks were caused by pressures generated by confined rust between the filler plates and back to back legs of the double angles. Field measurements of stresses were made at two locations along the arch span.

An early conclusion drawn from the test data was that the difference in the behavior of floortrusses under expansion joints and floortrusses under continuous spans was minimal and in some cases nonexistent. Thus, the quarter-span and mid-span test locations, which were located under expansion joints, were representative of all the floortrusses at the arch span.

Based on random and calibration field test data, the four outer diagonals (D1, D2, D5, and D6) were found to be the highest stressed members at both test locations. For these four critical members, the maximum extreme fiber stress ranges were 20 percent and 15 percent higher at floortrusses 4 and 8, respectively, than the axial stress ranges.

The percentage increases in stresses due to bending in these members was found to be unaffected by truck weight or lane position.

Stresses found in the four critical members using a general planar frame computer program were consistently higher yet comparable in most cases to the measured stresses.

The highest stress range found through field testing at either test location was 4.4 ksi. This worst case value, found at the extreme bottom fiber at the upper end of member D2 at floortruss 4 and floortruss 8, is less than half the design AASHTO fatigue limit of 10 ksi for the filler plate weld details. The conditions existing after the filler plate welds have cracked (failed) are not considered to be significantly worse than the as designed conditions.

Estimations and predictions concerning the double angle tension members based on fracture mechanics principles also suggested that fatigue cracking is not a threat to the integrity of the tied arch span floortrusses. Estimates of the fatigue-crack-initiation threshold indicate that fatigue cracking will not occur. Fatigue life calculations indicate that if fatigue cracks initiate, they will grow at a sufficiently slow rate to be found in the normal two year bridge inspections.

Therefore, based on the comparisons of maximum measured stress range to the fatigue limit and the results from the fracture mechanics calculations, fatigue cracking in the double angle tension members near the filler plate weld cracks is not problem.

RECOMMENDATIONS

Because of the conclusion that the development of fatigue cracking in the tension members of the tied arch span floortrusses is not a problem, removing the filler plates from those members and grinding out the welds is not necessary. However, if weld cracks

become severe enough to cause consecutive filler plates to break completely away from a compression member, buckling in that member is possible. Hence, for compression members having two or more consecutive failed filler plate welds, replacement of the filler plates using a new filler plate and a single high strength bolt is recommended.

REFERENCES

American Association of State Highway and Transportation Officials. (1991). Interim Specifications - Bridges, Washington, D.C.

American Association of State Highway and Transportation Officials. (1991). Guide Specifications for Fracture Critical Non-Redundant Steel Bridge Members, Washington, D.C.

Barsom, J.M. and Rolfe, S.T. (1987). Fracture and Fatigue Control in Structures, Prentice-Hall, Englewood Cliffs, N.J.

Fisher, J.W. (1978). "Fatigue Cracking in Bridges from Out-of-Plane Displacements," Canadian Journal of Civil Engineering, 5(4), 542-556.

Fisher, J.W., Yen, B.T., and Wang, D., "Fatigue of Bridge Structures - A Commentary and Guide for Design, Evaluation, and Investigation of Cracking," ATLSS, Advanced Technology for Large Scale Structural Systems, Lehigh University, July 1989, 89-102.

Keating, P.B. and Fisher, J.W. (1986). "Evaluation of Fatigue Tests and Design Criteria on Welded Details." Transportation Research Record 286, National Research Council, Washington, D.C., 6-16.

Kulicki, J.M. Prucz, Z., Sorgenfrei, D.F., Mertz, D.R., and Young, W.T. (1990). "Guidelines for Evaluating Corrosion Effects in Existing Steel Bridges." Transportation Research Record 333, National Research Council, Washington, D.C., 7-19.

Stallings, J.M., Cousins, T.E., Rotto, R.K., and Reid, C.B. (1993), "Evaluation of Fatigue Cracking in I-65 Mobile Delta Crossing Bridges, Volume I: Floorbeam - Girder Connections," Final Report, Alabama Highway Department Research Project 2019-16, Highway Research Center, Auburn University, Alabama, 186 pages.

Technical Manual for the Megadac Series 3008AC -Release 3.2.0 . (1991). Optim Corporation, Germantown, Maryland.

Yamada, K. and Albrecht, P. (1976). "Fatigue Design of Welded Bridge Details for Service Stresses." Transportation Research Record 607, National Research Council, Washington, D.C., 25-30.